THERAPEUTIC INVESTIGATION AND MODELING OF RESVERATROL AND SIRNA TARGETED COMBINATION DELIVERY TO LEUKEMIA CELLS

By
THIKRAYAT AL-ATTAR

Bachelor of Science in Chemical Engineering
United Arab Emirates University
Al Ain, UAE
2015

Master of Science in Chemical Engineering
University of California, Berkeley
Berkeley, California
2016

Submitted to the Faculty of the
Graduate College of the
Oklahoma State University
in partial fulfillment of
the requirements for
the Degree of
DOCTOR OF PHILOSOPHY
July, 2019

THERAPEUTIC INVESTIGATION AND MODELING OF RESVERATROL AND SIRNA TARGETED COMBINATION DELIVERY TO LEUKEMIA CELLS

Dissertation Approved:

Dr. Sundar Madihally

Dissertation Adviser

Dr. Josh Ramsey

Dr. Yu Feng

Dr. Peter Hoyt

DEDICATION

To Hasan, my little brother,

This project is dedicated to you and all children with leukemia

My little angel, you battled leukemia bravely,

but it took you away from me,

when you were only three,

in my heart you will always be…

ACKNOWLEDGMENTS

I would like to express my sincere gratitude and appreciation to my thesis advisor Dr. Sundar V. Madihally for the continuous support of my Ph.D. study and research, for his patience, motivation, enthusiasm, and deep knowledge. I would like to thank you for encouraging my research and for allowing me to grow as a research scientist. Your advice on both research as well as on my career is highly appreciated. I could not have imagined having a better advisor and mentor for my Ph.D. study.

I would also like to thank my committee members; Dr. Josh Ramsey, Dr. Yu Feng, and Dr. Peter Hoyt for serving as my committee members even at hardship. I also want to thank you for letting my defense be an enjoyable moment, and for your brilliant and insightful comments and suggestions. Thanks are extended to Dr. Heather Fahlenkamp - Chair in Chemical Engineering Department, Eileen Nelson, Carolyn Sanders, and Beth Kelly, for their generous administrative assistance. Special thanks to my family. Words cannot express how grateful I am to my parents for all of the sacrifices they made on my behalf. Your prayers for me were what sustained me this far. My heartfelt thanks to my husband, Masaaki Julian Ward. You have been my loving, patient, supportive partner and amazing friend throughout this journey. I am also grateful to my dear friends, Dr. Sara Azzam, with whom I shared a life journey, Altaies, Dr. Kevin Roehm, and Dr. Shailesh Dangwal, and my lab mates and colleagues Dr. Carrie German, Dr. Nicholas Flynn, and Dr. Abdurizzagh Khalf, who supported me along the way.

Name: THIKRAYAT AL-ATTAR

Date of Degree: JULY 2019

Title of Study: THERAPEUTIC INVESTIGATION AND MODELING OF RESVERATROL AND SIRNA TARGETED COMBINATION DELIVERY TO LEUKEMIA CELLS

Major Field: CHEMICAL ENGINEERING

Abstract: Nearly 10 million deaths are caused by cancer around the globe every year. Blood cancer is responsible for roughly 86,000 deaths in the United States. Patients' lifespan is improving as new technologies and controlled drug delivery techniques emerge. Cancer drug resistance and high required drug dosage remain the major hurdles towards improving cancer treatment. Nutraceuticals, such as resveratrol, are proven to be safe, and chemo-preventive action on a wide array of cancer have been used as a method to improve the sensitivity of the other drugs in combination therapy. Nutraceuticals, however, are non-specific, sparingly soluble in aqueous solution, and bioavailability *in vivo* is very low, leading to limited therapeutic effectiveness even at higher doses. Clinical trials with 150 mg/day of resveratrol given to healthy volunteers for 30 days showed plasma levels in the nanomolar range. Hence, arises the need for drug delivery of combination therapy to reduce the dose required and drug resistance. In this project, resveratrol is combined with leukemia-targeted small interfering RNA (siRNA), and encapsulated in electrospun microfibers, and holo-transferrin PEG-liposomes, respectively. Experiments were performed using single K562 cell cultures, as well as K562 and HUVECs co-cultures. Resveratrol (40 μM) content was analyzed using HPLC and cell viability was assessed using Annexin V (Non-viable), and Propidium Iodide (PI) (Necrotic) based flow cytometry. Electrospun microfibers with resveratrol were made using 1:1 PCL-GT blends. BCR-ABL siRNA (36 nM)-encapsulated holo-transferrin-conjugated PEG-liposomes were characterized using dynamic light scattering, and transmission electron microscopy. RT-qPCR was performed to assess silencing BCR-ABL gene. The combination therapy was additive, and controlled release in a timely manner resulted in 94.32 (±1.70)% K562 cells non-viability after 8-days of incubation. A computational fluid dynamics (CFD) model was developed in this project to assess the fluid flow impact on resveratrol release from electrospun microfibers. A custom-built bioreactor was designed to validate the model and study the stability of resveratrol in cell medium. Concentration profiles over 5 days were generated. The model suggested that perfusion velocity may not have a significant effect relative to cellular uptake rate and porosity of the surrounding tissue represented by that in the bone marrow microenvironment.

TABLE OF CONTENTS

LIST OF TABLES

Table Page

LIST OF FIGURES

Figure Page

CHAPTER I

INTRODUCTION

Cancer treatment has gained tremendous attention due to its global impact. Statistically, 18.1 million new cases of cancer will be diagnosed globally in 2018, of which, 9.6 million patients are expected to die [1]. Chronic Myeloid Leukemia (CML), also referred to as chronic myelogenous leukemia, is a type of blood cancer. It starts in the blood-forming cells of the bone marrow and invades the blood. Approximately every 3 minutes, a person is diagnosed with blood cancer in the US, and almost 171,550 people in 2016 are diagnosed with leukemia, lymphoma, and myeloma. Blood cancer accounts for almost 10.2% of new cancer cases in the US (**Figure 1**) [2].

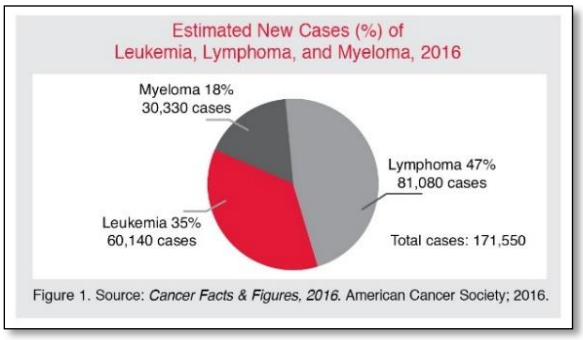

Figure 1.1: Estimated new cases of blood cancer in 2016.

Some of the available treatment options, apart from chemotherapy are molecular inhibitors of BCR-ABL pathway and tyrosine kinase pathway. Due to significant side effects with such medications, alternative therapies have been explored [3]. Supplementation with many nutraceuticals has been explored due to their proven safety [4].

Resveratrol, a naturally derived product found in red wine, grapes, fruits, peanuts, and pines, has been extensively investigated and shown to have a chemopreventive action on a wide array of cancer [5]. Resveratrol is, however, sparingly soluble in aqueous solution, and its bioavailability *in vivo* is very low when administered orally, leading to limited therapeutic effectiveness even at high doses. Alternatively, small interfering RNAs (siRNAs), which are 20-25 base pairs in length, have been shown to be very effective with local administration in silencing targeted genes since the first demonstration in 2010 [6]. However, systemic administration exacerbates side effects. Further, siRNA half-life is near 24 h [7], necessitating a higher dosage. In order to improve safety, targeting is required while minimizing the dosage, so that side effects could be eliminated. One unique approach shown to be more effective in targeting siRNA based delivery to cancer cells is transferrin-receptor based liposomal delivery [8, 9]. I propose combing these two approaches to treat cancer for its effectiveness. This is attributed to targeting different cellular pathways, through different mechanisms each drug induces. Hence, combination therapy lowers the probability of drug resistance in cancer cells. In order to control the release rates independently, two different delivery vehicles are explored. *I hypothesize that the synchronized combination treatment through controlled release of each drug, can reduce side effects, and induce higher levels of cancerous cells' non-viability.* To test my hypothesis, the following three aims are investigated:

Aim 1: Evaluate the influence of controlled release of resveratrol, in combination with siRNA on cell viability. Resveratrol-based therapy is hindered by achievable local therapeutic concentrations. Hence, I will test the controlled release of resveratrol using coaxial electrospun fibers. Poly(ε-caprolactone) (PCL) and gelatin (GT) blends were used to load resveratrol, HPLC was used to assess the controlled release profile. I also tested the combination therapy using siRNA, targeted towards BCR-ABL pathway to reduce the needed dosage of resveratrol. A factorial design is performed to evaluate the dosage requirements. I evaluated the apoptotic and necrotic effects of this treatment on K562 cells using Annexin V and Propidium Iodide staining. In the case of lipophilic

resveratrol, fiber configuration showed no significant effect on the release profile. Upon the controlled release of 40 μM resveratrol from single fibers, roughly 45% non-viable leukemia cells, after 8 days of incubation was measured. However, this percentage dropped to roughly 20% in the presence of 36 nM free BCR-ABL siRNA, which lead to further analysis in aim 2. Detailed findings of aim 1 are described in Chapter III.

Aim 2: Assess the effect of siRNA-loaded liposomes, in combination with controlled release of resveratrol on cell viability. In order to control the diffusion-dependent release of each drug independently, and eliminate any side interaction or side effects, a second delivery system was introduced. K562 cell line was treated with BCR-ABL siRNA-loaded PEG-liposomes. Liposomes 123 (±6.65) nm in size were formed using established techniques. Extrusion and dialysis were performed to obtain the desired size and purity. The surface of liposomes was modified with holo-transferrin, with 85.9 (±7.30)% conjugation efficiency, and the cell viability analysis was performed. Roughly 50% of non-viable leukemia cells was measured. PCL-GT microfibers containing resveratrol were then used along with siRNA-containing holo-transferrin-derived nano-liposomes. The treatment was tested in both single cultures of K562 cells, and co-cultures, in the presence of HUVECs. The treatment introduction was tested in a timely manner, showing that the delayed addition of liposomes increases K562 non-viability to 92.7 (±2.00)% and 94.32 (±1.70)%, in the absence and presence of HUVECs, respectively. HUVECs non-viability level was significantly lower. Experimental analysis and results are discussed thoroughly in Chapter IV.

Aim 3: Design a bioreactor to mimic the bone marrow microenvironment, and study the latter's effect on the proposed treatment. Due to the complexity of the biological microenvironment, it is very challenging to experimentally study certain effects of that microenvironment on the delivery system. A cost- and time- effective model was developed to predict these effects. Since liposomes are proposed to be injected intravenously, the main challenge would be predicting the release profile of locally-administered micro-fibers in the bone marrow. In order to understand the

various physical effects in the bone marrow microenvironment on the release of resveratrol from single fibers, a mathematical model is developed using COMSOL Multiphysics. This design included a cylindrical bioreactor, where inner walls were modified with fiber release of resveratrol. The model was used to test several variables, such as blood perfusion rate, cellular uptake, and the length of the reactor, on the release profile. Results showed that the release kinetics are diffusion-dominated. Cellular uptake was found to be the main variable affecting the release profile. The model parameters were obtained from literature, and in-house performed experiments, for which the stability of resveratrol under various conditions was established, aligning with that in literature. The model was successfully validated by performing a flow system experiment, under matching conditions such as temperature and flow rate, and analyzing the release of resveratrol using HPLC. To further develop the model to mimic the actual bone marrow microenvironment, an outer porous layer was added, showing similar simulation results. These results are presented in Chapter V.

Broader Impact: The proposed treatment can be applied to different types of cancer. The proposed two molecules interact additively to inhibit certain cellular pathways leading to apoptosis. The delivery systems allow the controlled release of each drug and can be introduced locally. The mathematical model is a powerful tool to predict certain effects of the extracellular environment. This can be useful in other application based on the selected system-specific parameters.

CHAPTER II

BACKGROUND

2.1 Single and multi-drug treatment for leukemia

Various drugs are investigated for the treatment of leukemia, these drugs are tested individually and in combination as shown in **Table 2.1**. BCR-ABL is a fusion gene found in most patients with CML. BCR-ABL protein downregulation by siRNA showed a reduction in the corresponding mRNA and early and late-stage apoptosis. It has been shown that 84% protein suppression can be achieved (no concentration specified for that suppression level, however, 50 nM and 100 nM are recommended) [10].

Myricetin, a small molecule inhibitor has shown high inhibition activity of the enzyme (hIMPDH1) [11]. That enzyme is partially localized in the nucleus of CML derived cells, or K562 cells (**Figure 2.1**). It promotes cell growth by controlling the guanine nucleotide pool size [12]. It has been shown that Myricetin Inhibition % of that enzyme reaches 64.78%, with IC_{50} of 6.98 ± 0.22 µM. In comparison, other small molecule inhibitors only caused less than 25% inhibition with IC_{50} of >30 µM [11]. The clinical potential of Myricetin has not been explored, therefore, side effects are not known.

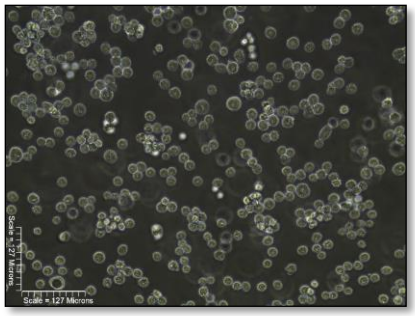

Figure 2.1: Microscopic image of K562 cell culture (72 hours of incubation).

Imatinib is a tyrosine-kinase (BCR-ABL) inhibitor that is used in CML (chronic myeloid leukemia) chemotherapy (3 µM lowers cell metabolism to around 20%) [13]. Imatinib is FDA approved and has passed clinical trials, it is used for CML treatment. Reported side effects include: mild to moderate nausea, myalgias, edema, fatigue, dyspepsia, diarrhea, and skin reaction. These side effects occur in less than 10% of CML patients. [14]. More occurring side effects include ocular, such as abnormal vision and intraocular pressure (Imatinib dosage is 400 mg/day – 800 mg/day) [14]. The side effect is also more occurring as skin reactions, including superficial edema (48-65% of cases treated), and macular-papular eruption (~67% of cases treated) [15]. ABL drug-related mutation has also been reported [13].

PPP2R5C pathway downregulation was studied using PPP2R5C-siRNA which drops the expression levels of PPP2R5C mRNA and protein to less than 15% [16].

Mithramycin is shown to inhibit the regulatory associated protein of mTOR - raptor (which regulates other downstream targets including kinases). Relative expression % of raptor dropped to 25% (cells were treated with 30 nM) [17]. However, mithramycin inhibition effect on K562 cells has been studied over the past two decades [18]. On the clinical level, it has only been shown effective on solid tumors [19]. Hence, it's expected to be a feasible option for this study.

As K562 cells are known to be TRAIL-resistant, it's been shown that this resistance can be suppressed using siRNA or Amurensin G to inhibit cell growth and cause apoptosis. The cytotoxicity

effect of TRAIL is induced through SIRT1 downregulation which leads to cell death. It's been shown that cell apoptosis reached roughly 22% when treated with SIRT1 siRNA, and 25 ng/ml of TRAIL, while that percentage is roughly 27% when treated with Amurensin G and 25 ng/ml of TRAIL [20].

Rilmenidine proliferation suppression effect has also been studied. Rilmenidine is a selective imidazoline I1 receptor agonist, that downregulates BCR-ABL pathway upon binding. It's been shown that the percentage of the apoptotic cells increased from 20%, using rilmenidine alone, to 42% when used synergistically with doxorubicin [21].

VEGF (Vascular Endothelial Growth Factor) has been frequently targeted to inhibit the growth of solid tumors. One study shows that VEGF is also expressed in leukemia cells. It's been shown that antisense-VEGF can be used to downregulate the expression of endogenous VEGF which lead to roughly 10% cell apoptosis [22].

Polyphyllin D, a compound derived from *Paris polyphylla rhizome* (Chinese herb), showed inhibitory activity on K562. It was shown that the IC_{50} is 0.8 μM for an inhibition percentage of around 90%. Induction of apoptosis takes place via the mitochondrial apoptotic pathway, through downregulation of BCR-ABL expression levels. Apoptosis of K562 was shown to be 25% using 0.8 μM. The suppression levels of BCR-ABL is 40%, while that of Bcl-2 is 85% [23].

Gallic acid has also been used to inhibit K562 growth. Gallic acid inhibits cell line growth by downregulation of COX-2, inhibition of BCR/ABL kinase, and NF-KB inactivation. Growth inhibition of K562 is gallic acid concentration dependent, where 10 μM causes around 15%, while 75 μM causes around 80% inhibition [24].

Some inhibitors resulted in high levels of mRNA/protein suppression, with noticeably low apoptosis levels. It is also noticed, apart from resveratrol, that only synergistic effect of Rilmenidine and doxorubicin resulted in 42% cell apoptosis, while all other inhibitors resulted in less 30%. These

results suggest that despite inhibiting certain pathways with high percentage, cells can still survive by undergoing alternative pathways, hence low apoptosis level is obtained. This suggests using a dual effect of siRNA with another inhibitor to achieve higher apoptosis level.

Resveratrol showed both high inhibition and apoptosis rates [25]. It inhibits the Sphingosine kinase 1 enzyme (SPHK1). This enzyme catalyzes the formation of Sphingosine-1-phosphate (S1P), which is mainly involved in regulating proliferation and survival. This study shows that the inhibition rate of K562 by resveratrol (using MTT assay and ELISA kit) reaches around 63% with a concentration of 40 µM. Apoptosis rate with the same concentration reaches 58.28% [25].

Many drugs have been investigated for their potential in treating cancer. It is inferred that a combination of multiple drugs gives higher cancer cell death levels. Although combination therapies tackle different cellular pathways in cancer or amplify the outcome of a single target, off-site targeting, and high dosing, are associated with problems. To address those, delivery devices are designed.

Table 2.1: Single and combination drugs investigated in leukemia treatment.

Inhibitor	**Target**	**Protein/mRNA suppression**	**Cell apoptosis**	**Mwt (g/mol)**	**Reference**
siRNA	BCR-ABL	84% protein suppression	-	13,300 (average)	[10]
Imatinib	BCR-ABL	80% cell metabolism suppression	-	493.603	[13]
Rilmenidine	BCR-ABL	-	20% cell apoptosis	180.251	[21]
Rilmenidine + doxorubicin	BCR-ABL	-	42% cell apoptosis	180.251 + 543.52	[21]
Gallic acid	BCR-ABL + COX-2 + NF-ƙB	80% growth inhibition	-	170.12	[24]

Myricetin	hIMPDH1	64.78% inhibition	-	318.2351	[11]
siRNA	PPP2R5C	85% suppression of mRNA expression		13,300	[16]
Polyphyllin D	Bcl-2	85% protein suppression	25% cell apoptosis	855.021	[23]
Mithramycin	Raptor (mTOR)	75% suppression of protein expression	-	1085.15	[18]
SIRT1 siRNA + TRAIL	SIRT1	-	≈22% cell apoptosis	120 kDa + 32,509 Da	[20]
Amurensin G + TRAIL	SIRT1	-	≈27% cell apoptosis	534.514 + 32,509	[20]
Antisense VEGF	VEGF	-	≈10% cell apoptosis	38,200	[22]
Resveratrol	SPHK1	63% inhibition	58.28% apoptotic cells	228.247	[25]

2.2 Delivery devices

Drug delivery refers to methods and techniques, developed for the purpose of transferring a certain drug, or multiple drugs, to the site of interest. Further advantages include lowering the required dose to exert an effect on the target and control the release of the drug over a desired period of time. In this review, three main methods of delivery are tackled. Scaffolds, nanoparticles, and electrospun fibers. For purposes of selection, the targeted medium properties, such as porosity, are essential to consider.

2.2.1 Scaffolds for cancer drug delivery

In the field of tissue engineering, highly porous biodegradable scaffolds are utilized to regenerate or repair damaged tissues. Mature cells and stem cells are seeded and allowed to attach to the porous structures. In order to stimulate those cells, stimulants have been sequestered either directly in the scaffold or after encapsulation in nanoparticles in order to influence cellular behavior and

create a heterogeneous environment. Similar notion has been extended for delivering molecules for cancer therapy. For example, the microenvironment and cell functionality can be manipulated through local gene delivery from scaffolds [26]. Gene delivery using scaffolds have shown improved control upon expression in promoting the regenerated tissue. Drug release from the scaffold is typically controlled by diffusion and cell migration, which limits control upon drug release. One group has shown that scaffolds with magnetic properties can provide remote control to deliver molecules such as mitoxantrone, plasmid DNA, and chemokines [27].

Biomaterials can also be directed for immunotherapy in treating cancer. A recent review illustrates immune therapies using chimeric antigen receptor (CAR)-T cell therapy, among other immunotherapies, using various biomaterial carriers [28]. This review is not re-iterating the mentioned reference, however, scaffolds can be combined with the reviewed immunotherapies, to provide local immunomodulation. This avoids systemic toxicity and allows lower dosage administration. A recent study has shown that locally delivered cancer drugs from engineered three-dimensional scaffolds, can potentially promote systemic antitumor immunity [29]. These recent studies foresee that immunotherapy has the potential of transforming cancer treatment in the near future. Cancer immunotherapy future lies mainly in combining T cells, and checkpoint inhibitors for tumor suppression [30].

2.2.2 Nanoparticles and ligands in cancer treatment

2.2.2.1 Nanoparticles in cancer treatment

Several types of nanoparticles have been investigated for delivery, mainly liposomes and polymeric nanoparticles (**Figure 3**). A previous study covered the use of polymers in the delivery of siRNA [31]. Small molecule cancer therapeutics problems are associated with pharmacokinetics as well as the delivery method. Using polymers can involve the incorporation of nanoparticles, such as carbon nanotubes, and gold nanoparticles, to enhance drug delivery. Although using polymers is

advantageous due to properties including, safety, and efficacy, surgery is required to remove the non-biodegradable polymer after the drug is released [32]. Delivery of siRNA is the main challenge for this type of cancer therapy. Hence, suggesting an effective delivery system is essential for treatment with the latter method. Nanoparticles are favored due to optimal achievable clearance [33]. Lipid-based nanoparticles delivery of siRNA is preferable to other methods. This potential is mainly based on biocompatibility and low toxicity.

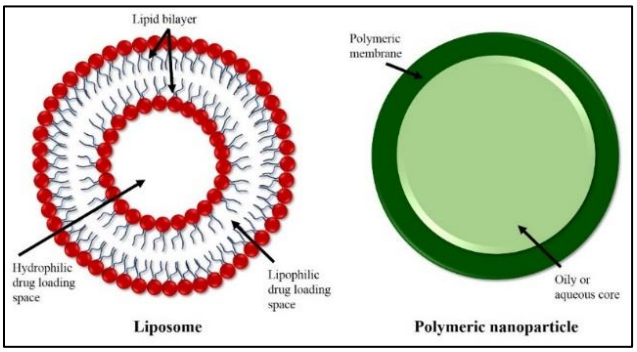

Figure 2.2: Schematic representation of liposomes and polymeric nanoparticles.

Endogenous characteristics of siRNA such as negative charge, rigid structure, size, and stability, make passive diffusion through cell membrane quite challenging. To address this challenge, endocytosis becomes an effective mechanism of delivery that can be achieved using lipid-based nanoparticles. [34]. Lipid-based nanoparticles are mainly delivered by a sub-category of endocytosis called Clathrin Endocytosis. In this method, vascular internalization of particles occurs with the aid of certain proteins, or Catherine, that can induce the formation of vesicles without direct action from the cell membrane [35].

Nanoparticle-based delivery provides various advantages such as increased efficacy, high stability, the ability to encapsulate both hydrophilic and hydrophobic molecules, and administer-ability by multiple methods [36]. Nanoparticles, however, have a relatively limited carrying capacity, compared to electrospun microfibers. Premature rupture of the nanoparticle membrane can lead to unintended off-target release drug release. The former self-assembles, and has a bilayer membrane

structure, while the latter is composed of biodegradable and biocompatible nanostructures. Both types deliver hydrophilic or hydrophobic molecules, while liposomes can deliver both simultaneously by encapsulating each drug in a separate layer. The inner layer of liposomes encapsulates hydrophilic molecules, while the outer layer encapsulates lipophilic molecules. Drugs are dissolved, entrapped or conjugated to the surface of the polymeric nanoparticles [37]. Higher loading efficiencies are typically achieved with liposomes (~95%) [38], [39] compared to polymeric nanoparticles (~90%) [40], [41].

2.2.2.2 Surface functionalization of nanoparticles

Ligand-targeted liposomes have shown great potential in many novel delivery systems, with high *in vivo* response due to their active targeting, increased stealth, and controlled drug release (**Table 2.2**). PEG coating (to overcome rapid clearance from circulation) and ligand attachment (to avoid non-specific binding) are specifically important to overcome the challenges associated with liposomal delivery systems [42].

Certain types of ligands (used for a certain type of cancer) provide higher binding efficiency and several folds decrease in IC_{50} value compared to non-targeted liposomes. Peptides, Lactose, monoclonal antibodies, folate, glucose, and transferrin are among the several ligands provided in the literature. [42]. For example, cancer cell proliferation requires a high intake of iron, hence cancer cells express a high concentration of transferrin receptor [44]. Transferrin and Holo-transferrin ligands have been used in the treatment of human leukemia (K562 cells). The former enhanced intracellular uptake with fivefold decrease in IC_{50} (treated with doxorubicin *in vitro*), while the latter has been used with BCR-ABL siRNA delivery (*in vitro*), and 2.5-folds enhancement in tumor uptake (compared to free Bcl-2-siRNA *in vivo*). Holo-transferrin attachment also showed improved tumor growth inhibition, and higher survival time compared to the non-targeted liposomal system. [42]. Besides several folds over-expression of the transferrin receptor in malignant cells, transferrin

is also expressed in the brain capillary endothelial cells [43]. Accordingly, using transferrin as a targeting tool helps to cross the blood-brain barrier, which is an obstacle in many cases.

Monoclonal antibodies have gained attention in cancer treatment due to overexpression of certain differentiation antigens and growth factors on tumor cells, e.g. epidermal growth factor. Antibodies have several affecting mechanisms on target cells, such as agonist activity upon binding to the surface receptor, induction of immune pathways, or stromal ablation [44]. Folate receptor is over-expressed in many tumor cells, such as ovarian, breast, and lung cancer, among others. This expression is significantly lower in normal cells. Folate activates certain cellular pathways, upon binding to the folate receptor, which eventually acts upon the nucleus, directly affecting transcription [45]. Nucleolin is another recent targeting method for liposomes and other nanoparticles, to deliver drugs such as siRNA and doxorubicin. Nucleolin is a ribonucleoprotein, which is overexpressed in cancer cells and is associated with cell proliferation and apoptosis [46]. It has been shown successful inhibition of tumor growth, with no observed non-specific binding [47].

Table 2.2: Ligands in cancer treatment targeting.

Ligand	**Treatment**	**Target**	**Results**	**References**
Transferrin	Doxorubicin	K562	Fivefold decrease in IC_{50} *in vitro*	[42], [43]
Holo-transferrin	BCR-ABL siRNA	K562	Selective *in vitro* delivery	[42]
Holo-transferrin	Bcl-2 siRNA	K562	2.5-fold enhancement in tumor uptake *in vivo* 80% Bcl-2 siRNA downregulation *in vitro* Tenfold decrease in IC_{50} *in vitro*	[42]
mAB	Bcl-2 siRNA	B-cell lymphoma	Induced apoptosis by immunostimulatory effects	[44]

Folate	Doxorubicin	Human cervical and ovarian lymphoma	Tumor growth inhibition	[45]
Nucleolin	siRNA	MDA-MB-231 breast cancer cells	Inhibit tumor growth	[46], [47]

2.2.3 Electrospun fibers for small molecules delivery

Electrospinning is a versatile polymer processing technique for the production of micro and nano diameter fibers through an electrically charged jet of the polymer solution. Characteristic diameters of the formulated electrospun fiber vary according to electrospinning conditions, such as voltage, and pumping speed. Nano- and microfibers varying from 630 nm to 6 μm in diameter have been formed by varying various solution parameters and processing parameters. Recent advances in electrospinning have facilitated the formation of fibers with desirable structural features such as reenforced core, hollow, porous, multicoated and tri-axial fibers will provide unique features for fabricated fibers. Controlling the fiber size and formation techniques have been extensively reviewed. Readers could refer to those review articles. This wide range of structure-dependent features makes electrospun fibers a good candidate for many applications (**Table 2.3**). Electrospun fibers have provided unprecedented opportunities that were recently applied in the field of cancer diagnosis and therapy.

Electrospun nanofibers and microfibers are employed in the treatment, diagnosis, delivery, and modeling of cancer. These fibers possess numerous properties including; high loading capacity, extremely large surface area, porosity, and high encapsulation efficiency [48]. Once administered in the body, electrospun fibers' degradation, like other properties, depends on their composition. Further information about that and the immune response is found in previous studies [49, 50]. Electrospun nanofibers and microfibers can be modified in terms of morphology and structure to

serve different purposes. Different properties were applied in different applications, those include; single fiber, multiaxial fibers, and surface functionalized fibers. Detecting circulating tumor cells is a challenge due to their low count in the bloodstream. Electrospun fibers have recently been studied as a potential selective cell capturing method, due to their cell adhesion, and high surface area properties. Electrospun polystyrene fibers attached to antibodies were used to detect cancer markers such as; alpha-fetoprotein (AFP), and vascular endothelial growth factor (VEGF) [51]. Ligand conjugated fibers have also been investigated for cancer targeting. For instance, folic acid modified electrospun poly(vinyl alcohol)/polyethyleneimine (PVA/PEI) nanofibers were used to specifically detect cancer cells overexpressing folic acid (FA) receptors such as ovarian and pancreatic cancer [52].

Another application based on the physicochemical properties of the electrospun fibers and their ability to selectively adhere to cancer cells. This property was specifically incorporated in the localized photothermal ablation to tumors. Poly(caprolactone)-based electrospun microfiber scaffold with covalent surface functionalization of graphene oxide (GO) (PCL_{MF}-GO) have enhanced selective cancer cell adhesion and proliferation properties. Graphene oxide can be used to enable localized photothermal eradication due to its near-infrared absorbance ability [53].

Artemisinin, a chemical compound that reacts with iron to produce free radicals, was incorporated in cancer cells treated for free radicals' ability to kill cells. Electrospun core/shell nanofibers were designed for the purposes of targeted delivery and preserve drug bioavailability. Hyperbranched poly(butylene adipate) (HB), which is used as a crystal suppressant for artemisinin, is the core material, and Poly(vinylpyrrolidone) (PVP) is the shell material. This delivery system effectively reduced prostatic cancer cell viability [54]. Mycophenolic acid (MPA) has been approved to inhibit many types of cancer cells growth. MPA degrades quickly due to liver uptake, hence a delivery method is essential to address this issue. Coaxial fibers of poly(ε-caprolactone) (PCL) core loaded

with MPA and PCL shell was used for controlled release of MPA [55]. This fiber system was applied to glioblastoma multiforme (GBM) tumor cells, which indicated strong cell suppression.

In addition to diagnosis, treatment and drug delivery, electrospun fibrous scaffolds (aligned PCL fibers) were employed to mimic the extracellular environment of tumors. A fibrous scaffold with random and aligned orientations was designed to study the three-dimensional structure of the extracellular matrix of breast cancer [56]. Breast cancer cells showed overexpression of transforming growth factor β-1 (TGF β-1), which is attributed to their response to the polymer scaffold. Despite promoting cell growth, it has, nevertheless, been shown that TGF β-1 can trigger cellular responses such as differentiation and apoptosis [57].

Table 2.3: Electrospun fibers in cancer treatment.

Electrospun Fiber	**Application**	**Year**	**Reference**
Polystyrene nanofibers	Cancer markers detection (AFP, CEA, and VEGF)	2013	[51]
PVA/PEI nanofibers	FA overexpressing- cancer cells	2016	[52]
PCL-GO microfibers	Breast cancer adhesion/localized photothermal ablation	2017	[53]
HB/PVP core/shell nanofibers	Artemisinin delivery to a prostatic cancer cell	2017	[54]
PCL/MPA / PCL core/shell fibers	MPA delivery to (GBM) tumor cells	2017	[55]
PCL fibers	Modelling ECM indicated by TGF β-1 overexpression	2011	[56]

Electrospun microfibers (**Figure 2.3**) has the potential to deliver higher doses of nutraceuticals due to their high surface area, and high carrying capacity. Microfibers, however, are associated with the limitation of systemic administration. Since the latter is not possible with this method of delivery, local administration is suggested. Similar to a bone marrow biopsy procedure, or stem cell local administration [58], microfibers can be placed in the bone marrow, for example, to controlla-

bly release and deliver nutraceuticals with therapeutic effects. This procedure requires further investigation, and future research can reveal possible methods for local administration, required amounts microfiber, and dosages of delivered therapeutic. Investigating this approach might be challenging and would require *in vivo* testing, however, local delivery of therapeutic nutraceuticals can sensitize the target cells for further targeted treatment. The latter can be administrated systemically in series with local drug delivery, where cells are primed for the targeted treatment [59].

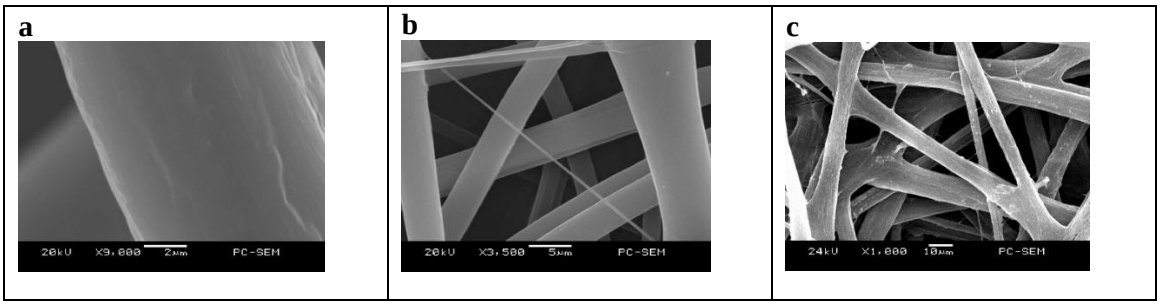

Figure 2.3: Scanning Electron Microscope (SEM) images of electrospun microfibers at different magnifications (a ×9000, b ×3500, and c ×1000).

2.3 Combined drug delivery

This section will discuss the advantages and challenges associated with delivery systems for combination therapy. When selecting a delivery method, a researcher is advised to go through the following steps:

1) Define the target tissue/organ/cells, and have a good understanding of the target microenvironment.

2) Define the chemical and physical properties- such as molecular weight, size, charge, and hydrophilicity.

3) Select the required scale; nanotechnology or Microsystems can be selected based on medical needs, drug loading requirements, and level of release control.

This section provides a comprehensive view that will help in selecting the appropriate delivery method based on recent literature findings.

2.3.1 Multi-drug therapy using a single delivery method

Combinatorial therapy has been explored for its synergistic effect in treating drug-resistant cancers **(Table 4)**. Higher doses can be delivered inducing desired effects, however, the release profile of each drug usually differs, creating further challenges. Controlled release is essential to achieve the required dose of each drug at the site of interest.

Nanoparticles have been used to carry multiple drug payloads. Multiple drugs are incorporated into the delivery vehicle and released in a controlled manner. Lipid bilayer spherical vesicles, or liposomes, are one approach for combination drug delivery. One example is CPX-351 liposome used for leukemia treatment. This liposomal system can be loaded with cytarabine and daunorubicin [60]. Another method is polymeric-nanoparticles which consist of solid polymeric cores. The latter is more suitable for delivering water-insoluble drugs. Polymer-drug conjugates have also been explored. They show enhanced delivery of water-soluble molecules such as paclitaxel, doxorubicin (DOX), and camptothecin. The delivery system improves the pharmacokinetics and efficacy of these drugs [61].

Others have investigated core-shell nanoparticles for combination delivery. For example, tumor necrosis factor-related apoptosis inducing ligand (TRAIL) and DOX have been co-encapsulated into a core-shell nanoparticle, resulting in a synergistic effect by targeting different pathways [62]. Nanoparticles have emerged as promising carriers for multidrug delivery. Small molecule drugs can be co-encapsulated into the same nanoparticle. Both hydrophilic and hydrophobic drugs can

Table 2.4: Combination of treatment delivery for cancer applications.

Delivery method	Loaded drugs	Target	Reference
Polymer drug conjugates	Verapamil, and DOX	Leukemia	[61]
Core-shell nanoparticles	TRAIL and DOX	Lung cancer	[62]
Liposomes	cytarabine/daunorubicin (CPX-351)	Acute Myeloid Leukemia	[60]
Lipid micelles	Hydrophobic inhibitor of transforming growth factor β (TGF-β), and the hydrophilic protein interleukin-2	Tumors and stromal cells	[63]
Liposomal hydrogel scaffolds	Regenerative cells, protein, and growth factor	Implant at the target site	[64]
Co-electrospun nanofibers	BSA and myoglobin	Improve cellular interactions, (cell adhesion, proliferation, and differentiation)	[65]

be encapsulated. The solvent selection process for these drugs is a key requirement for successful encapsulation of different polarity drugs [66]. This delivery method has enhanced the synergy, and pharmacokinetics associated with each drug [67]. Many types of nanoparticles have been explored for their potential in multidrug delivery. Liposomes have been used to deliver and enhance the efficacy of chemotherapy pairs. Lipid micelles have been utilized for their high drug loading capacity and tunable sizes. Also, they have shown promising results in clinical trial phase I for a variety of cancers [63]. Liposomal hydrogel scaffolds have been explored for localized delivery. These scaffolds can be pre-designed outside the body to form its three-dimensional shape to be administrated locally [64]. Others have explored co-electrospun nanofibers for multidrug delivery. A composite system of this delivery method can be formulated for loading multiple drugs, where the system is composed of a mixture of different-drugs-loaded electrospun nanofibers [65].

2.3.2 Multi-drug therapy using multi-delivery methods

Although several combination delivery techniques have been explored, the multi-delivery method has not been thoroughly addressed. Nanocarriers, for example, have been used as a single delivery method for multi-drug delivery [68]. However, using multiple, different, delivery methods can improve the release profiles and time of administration for combination therapy. This method reduces multidrug resistance in cancer cells, attributed to the optimal synergistic effect achieved by sequential administration of each drug. For instance, liposomes can be combined with other types of nanoparticles, such as core-shell nanoparticles, to deliver two or more different drugs. Using this method of delivery introduces better flexibility regarding the time of administration, and control upon the optimal effect on each drug, based on their kinetic profiles (of uptake and release). Nanoparticles co-administration of multiple drugs improve both the uptake and the cytotoxicity of the combination therapy [69]. DOX-encapsulated nanoparticles were administrated in combination with verapamil-encapsulated nanoparticles, inducing higher toxicity effects on NCI/ADR-RES cells compared to the single delivery method [70]. Administration of electrospun fibers, however, remains a challenge. As nanoparticles could be administered intravenously, local administration is suggested for electrospun fibers. This procedure has been explored to promote cartilage regeneration [71]. However, the area of local administration of electrospun fibers for drug release remains nascent.

2.4 Kinetic and parametric modeling of electrospun fibers and nanoparticles

Electrospun fibers delivery is carried out through two main routes: 1) drug release from the fibers and 2) cellular uptake of the drug. Each step includes several factors to be taken into consideration when designing fibers as delivery vehicles. In the first step, the hydrophilicity/lipophilicity of the drug affects its diffusion and permeability as it is released from the fiber. These parameters can be modeled as discussed later in this section. The second step occurs once the drug is released **(Figure 2.4)**, and it is dependent on the drug's chemical nature, and the microenvironment at the target site.

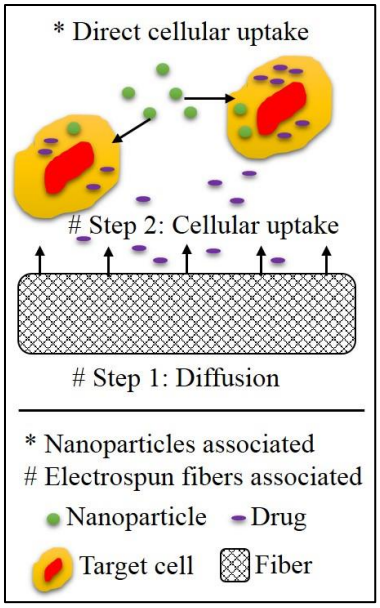

Figure 2.4: Schematic representation of drug release and uptake.

Certain enzymes or side targets cellular uptake may take place and may lead to significant depletion of the drug even if maximum release is reached. Both steps should be taken into account in order to achieve a fully controlled delivery process. As opposed to electrospun fibers, nanoparticles, such as liposomes, are not associated with release rates, but rather uptake rates. Hence, loading efficienc and particle rigidity are more relevant parameters that are introduced in this section.

Electrospun fibers have the potential to deliver various cancer drugs and have a wide range of applications. It is essential to establish a release profile for the electrospun fiber, as the controlled release is achieved through a well-established release model. A previous review [72] has shown various models associated with different types of electrospun fiber. Both lipophilic and hydrophilic molecules have been released from electrospun fibers. It was found that the structure of electrospun microfibers (single, co-axial, or tri-axial) has an effect on releasing hydrophilic molecules, while this effect is negligible when releasing lipophilic molecules [73, 74]. This is attributed to the mass transfer dominating process occurring in each case. Lipophilic drugs are mainly replaced by water molecules resulting in a dominating partition coefficient factor (**Eq. 1**) [75]. This number is a

measure of solubility of molecules in an organic (octanol) versus aqueous (water) solution. The larger the partition coefficient value, the more lipophilic the molecule. Hydrophilic molecules, however, are released by a dominating diffusion factor which can be experimentally determined as given by Fick's law (**Eq. 2**) [76]. The concentration profile can be generated experimentally, and the diffusion coefficient can be determined by the slope of flux versus concentration-distance gradient line. For release from single layer fibers of (1:1 of PCL and GT), the diffusion coefficient is generally > 10^{-10} m^2/hour for lipophilic molecules, and < 10^{-10} m^2/hour for hydrophilic molecules [73], [74].

$$K_c = \frac{C_{octanol}}{C_{water}} \quad (1)$$

$$J = -D_{ab}\frac{dC}{dx} \quad (2)$$

Where K_c is the partition coefficient, J is diffusional flux (given in mol m^{-2} s^{-1}), C is drug's concentration, D_{ab} is the diffusion coefficient, and x is the diffusion path length.

Nanoparticles are also characterized by their rigidity and loading capacity. The diffusion coefficient of nanoparticles depends on the particle's rigidity [77]. It has been shown that soft nanoparticles (10 nm) in polymeric matrices (20 nm) increases their diffusion coefficient. Another study describes rigidity models for nanoparticles [78], where the stiffness factor is given by **Eq. 3**.

$$C_s = \varepsilon\left(\frac{C_a}{C_b}\right)^2 \quad (3)$$

where $C = \sqrt{\frac{E}{\rho}}$ is the one-dimensional speed of sound in the solid, E is the Young's modulus and ρ is the density, a and b refer to the adsorbate and the cantilever, respectively, and ε is a dimensionless parameter. It is shown that the stiffness coefficient for gold nanoparticles is roughly 0.03.

Loading efficiency and capacity, as well as kinetic studies, can be performed on nanoparticles. A recent investigation of the kinetics of polymyxin B (PMB) loading onto anionic mesoporous silica nanoparticles (MSN) is presented in another study [79]. The loading capacity (LC) is given by **Eq. 4**.

$$LC = \frac{(total\ mass\ of\ applied\ PMB - mass\ of\ nonadsobred\ PMB)}{total\ mass\ of\ MSN} \quad (4)$$

Loading capacity depends highly on the particles and drugs chemical and physical nature. Emulsions, for example, result in significantly higher loading capacities compared to suspensions. This is due to drug solubilizing effect by a liquid matrix of particles, compared to that of the solid crystalline matrix. It has been shown that up to 50% higher loading is achieved by emulsions compared to suspensions [80].

CHAPTER III

CONTROLLED RELEASE OF RESVERATROL, IN COMBINATION WITH SIRNA, EFFECT ON LEUKEMIA CELLS VIABILITY

3.1 Introduction

Resveratrol gained significant attention in the early 1990s, consumption of red wine in France was attributed to the low incidence of cardiovascular diseases, despite higher consumption of saturated fat [81]. This was termed "French paradox," and provided significant impetus to exploring resveratrol as a dietary supplement in cardiac and cancer therapies [82, 83]. Molecular mechanisms through which resveratrol mediate such interactions is explored in various disease models, including cancer [84]. *In vitro* studies show that resveratrol induces apoptosis via sphingosine kinase 1 (SphK1) inhibition, which is associated in promoting various types of cancers including CML [85], and prostate cancer [86]. Others have shown that resveratrol causes autophagy in K562 cells, the erythroleukemia cell type commonly used to study CML [87] and the formation of intracellular autophagosomes [88]. Resveratrol is shown to cause changes in mitochondrial activity [89] using tetrazolium salt-based calorimetric assays, which is reduced to formazan.

Clinical trials performed by administering 500 mg of trans-resveratrol showed no significant side effects [90]. Another study with 150 mg/day of trans-resveratrol given to healthy volunteers showed signs of calorie restricted diet effects [91]. However, plasma levels after 30 days were in the nanomolar range, nearly 3 orders of magnitude less than required to cause apoptosis in cancer cells *in vitro*.

Rapid reduction in the bioavailability of resveratrol after systemic administration is attributed to various factors, including biotransformation, short half-life (1-3 hours), rapid uptake by cells, and lipophilic characteristics with limited solubility in water [92, 93]. Metabolism of resveratrol also varies from person to person due to alterations in gut-associated bacteria [94]. In order to obtain therapeutic levels needed for inducing apoptosis, controlled release of trans-resveratrol at the site of interest is necessary. In addition, combining resveratrol with other drugs targeting other cellular pathways could reduce the dosage requirements [95, 96].

Recently, electrospun fibers have emerged as ideal candidates in drug delivery systems, as they offer a better degree of control over the release kinetics relative to competing methods such as nanoparticles [97]. In particular, the formation of multilayered core-shell fibers using multiaxial electrospinning allows sequestering stimulants in different compartments to modulate the release kinetics [98]. Also, one could blend lipophilic polymers, such as poly(ε-caprolactone) (PCL), and hydrophilic polymers, such as gelatin (GT), in various ratios and form fibers. These combinations allow encapsulation of both hydrophilic and lipophilic (or hydrophobic) drugs while providing a high surface to volume ratio, cell attachment, and drug loading. These polymers are also biocompatible and biodegradable i.e., they can be locally implanted with the expectation of complete degradation. However, there is a lack of model-based fundamental understanding of the influence of such layering and polymer selection on the permeability of lipophilic drugs.

In this regard, I first tested the combination effect of resveratrol and small interfering RNA (siRNA), to downregulate the fused breakpoint cluster region (BCR)-Abelson (ABL) tyrosine kinase gene pathway; BCR-ABL deregulation is shown to be sufficient to sustain CML phenotype [99, 100]. Based on the literature reports, resveratrol [85] and siRNA [10] dosage were selected. Combination of resveratrol and siRNA was more effective in inducing apoptosis even at lower doses. Next, I selected 40 μM resveratrol and formed PCL-GT hybrid coaxial fibers using a common solvent and a previously published method [101]. I evaluated the release profile of resveratrol

and its effect on K562 cells. Loading resveratrol into electrospun fibers provided a delivery method needed to obtain dosage levels locally. Evaluation of permeability using resistance in series model showed no dependency on layering, suggesting that the rate of lipophilic drug release is less dependent on various layers.

3.2 Materials and methods

3.2.1 Materials

PCL (80 kDa, Mn = 80,000), Type A gelatin (porcine 300 Bloom), 2,2,2-trifluoroethanol (TFE), Caffeine, propidium iodide (PI) powder, sterile dimethyl sulfoxide (DMSO), and trans-resveratrol were purchased from Sigma-Aldrich (St. Louis, USA). A custom-synthesized BCR-ABL siRNA (5′-GCAGAGUUCAAAAGCCCTT-3′), and a corresponding scrambled siRNA (5'-GCCCCAA-GATATAGGTTCA-3') were purchased from Integrated DNA Technologies (Coralville, IA). Annexin V FITC conjugate was purchased from Thermo Fisher Scientific. K562 cells were purchased from ATCC (Manassas, VA) and cultured in RPMI 1640 medium (Sigma-Aldrich, St. Louis, USA), 2 mM Glutamine, prepared with 10% FBS obtained from ATCC (Manassas, VA).

3.2.2 Cell culture maintenance

K562 cells were cultured in T75 cell culture flasks following the vendor's protocol. In brief, cells were incubated in 5% CO_2/95% air, at 37 °C and culture medium was changed every 3 days by centrifuging cell suspensions for 5 minutes at 840 ×g and 4 °C. The formed cell pellet was re-suspended in 9 mL of fresh culture medium and plated in a fresh T75 flask. All cultures were routinely monitored under an Evos™ AME-i2111 Digital Inverted Microscope, and when necessary, phase contrast micrographs were obtained at random locations.

3.2.3 Resveratrol and siRNA dosage effect in solution

For all experiments, cells were harvested, counted using the hemocytometer, and 2×10^5 cells/mL were cultured in a 6-well plate with 2 mL of fresh media for each well. All cell cultures were incubated for 72 hours prior to analysis for viability as described in cell viability section.

Resveratrol alone: A 40 mM stock solution of resveratrol was dissolved in DMSO and stored at 4 ^{o}C until further use. Based on a previously published report [85], samples were prepared with 0, 10, 20, 40, 80, and 160 µM resveratrol concentrations. Zero concentration condition had DMSO equivalent to that present in 160 µM resveratrol condition, added directly.

siRNA alone: A stock solution of 625 nM siRNA in 150 mM NaCl was prepared. Based on a previously published report [10], samples were prepared with 0, 12, 24, 36, 48, and 60 nM range of siRNA concentration. Zero concentration condition contained NaCl equivalent to that present in 60 nM siRNA condition, was added directly. Scrambled siRNA was tested at 36 nM concentration.

Resveratrol and siRNA combination experiments: Three conditions were used based on a factorial design of experimental approach:

i) 40 µM resveratrol and 36 nM siRNA.

ii) mid-point concentrations using 20 µM resveratrol, and 18 nM siRNA

iii) Control samples were prepared by directly adding DMSO and NaCl solution equivalent to that present in 40 µM resveratrol solution and 36 nM siRNA solution.

3.2.4 Cell viability analysis

After various incubation times, cells were centrifuged at 840 ×g for 5 minutes, and washed with phosphate buffer solution (PBS, 7.2 pH, prepared in-house using 8 g NaCl, 0.2 g KCl, 0.2 g

KH_2PO_4, and 2.17 g Na_2HPO_4-$7H_2O$ in 975 mL DI water) with 0.1% BSA (1 mL for every 2×10^5 cells). Then cells were stained with Annexin V buffer, using the vendor's protocol. In brief, cells were centrifuged again and washed with Annexin V buffer solution (140 mM NaCl, 4 mM KCl, 0.75 mM $MgCl_2$ and 10 mM HEPES in DI water). Cells were centrifuged and re-suspended in Annexin V buffer solution (50 µL per 10^5 cells). Then, 1 µL per10^5 cells of Annexin V FITC conjugate were added and incubated on ice for 15 minutes. Also, 50 µL per 10^5 cells of Annexin V buffer was added, followed by 4 µL of PI (100 mg/L), and then incubated in ice for another 15 minutes. Cells were washed with 500 µL of Annexin V buffer solution, and the suspension was then discarded. The cells pellet was re-suspended in 500 µL of Annexin V buffer solution and incubated on ice for 10 minutes before samples were analyzed using a FACSCalibur (Becton Dickinson, San Jose, CA) flow cytometer. Unstained samples and individually stained samples were used as controls. Obtained data for each sample was plotted in dot plots, where the cell populations separate into at least two groups: live cells with a low level of fluorescence and non-viable cells with substantially higher fluorescence intensity. Dead cells were labeled with both the PI and Annexin V conjugate. Based on this information, percentages of dead cells were obtained using a standard quadrant analysis.

3.2.5 Stability of resveratrol in culture medium

In order to understand the changes in resveratrol concentration during 3-day incubation, cell culture experiments were performed in 6-well plates in two groups: i) with 2×10^5 K562 cells/mL cells and ii) without cells, but with the same amount of cell culture medium. In both groups, 40 µM resveratrol was added to the culture medium using the same stock solution used in viability. All conditions were incubated in 5% CO_2, and 37 °C. From each group, the culture medium was collected every 24 hours and analyzed for resveratrol content using HPLC. Samples with cells were centrifuged at 840×g to remove the cells. Resveratrol concentration (released drug) was measured using an

HPLC, using a previously reported method with minor modifications [102]. In brief, a 4.6 × 150 mm C18 column (Acclaim, National Scientific Rockwood, TN) was used, with a 5 µm particle diameter, and a 120 Å pore size. A 4.6 × 10 mm C18 guard column with a 5 µm particle diameter (Acclaim, National Scientific Rockwood, TN Guard Cartridge, and Cartridge Holder) was also used. The mobile phase consisting of 30% acetonitrile, and 70% 25 mM sodium phosphate mono-basic at pH 4.0 was prepared using HPLC grade chemicals. Mobile phase flow rate was set at 4 mL/min, and the injection volume was set to 25 µL. Caffeine was used as the internal standard. Resveratrol samples were dissolved in the mobile phase, while the internal standard was dissolved in methanol, and a ratio of 2:1 of resveratrol to internal standard was used. HPLC system was controlled using Chromeleon software (version 6.8 Dionex Sunnyvale, CA). A calibration curve was also prepared (in the range of 0 to 160 µM) similarly, using known resveratrol concentrations.

For each group, at least three samples were used. Obtained data at different time points were plotted as an average (± standard deviation) and curve fitted to understand the kinetic behavior.

3.2.6 Preparation of electrospun fibers with resveratrol

Based on prior studies [103], 10 and 17 wt% concentrations of PCL and GT, respectively, were dissolved independently in the common TFE solvent. All solutions were stirred for 24 hours. Then 1:1 (volume basis) ratio of PCL and GT solutions were mixed together prior to electrospinning. Electrospinning was performed using the methodology described previously, with minor modifications [101]. In brief, setup (**Figure 3.1a**) consisted of two syringe pumps (74900 series, Cole-Parmer, Vernon Hills, IL), coaxial needles, syringes, high voltage power supply (ES30P-5W/DAM, Gamma High Voltage Research, Ormond Beach, FL), earth grounding, and a collection mandrel. Solutions were loaded into a 10 mL syringe and fed to a spinneret held at 17 kV. Core needle inner diameter was 0.4 mm while the shell inner diameter was 1.00 mm. Syringes were connected to the spinneret via 30 cm long 20-gauge PTFE tubing (Sigma Aldrich, St. Louis, MO). Core solution

was pumped independently at 1 mL/h, while the shell solution was pumped at 3 mL/h. Electrospinning was performed in low humid conditions (<50%) at 22 °C. The distance between the collector plate and the spinneret was 15 cm. A collector plate made of aluminum foil wrapped around a 6-well tissue culture plate was used as described previously [104]. In order to improve the handling of the prepared structures, circular voids were created in the collector plate that corresponded to a diameter suitable to fit a 6-well plate. The amount of resveratrol added to the fiber preparation was based on correlating the well area (35 mm diameter) to the volume of resveratrol added. These calculations showed that 2 µL of 40 mM resveratrol stock solution was needed for each well, i.e., 12 µL per 2 mL of fiber solution when collected on a 6-well plate. Since fibers were deposited in areas around the circular void (~ 38% of the total solution), the amount of resveratrol added was proportionally increased. Hence, 16.56 µL of 40 mM resveratrol stock solution was loaded into 2 mL of core fiber solutions.

Then setup was configured to form fibers in four configurations as follows:

i) *Control*: With an outer PCL-GT and an inner core of PCL-GT without resveratrol (**Figure 3.1b**)

ii) Single: Only one stream of PCL-GT with resveratrol (**Figure 3.1c**)

iii) Co-Single: With an outer PCL-GT and an inner core of PCL-GT containing resveratrol, providing a single phase (**Figure 3.1d**), but loading resveratrol in the core increased the distance the drug has to travel.

iv) Co-PCL: With an outer PCL-GT and an inner core of PCL containing resveratrol (**Figure 3.1e**), as PCL core allows evaluating resveratrol release from a hydrophobic polymer, which is compatible with hydrophobic (or lipophilic) resveratrol.

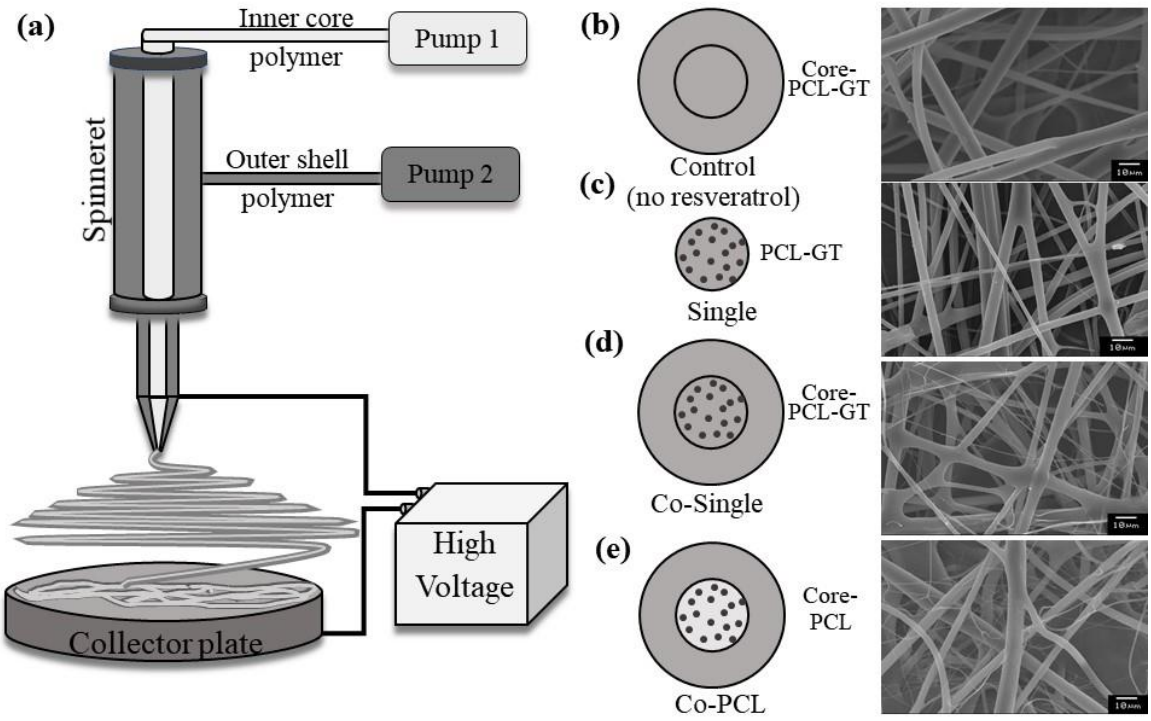

Figure 3.1: Resveratrol loaded electrospun fibers formation (a) Schematic of coaxial electrospinning showing various components. (b) Control configuration showing coaxial PCL-GT fiber with PCL-GT inner core and no resveratrol schematic and corresponding micrograph. (c) Single PCL-GT fiber with resveratrol schematic and corresponding micrograph. (d) Coaxial PCL-GT fiber with PCL-GT inner core with resveratrol schematic and corresponding micrograph. (e) Coaxial PCL-GT fiber with PCL inner core with resveratrol schematic and corresponding micrograph. Small circles within the inner core represent resveratrol.

3.2.7 Fiber characterization

Dry fibers from all configurations were analyzed using a scanning electron microscope (SEM) (Jeol JOEL 6360USA Inc., Peabody, MA), similar to a previous publication [104]. In brief, samples were cut into 2-mm strips, attached to an aluminum stub using double-sided conductive tape, and sputter-coated with gold for 1 min to make the samples conductive. Samples were visualized at 24 kV accelerating voltage, and 1000× magnification. Using the digital micrographs in ImageJ, fiber size and porosity were analyzed, similar to a previous publication [101].

In order to determine the initial loading of resveratrol, it was selectively extracted from each fiber configuration using 30% acetonitrile, and 70% 25 mM sodium phosphate mono-basic at pH 4.0. Samples were incubated for 48 hours at room temperature, where the containers were completely wrapped using parafilm. Samples were collected while ensuring there were no fiber components prior to analysis using HPLC as described above.

3.2.8 *In vitro* release of resveratrol

PCL-GT electrospun fibers from all four configurations were cut to the circular area (35 mm in diameter) formed at each well of the void collector plate. Fibers were sterilized before introduction to cell culture using the following process: 2 mL of 100% ethanol was added to each well for 25 minutes. Ethanol was removed, sterile PBS was added for 20 minutes, which was replaced by 2 mL of fresh medium. Then, the medium was removed, and fibers were kept under UV for 1 hour inside a biosafety cabinet. Then, 2 mL of 2×10^5 K562 cells/mL solution was added to each well and incubated in 5% CO_2, and 37 °C. After 1, 4, 9, 24, 26, 48, 72 and 96 hours of incubation, 25 µL samples were collected from each condition. Each sample was centrifuged at 840×g to remove the cells, resveratrol concentration was determined using the HPLC method as described above. For each group, at least three samples were used. Obtained data at different incubation times were plotted as an average (± standard deviation) and curve fitted to understand release behavior.

In order to determine cell viability, additional experiments were performed where they were terminated at day 3, day 5 and day 8. For each day, at least three samples were used. Cells were collected at these time points and viability was determined using Annexin V and PI staining as described above.

Cell cultures were also performed using fibers and siRNA at 36 nM concentration added directly to the cell culture. These cultures were terminated at day 3. Cells were collected at these time points and viability was determined using Annexin V and PI staining as described above

The cell-containing samples were fixed in 3.7% formaldehyde for 30 min at room temperature, washed with ethanol, and stored in the desiccator for 48 hours, prior to sputter coating with gold at 40 mA for SEM analysis.

3.2.9 Statistical Analysis

All experiments were repeated three or more times. Average values along with standard deviation were calculated. Significant differences between two groups were evaluated using a one-way analysis of variance (ANOVA) with a 98% confidence interval. When $P < 0.02$, differences were considered to be statistically significant.

3.2.10 Modeling resveratrol permeability in PCL-GT fibers

In order to determine the permeability of resveratrol through different layers of coaxial PCL-GT fibers, the model described in the previous publication [101] was used with minor modifications. In brief, based on model studies using the Korsmeyer-Peppas power-law model [105, 106, 107], drug release from PCL-GT fibers was assumed to obey Fickian diffusion, given by:

$$\frac{dC_{Res,0}}{dt} = \frac{PS}{V}(C_{Matrix} - C_{Res,0}) \qquad (5)$$

where S is the total surface area of the matrix (7479 mm^2), and V is the total volume (2000 mm^3) of the RPMI medium used to incubate the matrix, C_{Matrix} is the resveratrol concentration in the matrix, and $C_{Res,0}$ is the actual resveratrol concentration in the solution prior to decay. In order to calculate C_{Matrix}, volume of solids in the matrix was calculated using the fiber fraction (ϕ) and the sample volume. Then, C_{Matrix} was obtained by dividing resveratrol content by the volume of solids.

Using the initial boundary condition when $t = 0$, $C_{Res,0} = 0$, integrating **Eq. 5** gives **Eq.6**:

$$\ln\left(\frac{C_{Matrix}-C_{Res,0}}{C_{Matrix}}\right) = -P\frac{tS}{V} \quad (6)$$

From the obtained concentrations at various times, $\ln(1-\frac{C_{Res,0}}{C_{Matrix}})$ was calculated. Using a linear fit, overall permeability (μm/h) for each configuration was calculated based on the slope value. In order to test the effectiveness of multiple layers on permeability, overall resistance (inverse of overall permeability) to the transport of resveratrol can be considered as the sum of the resistances (inverse of individual permeability) from individual layers. This is given by **Eq. 7**:

$$\frac{1}{P_{overall}} = \frac{1}{P_{\frac{PCL}{GT sheath}}} + \frac{1}{P_{core}} \quad (7)$$

Assuming that the Permeability of single PCL/GT fiber remains the same in the outer sheath in coaxial fibers as the concentrations of polymers and flow rates were identical, the resistance of the inner core was calculated for different configurations.

3.3 Results

3.3.1 Effect of resveratrol and siRNA on K562 cells in cell culture medium

Based on literature reports regarding the effect of resveratrol concentration added directly to the cell culture medium [85], first I investigated that effect on K562 cells viability. These results (**Figure 3.2a**) showed that when resveratrol is added directly to the cell culture medium, it induces K562 cell death in a dose-dependent manner, in agreement with published reports [85]. However, MTT assay was used in that study, rather than Annexin V and PI. Cell death can be caused by either apoptosis or necrosis (death due to cell damage). Annexin V binds to the outer membrane of the apoptotic cells and to the inner membrane of necrotic cells. In contrast, PI binds to the nucleus of necrotic cells only as it cannot permeate through an intact cell wall. From Annexin V staining, 50.35(±5.88)% of cells were non-viable with resveratrol concentration of 40 μM. All cultures showed a significantly higher percentage of non-viable cells relative to control (with

DMSO), suggesting that the observed cell death is not due to DMSO solvent used in resveratrol. Both Annexin V and PI stained populations showed similar percentages, suggesting that cell death is primarily mediated via necrosis when directly treated with resveratrol. To my knowledge, the difference between apoptotic and necrotic effects of resveratrol on K562 cell line has not been reported.

Using formazan reduction assay, siRNA targeting BCR-ABL pathway is shown to induce K562 cell death when added directly to the culture medium [10]. Similar results were observed with Annexin V staining in a dose-dependent manner. These were significantly higher than the control sample, suggesting that these interactions are not due to NaCl present in the buffer used for siRNA. Further, the presence of scrambled siRNA showed significantly lower non-viable cell percentages at similar concentrations, confirming the specificity of the siRNA. However, PI stained non-viable cells were significantly lower than the Annexin V stained population (**Figure 3.2b**), suggesting that siRNA induced cell death is primarily mediated by apoptosis.

In order to understand whether a combination of resveratrol and siRNA act synergistically or antagonistically, cells were exposed to a combination of 40 μM resveratrol and 36 nM siRNA. These results (**Figure 3.2c**) showed that the combination was more potent than the highest concentration of siRNA, and nearly that of the highest concentration of resveratrol. These increases are not due to the DMSO and NaCl as the control samples showed significantly less non-viable cells. Combining both molecules had an additive effect on cell death; 72 (±2.9) % cells (25 (±1.8) % midpoint) were apoptotic and/or necrotic under these conditions. When both siRNA and resveratrol were added together, the necrosis level dropped, compared to that observed when using individual drugs separately (indicated by PI stain). Thus, apoptosis mechanism could be triggered when using combination therapy. By inducing necrosis, the internal compartments of the cell spread out affecting the surrounding environment, hence, inducing apoptosis is more desirable.

In order to optimize the concentrations of resveratrol and siRNA on apoptosis, experiments were designed via 2^3 full-factorial Central Composite Design, in which three experimental levels (i.e., concentrations) were tested for each factor (i.e., the resveratrol and siRNA). A multiple linear regression model was fitted to the experimentally obtained non-viable data points using the regression function in Microsoft Excel. A seven-parameter model was used as shown in **Eq. 8**:

$$NV_{K562} = \alpha_0 + \alpha_1 C_{Res} + \alpha_2 C_{siRNA} + \alpha_3 {C_{Res}}^2 + \alpha_4 {C_{Res}}^2 C_{siRNA} \quad (8)$$

Where NV_{K562} is non-viable K562 cell count, the α parameters are the regression coefficients estimated from the factorial design, C_{Res} and C_{siRNA}, are resveratrol and siRNA concentration in medium, respectively. Using MS Excel® output, a relation between non-viable cells percentage and the concentrations of resveratrol and siRNA was found to be as shown in **Eq. 9**:

$$NV_{K562} = 14.31 + 0.62\, C_{Res} + 0.83\, C_{siRNA} - 4.65 \times 10^{-3}\, {C_{Res}}^2 + 1.31 \times 10^{-4} {C_{Res}}^2 C_{siRNA} \quad (9)$$

Using Eq. 9, a surface plot showing the effect of resveratrol concentration and siRNA concentration was generated (**Figure 3.2d)**. The intent was to understand the required dosages of resveratrol and siRNA to obtain 100% non-viable cells. The surface plot shows several combinations of resveratrol and siRNA concentrations. Predicted values using the optimization equation were evaluated using several experimental measurements. These results showed 5 to 10% error in model predicated non-viability values, suggesting that the model is valid.

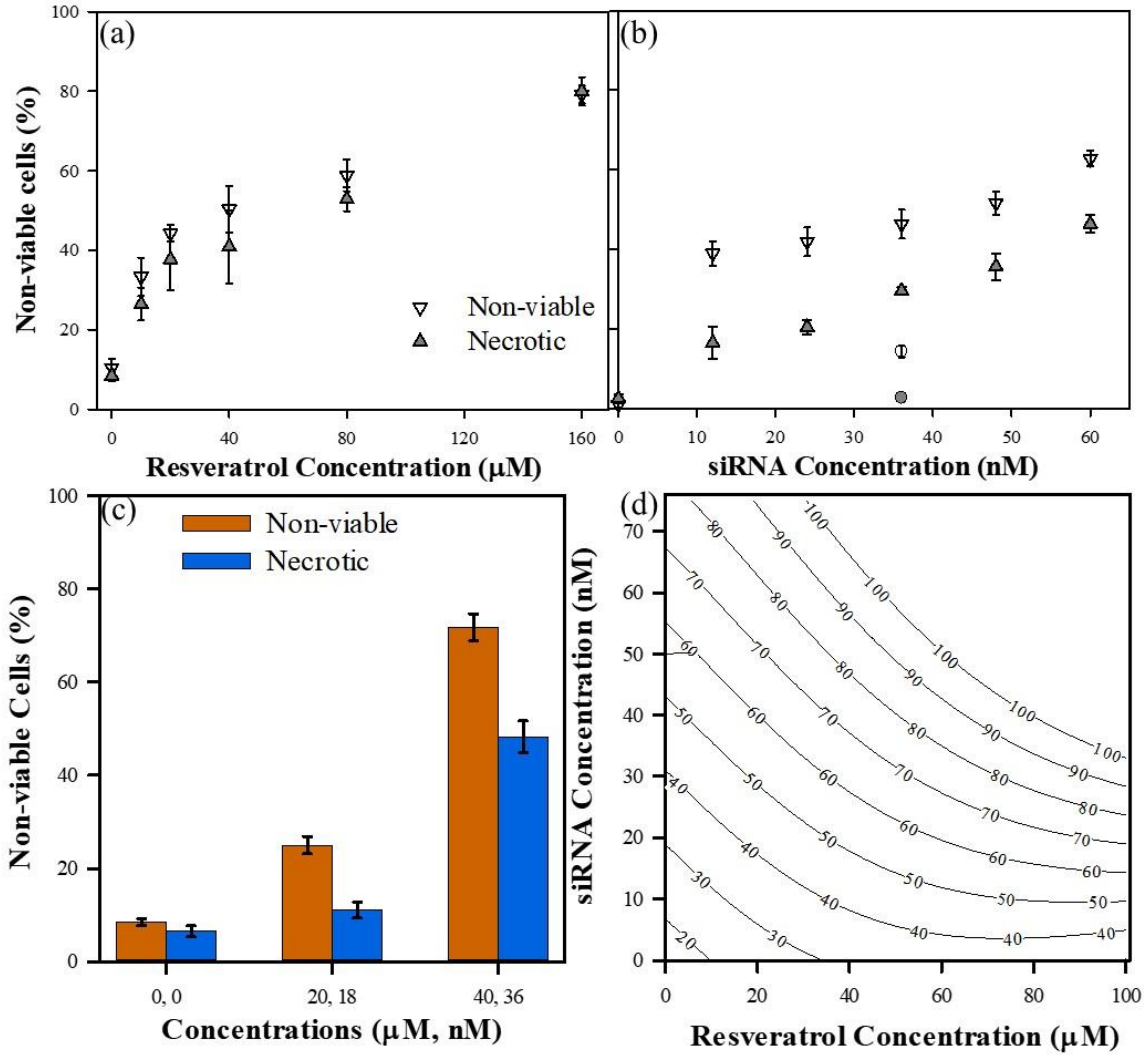

Figure 3.2: **Influence of resveratrol and siRNA on K562 cell viability after 72 hours**. (a) Effect of resveratrol concentration. Control corresponds to cell culture without resveratrol but with DMSO equivalent to that in 160 μM resveratrol (b) Effect of siRNA concentration. Circular symbols correspond to the scrambled siRNA and control corresponds to cell culture without siRNA but with NaCl present in 60 nM siRNA concentration. (c) Effect of combination of resveratrol and siRNA. Control corresponds to cell culture with DMSO corresponding to that present in 40 μM resveratrol and NaCl present in 36 nM siRNA concentration. (d) Surface plot obtained using the factorial design of experiments equation showing the dosages of combination therapy need to obtain various level of non-viable cell percentage.

In order to confirm cell death via different approaches, digital micrographs were acquired during the culture duration of 3 days (**Figure 3.3**). These results showed the presence of necrotic cells in resveratrol-containing cultures, indicated by cell membrane damage, and cell content leakage.

Smaller fragments were formed replacing the circular shaped cells indicating apoptosis. More importantly, the number of cells was significantly less in these cultures, relative to cultures not treated with resveratrol (control) but containing a similar amount of DMSO. The latter showed a significantly higher number of K562 cells. This confirmed cell death caused by resveratrol.

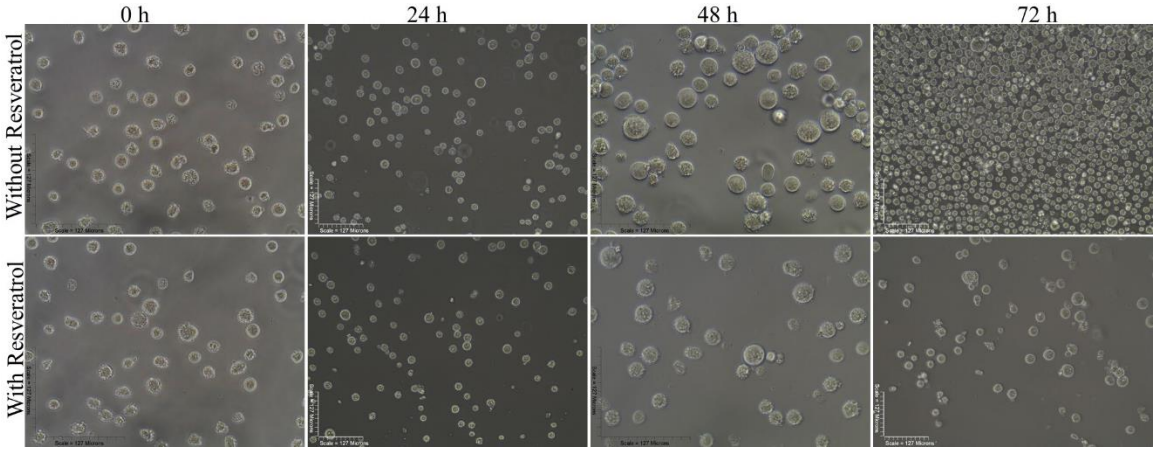

Figure 3.3: Effect of resveratrol on K562 cell morphology. Micrographs were taken every 24 hours, in both with 40 μM resveratrol and without resveratrol, with the same amount of NaCl.

3.3.2 Fate of resveratrol in cell culture medium

In order to understand the fate of resveratrol during the 3-day cell culture duration, samples were analyzed using HPLC. A calibration curve was developed (**Figure 3.4a**) using the internal standard caffeine. In the presence of K562 cells, resveratrol concentration showed a linear reduction (**Figure 3.4b**). Resveratrol was not detectable in a 72-hour sample. In order to predict the depletion time, the linear fit equation was extrapolated (dashed line) to determine the x-intercept, the required time to reach zero concentration. This gave a value of 70.4 hours, confirming the observed complete depletion of resveratrol at 72 hr.

Since drug clearance typically follows a non-linear decay in a single compartment such as cell cultures, a linear depletion of resveratrol could be due to the diffusion of resveratrol into the cells

i.e., direct uptake by cells. Others have shown that resveratrol uptake by K562 cells is mediated via binding to lipoproteins and albumin found in cell culture medium [108]. In order to understand the stability of resveratrol in the cell culture environment, experiments were performed in the absence of cells. These results showed an exponential decay curve, much slower than in the presence of cells (**Figure 3.4c).** To find the decay rate, k_D, resveratrol concentration at different points in time t, was related to the initial concentration $C_{Res,0}$ (when $t = 0$), using a first order exponential decay rate as shown in **Eq. 10**:

$$\frac{C_{Res}}{C_{Res,0}} = e^{-k_D t} \qquad (10)$$

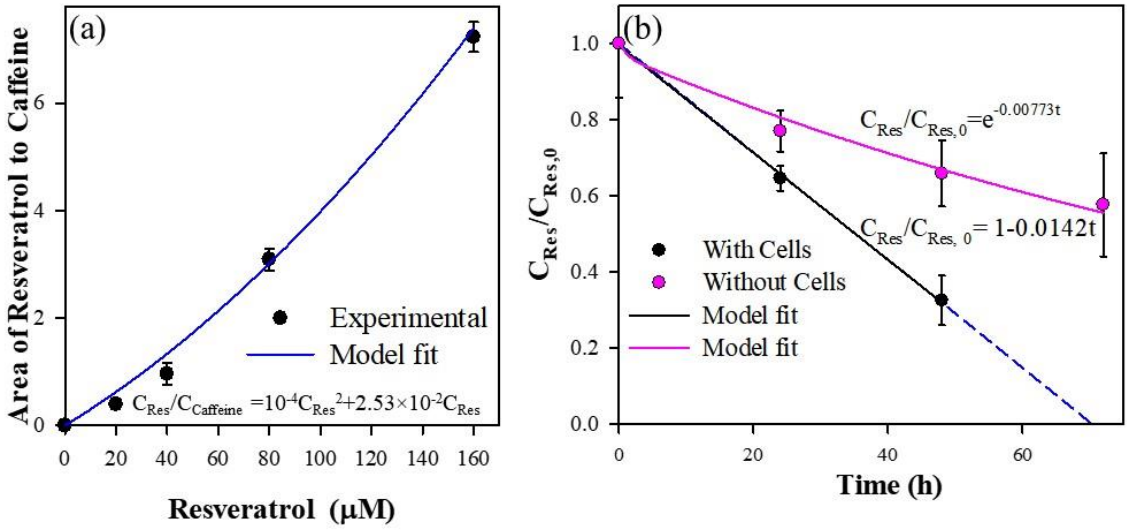

Figure 3.4: Resveratrol characterization and stability in the medium. (a) Calibration curve using HPLC. (b) Resveratrol concentration change in cultures with and without K562 cells incubated at 37 °C and 5% CO_2. Values are plotted as a fraction of the initial dosage $C_{res,0}$ of 40 μM resveratrol. The dashed line corresponds to the extrapolated trend line obtained using the shown linear equation.

Experimental data were fitted with an exponential function to obtain k_D values. Using the k_D value and the relation $t_{\frac{1}{2}} = \frac{\ln(2)}{k_D}$, the half-life of resveratrol in medium the was calculated to be 89.6 hours in the cell culture, much longer than that reported in the plasma [92]. These differences could

further explain the lack of achieving a high concentration of resveratrol even with 500 mg dosage per day *in vivo* [93].

3.3.3 Resveratrol loaded fibers characteristics

Based on the stability of directly added resveratrol in the cell culture medium, I questioned the possibility of encapsulating resveratrol in PCL-GT electrospun fibers. Since these fibers have to interact with cells, all formed fibers had the same PCL-GT outer layer, in order to eliminate different cell-polymer interactions at the surface. However, resveratrol is a lipophilic molecule and requires appropriate polymer selection for uniform distribution. Hence, two inner core conditions were selected in co-axial fibers: i) inner hydrophobic PCL layer with resveratrol and ii) inner PCL-GT layer with resveratrol providing a continuous phase in the fiber which could minimize interfacial resistance during the transfer of resveratrol while providing a medium for uniform distribution of resveratrol. Since hydrophilic GT environment is not compatible with loading lipophilic resveratrol, I did not consider forming coaxial fibers with PCL-GT and GT as the inner core. In order to compare the effect of controlled release of resveratrol, a 40 μM concentration of resveratrol was used in forming the electrospun fibers.

These results showed successful formation of fibers in all these configurations, without any difficulty. Analyzing SEM micrographs (**Figure 3.1b-e**) showed no beaded fibers, confirming the stability of the electrospinning jet. Also, the surface of the fibers appeared to be smooth, without any particulate structures on single fibers, suggesting no phase separation of resveratrol due to compatibility issues between resveratrol and the PCL-GT. It has been shown that GT is uniformly distributed within the fiber and it is stable for more than two weeks [101]. Similar to previous results, all configurations produced fibers in microsize range suggesting process parameters and solution parameters are adequate to form PCL-GT fibers with resveratrol [101]. Co-single coaxial fibers had

larger diameters compared to single fiber, due to additional layers and an increase in the volume of the spinning solution. Random analysis of micrographs collected using SEM via an image analysis software confirmed that the fiber diameter, porosity, and matrix thickness were identical to that reported in the literature [101]. Hence, the addition of a small amount of resveratrol did not alter the fiber size and matrix characteristics relative to previous analysis.

3.3.4 Influence of fiber configuration on the resveratrol release profile

In order to understand the loading efficiency of resveratrol in different fiber configurations, I evaluated the amount of resveratrol in fresh fibers. All three fiber configurations demonstrated a very high loading efficiency of 88.3 (±8.06) %, 81.8 (±1.47) %, and 76.9 (±4.55) % (**Figure 3.5a**), for single fiber, Co-single phase, and Co-PCL, respectively.

The intent of forming different configurations was to test the possibility of controlled release of resveratrol and increase its concentration beyond 3 days. The amount of resveratrol in the culture medium was evaluated. These results showed a release profile saturating at day 5 (**Figure 3.5b)**. The values provided were based on resveratrol available in the cell culture medium in the presence of cells. They did not account for the decay or the uptake of resveratrol by cells during the incubation time. Without those corrections, nearly 95% of resveratrol was present after 100 hours from single fibers. Coaxial fibers in both configurations showed similar release profiles, suggesting no significant influence of the outer sheath layer. This suggests that the release of resveratrol is independent of fiber's configuration.

In order to understand this, the permeability of resveratrol was calculated using resistance in series model [101]. Calculated permeability values for all three configurations provide similar permeability values (**Figure 3.5c**); where single fiber matrix determined permeability was 10.6 μm/h. Although resveratrol (MW = 228.25 g/mol) is nearly half the molecular weight as doxycycline (MW = 444.43 g/mol), obtained permeability was similar in single fibers [101]. Permeability of fibers

or membranes is a function of both lipophilicity and diffusivity. Hence, resveratrol release process may be significantly dependent on its lipophilicity, as water molecules diffuse through the fiber layers and replace the drug, forcing it to be released.

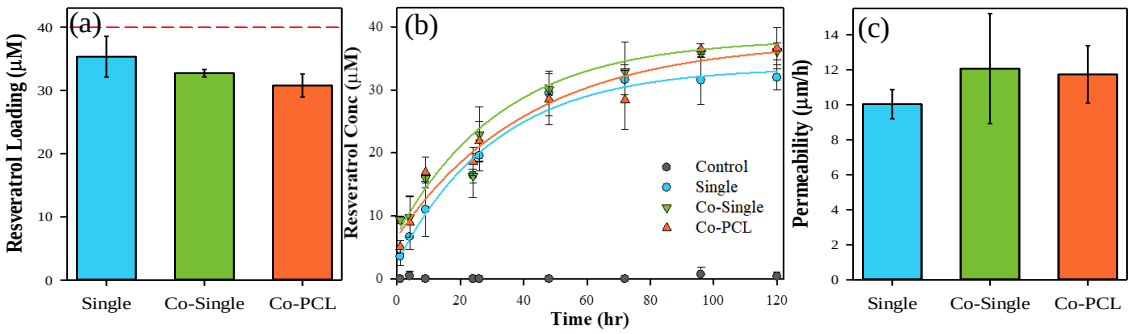

Figure 3.5: Resveratrol loaded electrospun fibers. (a) Comparison of drug loading in different configurations. The dashed line corresponds to the initial concentration of resveratrol added to the polymer solution. (b) Resveratrol release behavior from various fibers. (c) Effect of fiber configuration on the permeability constant.

3.3.5. Effect of resveratrol loaded fibers on cell death

In order to understand the bioactivity of resveratrol released from the electrospun PCL-GT fibers, K562 cell viability was analyzed for three, five, and eight days. These results showed a time-dependent increase in the level of apoptosis indicated by Annexin V (**Figure 3.6a**) staining, correlating to the release profile. Further, the control group containing co-single fibers but without resveratrol showed no significant changes during the incubation time. This suggested that the released resveratrol from fibers is bioactive and the observed non-viability is not due to solvents used in fiber generation or sterilization. More importantly, the apoptotic level at day 8 was similar to that observed at day 3 when 40 μM resveratrol was added directly to the cell culture medium. One needs to extend the studies to ten days to see whether increased cell death mimics day 5 results when 40 μM resveratrol was added directly to the cell culture medium. When PI staining results were evaluated, day 3 results were similar to that of the control group containing co-single fibers without resveratrol. On day 5 and day 8, cell death increased in all containing resveratrol, in tandem

with the release profile (**Figure 3.6b**). However, necrosis was moderately lower. This could be due to the controlled release process, which enhanced the level of apoptosis.

In order to understand further, cell cultures were observed at different days during the culture time. On day 8, apoptotic bodies were observed (**Figure 3.6c**) in all three fiber configurations compared to the control sample. Apoptotic bodies were more prevalent than vacuoles formation, indicating lower levels of autophagy. Using the controlled delivery system, the level of apoptosis significantly increases compared to that of necrosis. Since cellular uptake is diffusion i.e., concentration-dependent, it is possible that the controlled release could decrease the uptake of resveratrol by the cells, compared to direct introduction to the cell culture medium due to reduced concentration gradient. Hypothetically, the controlled release provides a specific concentration of the drug associated with apoptosis, over a certain period, triggering the process. In comparison, introducing the same total concentration to the cell medium caused necrosis.

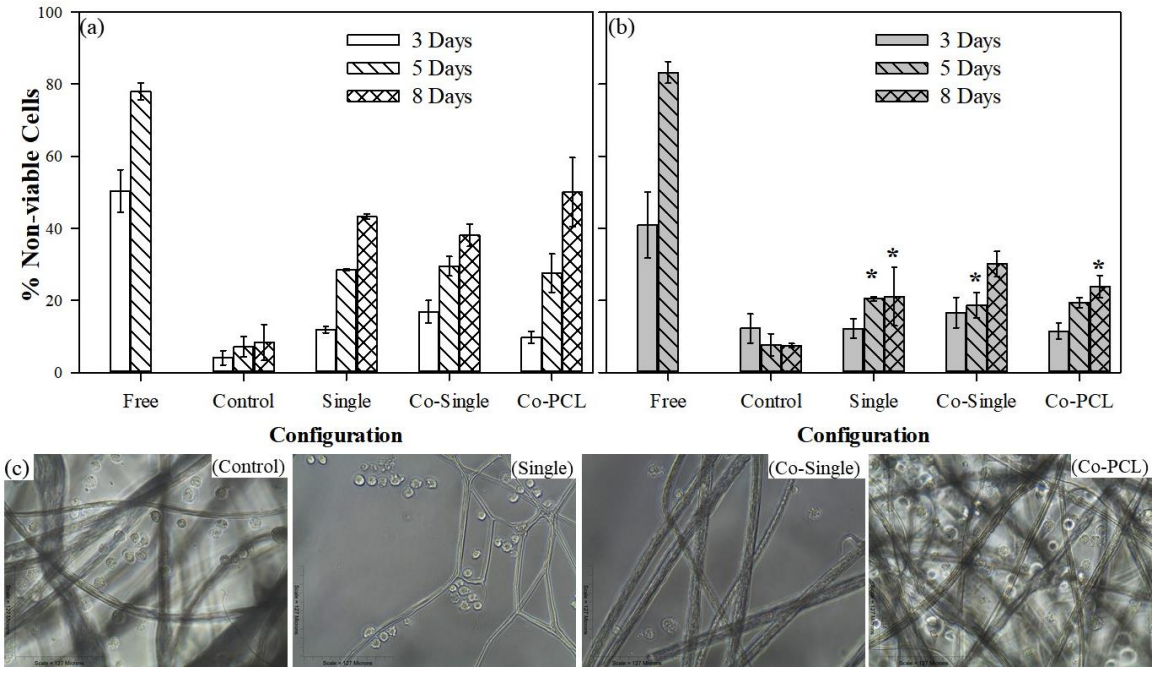

Figure 3.6: Influence of fiber configuration on resveratrol-mediated K562 cells death. (a) Annexin V stained non-viable cells. (b) PI stained necrotic cells. Condition "Free" corresponds to 40 μM resveratrol added directly to the medium. Condition "control" corresponds to Co-Single fibers without resveratrol. * represents statistical significance with $p < 0.02$ between Annexin V and PI

stained cell populations in the same fiber configuration for the same day. $ represents statistical significance with $p < 0.02$ between experiments with and without siRNA in the same fiber configuration stained with Annexin V. (c) Micrographs showing the morphology of K562 cells in presence of fibers in culture after eight days of incubation.

In order to understand changes in fiber stability during the incubation time, samples were analyzed via SEM after 3 and 5 days of incubation. Comparison of results in the presence and absence of resveratrol showed no significant differences between configurations (**Figure 3.7**). However, single fiber and Co-PCL configuration had more cells trapped in the fibers, which increased over time, compared to Co-single phase fibers. This could be attributed to the nanostructures that formed in single fiber and Co-PCL configurations. This could affect the determination of cell viability using flow cytometry since certain cell count is lost due to cell entrapment.

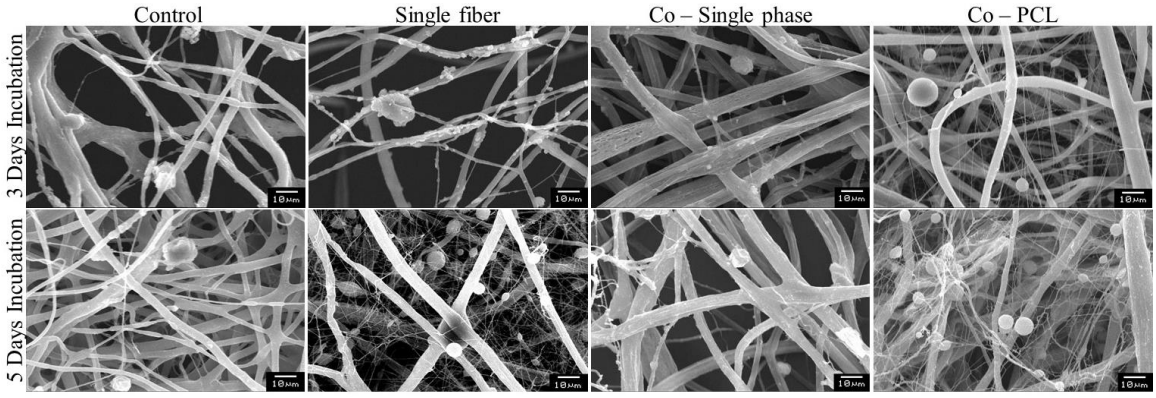

Figure 3.7: Morphology of fibers after incubation for 3 days and 5 days with K562 cells. Micrographs were obtained after drying the samples from respective time periods. Also present are some of the cells trapped within the fibers.

3.3.6 Effect of siRNA in the presence of resveratrol-containing fibers

Additional experiments were performed by adding siRNA to the culture medium, where PCL-GT fibers were present. Interestingly, there seemed to some interaction between the siRNA and fibers.

In the control group (**Figure 3.8**), where no resveratrol was present, there was a significant reduction in non-viable cells in comparison to 36 nM siRNA concentration added directly to the cell culture medium (**Figure 3.2b**); at 36 nM siRNA alone, 46.3% non-viable cells were observed which reduced to 21.5% in the presence of fibers. A similar reduction was also observed with PI staining; at 36 nM siRNA alone, necrotic cells were 29.5%, which reduced to 16.4% in presence of PCL-GT co-single fibers. In the presence of resveratrol-containing fibers, these numbers decreased further. In order to realize a similar combination effect, developing a delivery system for siRNA to ensure controlled release needs to be studied. Furthermore, one could investigate the targeted delivery of siRNA, which could further reduce the dosage requirement.

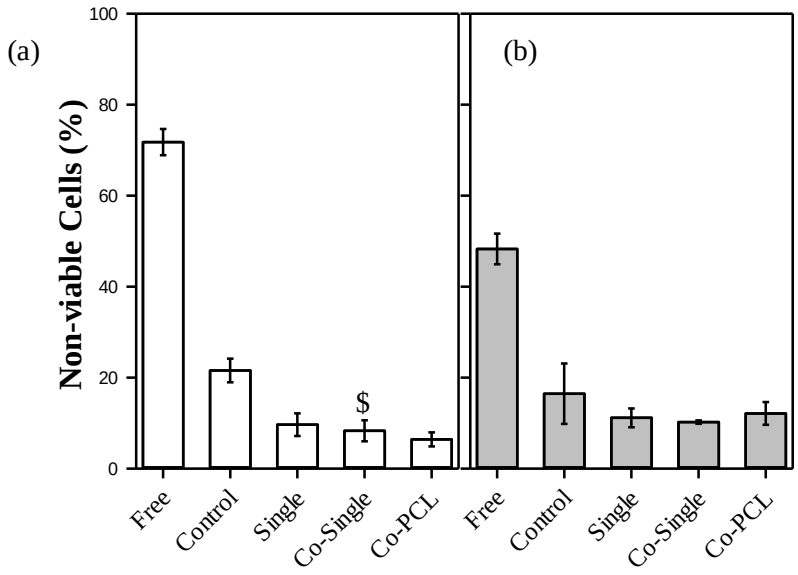

Figure 3.8: Influence of a combination of 36 nM siRNA added to medium and fibers containing resveratrol on K562 cells on day 3. (a) Annexin V stained non-viable cells. (b) PI stained necrotic cells. Condition "Free" corresponds to 40 μM resveratrol and 36 nM siRNA added directly to the medium. Condition "control" corresponds to 36 nM siRNA with the Co-Single fibers without resveratrol.

3.4 Discussion

Based on many studies showing the protective effects of resveratrol, clinical trials have been performed [90] and further explored in cancer therapy [82, 83]. However, these results have shown less success of resveratrol when systemically administered due to the pharmacokinetic characteristics of resveratrol. In an attempt to enhance the bioavailability of resveratrol, controlled release of resveratrol has been investigated [109]. Controlled release of resveratrol from electrospun PCL-GT fibers seems to be more effective in loading and controlled release in relation to other delivery systems. Using chitosan-based nanoparticles, *in vitro* release of resveratrol was studied at pH 6.8 for eight hours [110]. Adherent fibroblasts non-viability showed only resveratrol to be better at tested doses. Controlled release of resveratrol was tested using lecithin mixed micelles [111], where the release of resveratrol was extended to 24 h. Some reported higher loading efficiency using mPEG-poly(ε-caprolactone)-based nanoparticles, and cumulative controlled release was extended to five days [112]. Others have explored forming resveratrol containing core-shell nanoparticles to improve the bioavailability [110, 113]. Hence, my delivery method using PCL-GT blends, to encapsulate higher loading of resveratrol, offers a new approach for delivering hydrophobic drugs for a longer duration.

In coaxial PCL-GT electrospun fibers, the inner core can be chosen based on the properties of the therapeutic agent. Previously, hydrophilic doxycycline was delivered using GT and PCL-GT inner cores, while lipophilic resveratrol can be delivered using PCL and PCL-GT inner cores. Blended hydrophilic GT with hydrophobic PCL helps load a broad range of components. The encapsulation efficiency of lipophilic drugs after electrospinning in hydrophobic polymers is known to be significantly higher [114], similar to my observation. Further, electrospun PCL-GT fibers have also been investigated for their biodegradability and biocompatibility [115]. Hence, PCL-GT fibers can be locally administrated into the bone marrow to achieve a local therapeutic concentration of resveratrol. Similar ibuprofen-loaded polylactic-co-glycolic acid (PLGA) biodegradable fibers have been

explored in reducing fibrosis after lumbar laminectomy in a local implantation model [116]. In order to better understand the utility of such fibrous mats, further studies are required using animal models.

There have been many studies showing the usage of electrospun fibers in local delivery with many coaxial configurations [98]. However, the modeling of the release profile from such fibers is limited to understanding whether the release behavior is dictated by Fickian diffusion. In this regard, I extended such modeling to understand the changes in the permeability of the drug with various combinations of the polymeric blends. Permeability of lipophilic resveratrol was not controlled by the configuration of electrospun fibers, unlike that observed with hydrophilic doxycycline [101]. Others have reported similar results in co-axial fibers using poly(butylene succinate) with lipophilic curcumin [117]. Curcumin release from different configurations into ethanol showed no dependency on structures, consistent with my observation in this Chapter. This suggests that the partition coefficient may be a dominant factor, rather than diffusion in the controlled release of lipophilic drugs. In this Chapter, the mass ratio of PCL and GT were similar and as they both have similar molecular weight, the molecular ratio is, also similar. In order to understand the changes in the partition coefficients, one has to test the effect of altering the ratio of PCL-GT in the outer sheath. Determining the permeability values of individual layers helps in correlating the diffusion in order to understand the effect of partition coefficient. Such an analysis would be valuable in tuning the release profile of other lipophilic therapeutic agents.

This study explored combining resveratrol and siRNA to induce 100% non-viability of cancer cells. Using a factorial design approach, I estimated the dosages required of both drugs when administered into the cell culture medium. However, the influence of siRNA in the presence of PCL-GT fibers was reduced, probably due to non-specific interactions between the naked siRNA and the fibers. In addition, endogenous characteristics of siRNA such as negative charge, rigid structure, size, and stability, make passive diffusion through cell membrane quite challenging. Some have

addressed this challenge by delivering siRNA using endocytosis with liposomes [34]. Ligand-targeted liposomes have shown great potential in many novel delivery systems, with high *in vivo* response due to their active targeting, increased stealth, and controlled drug release. PEG coating (to overcome rapid clearance from circulation) and ligand attachment (to avoid non-specific binding) are specifically important to overcome the challenges associated with liposomal delivery systems [42]. Based on the type of cancer, certain types of ligands provide higher binding efficiency and many fold decrease in IC_{50} value compared to non-targeted liposomes. Holo-transferrin containing liposomes show enhanced intracellular uptake compared to free Bcl-2-siRNA *in vivo* and decreased IC_{50} (treated with doxorubicin *in vitro*) values. Holo-transferrin attachment also showed improved tumor growth inhibition, and higher survival time compared to the non-targeted liposomal system [42]. Chapter IV provides a detailed study of the combined delivery system of electrospun microfibers and holo-transferrin-conjugated-PEG liposomes (referred to as liposomes in this manuscript, unless stated otherwise).

CHAPTER IV

ASSESSMENT OF THE COMBINATION TREATMENT OF LEUKEMIA CELLS, USING SIRNA-LOADED LIPOSOMES, AND CONTROLLED RELEASE OF RESVERATROL

4.1 Introduction

To eliminate side effect, and drug interaction, the combined delivery system has gained my attention towards achieving the second aim of this project. Small interfering RNAs (siRNAs), which are 20-25 base pairs in length, have been shown to be very effective in silencing targeted genes since the first demonstration in 2010 [6]. siRNA's half-life is approximately 24 h [7], which necessitates a higher dosage. Although local administration of siRNA has limited side effects, systemic administration exacerbates side effects, which lead to early termination of clinical trials [118]. siRNA endogenous characteristics such as negative charge, rigid structure, size, and stability, make passive diffusion through cell membrane quite challenging [119]. To address this challenge, endocytosis becomes an effective mechanism of delivery that can be achieved using lipid-based nanoparticles [34]. In order to improve safety and minimize the dosage of drugs, targeting based on increased expression of certain receptors in cancer cells has been a strategy.

Leukemia-specific siRNA has been investigated to downregulate the fused breakpoint cluster region (BCR)-Abelson (ABL) tyrosine kinase gene pathway. This silencing technique is shown to be sufficient to sustain CML phenotype [120]. As mentioned earlier, ligand-targeted liposomes with PEG coating (to overcome rapid clearance from circulation) and holo-transferrin attachment showed improved tumor growth inhibition, and higher survival time compared to the non-targeted liposomal system [42].

In this chapter, I discussed in detail my evaluation of the effect of two different drug delivery devices on inducing cancer cell death selectively. Treatment with resveratrol or siRNA increases response sensitivity in cancer cells [121]. The combination of these two drugs enhanced the effectiveness and drug resistance in cancer cells. I hypothesize that combining two drugs using two different drug delivery devices leads to an improved therapeutic effect of each drug with reduced dosage. To test the hypothesis, I used a model study comprising; i) delivering resveratrol using microfibers, and ii) delivering siRNA targeting BCR-ABL expression using liposomes. This allows the controlled administration of each drug in a timely manner. In addition, I used a co-culture system comprised of K562 cells and HUVECs, which also helps understand the device-blood vessel interactions. I show that resveratrol released from PCL-GT electrospun fibers and delayed siRNA delivered through holo-transferrin conjugated PEG-liposome induces 92.7 (±2) % non-viability by day 8. The use of co-cultures introduces a unique tool to estimate treatment effect on healthy cells as well as target cancerous cells in an *in vitro* setting.

4.2 Materials and Methods

4.2.1 Materials

In addition to materials introduced in section 3.2.1, holo-Transferrin, Traut's reagent, and cholesterol were from Sigma-Aldrich (St. Louis, USA). Distearoyl phosphatidylethanolamine–PEG [2000 d] was purchased from Shearwater Polymers (Huntsville, AL). HUVECs derived from single donors were purchased from BD Biosciences (San Jose, CA). Medium 200 phenol red free (PRF), low serum growth supplement (LSGS), trypsin/EDTA, and trypsin neutralizer solution were all purchased from Life Technologies Corporation (Carlsbad, CA).

4.2.2 Cell culture maintenance

K562 Cell Culture: This culture was described in section 3.2.2.

HUVECs Culture: HUVECs were plated in T75 flasks and fed with fresh medium every 36 hours. When confluent, cells were detached with 0.025% trypsin and 0.01% EDTA in PBS, neutralized with trypsin neutralizer solution (phosphate-buffered saline (PBS) containing calf serum), centrifuged at 125 ×g for 5 minutes, and re-suspended in the growth medium.

All cultures were routinely monitored under an EvosTM AME-i2111 Digital Inverted Microscope, and when necessary, phase contrast micrographs were obtained at random locations.

4.2.3 Synthesis siRNA containing liposomal particles [122], [123]

A mixture of 260 nmol of distearoyl phosphatidylethanolamine–PEG [2000 d] and 3877 nmol of cholesterol was added to 5 mL of chloroform. The lipid film was formed by allowing the solvent to evaporate overnight. Then, 5 mL of MES buffer was added and stored in the dark for 2 hours. Liposomes were formed by strong vortex, 15 seconds of heating at 38 ^{o}C in a water bath, followed by strong vortex. At this stage, the samples were split into two groups: the first group was used, then stored for further testing, and the second group was used in holo-transferrin conjugation.

Holo-transferrin conjugation: A mixture of 260 nmol of holo-transferrin, and 10390 nmol of Traut's reagent was prepared in 2 mL of EDTA buffer (pH: 8.5). The mixture was shaken in the dark for 1 hour. The solution was re-concentrated to 0.2 mL using Amicon® Ultra-2 filters (3 kDa, Sigma Aldrich) by centrifugation for 12 mins 3500 rpm at room temperature. The concentrated solution was added in a 1:1 ratio to the freshly prepared micelles, as described above. The mixture was stirred in the dark for 24 hours. The samples were divided into two groups: the first group was stored for further testing, and the second group was used for siRNA.

siRNA encapsulation: A 2.5 µM stock solution of siRNA was prepared in citrate buffer (pH 6.0 – Sigma Aldrich). The lipid was dissolved in 100% ethanol, heated at 60 ^{o}C, and added to siRNA solution (36 nM final concentration) under strong vortex. Micelles were formed as stated above.

Sizing and purification: The prepared liposomes solution was extruded through an extrusion device (T&T scientific corporation, Knoxville, TN, USA) with a 100-nm diameter filter, 21 times, following the vendor's instructions. Dialysis was then performed in HBSS through MWCO 6000-8000 (Cellu Sep T2, Membrane Filtration Products, Inc., Seguin, TX, USA) for 3 hours at room temperature to remove the ethanol and raise the external pH. Sepharose CL-4B ((Sigma Aldrich, St. Louis, MO) was packed into columns (Sigma Aldrich, St. Louis, MO), allowed to settle overnight at 4 °C and used to remove unconjugated transferrin and other impurities.

Dynamic light scattering (DLS) was performed using a zeta potential analyzer (Brookhaven Instruments Corporation, NY, USA). Using the associated software, the effective diameter of the particles population and its polydispersity were determined. The zeta potential was also determined using the same apparatus.

Transmission electron microscopy (TEM) was performed using JEOL JEM-2100 with Evex EDS (Peabody, MA) to visualize the liposomal particles. Samples were stained with phosphotungstic acid, then placed on a TEM grid and imaged immediately. The images show that the particles are spherical in shape and are less than 100 nm in size.

4.2.4 Loading efficiency of siRNA in liposomes

Liposomes were encapsulated with Alexa-Flour 488-conjugated BCR-ABL siRNA (F-siRNA, Integrated DNA Technologies) to detect encapsulation efficiency and uptake by cells. Since both free F-siRNA and encapsulated F-siRNA contributes to the fluorescence intensity, samples were collected before and after purification via Sepharose CL-4B packed column. Fluorescence intensities were measured using a Gemini XPS spectrofluorometer (Molecular Devices, CA) at an excitation wavelength of 488nm and an emission wavelength of 530 nm. Liposomes with siRNA were used as blank controls. A calibration curve was prepared using 0 – 0.25 μM concentration of free

F-siRNA to convert, fluorescent intensities into concentration. Loading efficiency was determined by taking the ratio of the two concentrations.

4.2.5 Holo-transferrin conjugation efficiency

Holo-transferrin-conjugated liposomes were purified using a Sepharose CL-4B packed column to remove any unconjugated particles. The amount of holo-transferrin conjugated to liposomes was determined using BCA assay (Thermo Fisher Scientific, Waltham, MA), according to the vendor's protocol. In brief, absorbance was measured using Spectramax Emax (Molecular Devices, CA) at 595 nm in a 96 well plate. Based on a calibration curve prepared using standard solutions (125 – 2000 µg/mL), the total amount of protein in the sample was quantified. Using the total amount of holo-transferrin added during preparation, the conjugation efficiency was calculated.

4.2.6 Determination of BCR-ABL downregulation using quantitative polymerase chain reaction (q –PCR)

Free siRNA (36 nM) was incubated with 2×10^5 K562 cells/mL for 72 hours. The samples were snap frozen at -80 ^{o}C. An RNeasy mini kit was used to purify RNA samples and RNA concentration in each sample was measured using NanoDrop Spectrophotometer (ND-1000). The complementary DNA (cDNA) kit, iScript Reverse Transcription Supermix for RT-qPCR (BIO-RAD), was used to obtain cDNA for the collected RNA samples. Mastercycler (Eppendorf) was used to run the reverse transcription process. β-glucuronidase (GUSB) was used as the standard gene, as suggested for K562 cells [124]. Primers for the GUSB were designed using Primer-BLAST while the primers for the BCR-ABL gene were purchased (ThermoFisher Scientific,) based on literature reports [125]. SYBR Green Supermix (BIO-RAD) was added to all samples. qPCR was performed by CFX Connect Real-Time System (BIO-RAD), and the results were analyzed using Bio-Rad CFX Manager 3.0, and MS Excel. The expression fold change (EFC) method was used to quantify BCR-ABL downregulation in K562 cells.

4.2.7 siRNA-loaded liposomes effect on cell viability

For all experiments, K562 cells were harvested, counted using a Hemocytometer, and 2×10^5 cells/mL were cultured in a 6-well plate with 2 mL of fresh media for each well. siRNA concentration was 36 nM in all the samples as follows: i) controls prepared by directly adding citrate buffer solution equivalent to that present in 36 nM siRNA solution, ii) free siRNA, iii) scrambled siRNA, iv) PEG-Liposomes with no siRNA, v) siRNA- loaded PEG-liposomes, and vi) siRNA-loaded-holo-transferrin conjugated PEG-liposomes. All cell cultures were incubated for 72 hours, K562 cells were collected by centrifugation at 840 ×g for 5 minutes, and viability was determined using the method previously reported [73]. In brief, cells were washed with phosphate buffer solution (PBS, 7.2 pH, prepared in-house using 8 g NaCl, 0.2 g KCl, 0.2 g KH_2PO_4, and 2.17 g Na_2HPO_4-$7H_2O$ in 975 mL DI water) with 0.1% BSA (1 mL for every 2×10^5 cells). Then cells were washed with Annexin V buffer solution and stained with 2 µL Annexin V FITC conjugate, then with 4 µL of PI (100 mg/L), and then incubated in ice for another 15 minutes. Samples were analyzed using a FACSCalibur (Becton Dickinson, San Jose, CA) flow cytometer. Unstained samples and individually stained samples were used as controls. Based on the obtained information, the percentages of dead cells were determined using a standard quadrant analysis.

4.2.8 Cellular uptake of siRNA and siRNA-loaded liposomes

Free F-siRNA, F-siRNA-loaded and unloaded holo-transferrin-PEG-liposomes were prepared. The samples were incubated for 5 days i) without any cells, ii) with K562 cells, and iii) with K562 cells and HUVECs. HUVECs were seeded on 6-well plates in preparation for experiments. The other cell line and treatment elements were then added. Cell medium was prepared in 1:1 (by volume) of RPMI: 200 medium. Micrographs were collected for all conditions after 0, 24, 72, and 120 hours using an Evos digital microscope. Non-adherent K562 cells were gently collected by withdrawing 100 µL cell medium each day and analyzed by flow cytometry for the presence of F-

siRNA. On the fifth day, all K562 cells were removed by gentle mixing and then HUVECs were detached using trypsin/EDTA and analyzed for the presence of F-siRNA. In order to minimize the presence of both cell types, forward scatter and side scatter data were used as both cells have different sizes and granularity. Three biological samples were prepared for each condition.

4.2.9 Influence of resveratrol on HUVECs

In order to assess the effect of released resveratrol, changes in Sphingosine 1-phosphate (S1P) was measured using ELISA kit (MyBioSource Inc., CA) following the vendor's protocol. Following conditions were prepared in 1:1 RPMI:200 PRF cell medium: i) 2×10^5 cells/mL K562 cells without resveratrol; ii) 2×10^5 cells/mL K562 cells with 40 µM of resveratrol; and iii) Both K562 cells and HUVECs (2×10^5 cells/mL) where HUVECs were seeded first, allowed to attach, and then K562 cells were added along with 40 µM of resveratrol. Cell culture medium without any cells was also cultured in tandem with cell cultures. Samples (50 µL) were collected at 0, 24, 48, and 72 hours, and stored at -20 ^{o}C for further analyses. Absorbance was measured using Spectramax Emax (Molecular Devices, CA) at 450 nm in a 96 well plate. Based on a calibration curve prepared using standard solutions (0 – 200 ng/mL), the S1P content in the sample was quantified. S1P activity in the culture medium without cells was used as blank for respective time points.

4.2.10 Resveratrol and siRNA combination effect on K562 cell viability

Effect of resveratrol encapsulated microfibers in combination with siRNA-loaded liposomes on K562 cell viability was evaluated over 8 days. For all conditions, K 562 cells at 2×10^5 cells/mL were used with PRF cell culture medium. The following conditions were prepared: i) 36 nM siRNA and 40 µM resveratrol both introduced directly to the cell culture medium; ii) Controls prepared by adding fresh medium only; iii) Fibers (with no resveratrol) introduced into cell medium on day 0; iv) Fibers with 40 µM resveratrol and liposomes with 36 nM siRNA both introduced at

the same time on day 0; v) Fibers with 40 μM resveratrol introduced on day 0, and liposomes with 36 nM siRNA introduced on day 3 referred to as delayed liposomes + microfibers. Micrographs were taken at random locations after 0, 72, 120, and 192 hours for each sample. On days 3, 5 and 8, cultures were mixed gently and 50μL samples were collected. These samples were analyzed for K562 cell viability using two-color flow cytometry.

4.2.11 Resveratrol and siRNA combination effect on K562 cell viability in the presence of HUVECs

In order to understand the combination effect in presence of HUVECs, co-culture experiments were performed. HUVECs were seeded first, allowed to attach, then fibers were introduced followed by the addition of K562 cells. All samples were incubated in 1:1 ratio of RPMI (with 10% FBS) and 200 PRF medium. The following groups were used: i) controls prepared by adding fresh medium only; ii) Fibers with 40 μM resveratrol and liposomes with 36 nM siRNA both introduced at the same time on day 0; iii) Fibers with 40 μM resveratrol introduced on day 0, and liposomes with 36 nM siRNA introduced on day 3 referred as delayed liposomes + microfibers. Micrographs were taken at random locations after 0, 72, 120, and 192 hours for each sample. On days 3, 5 and 8, cultures were mixed gently and 50μL samples were collected. These samples were analyzed for K562 cell viability using two-color flow cytometry.

4.3 Results

4.3.1 Liposomes characterization

Liposomes were prepared in-house as described in the previous section. Hence, I first characterized the particle size and efficiency of holo-transferrin conjugation. Then samples were visualized in TEM, which (**Figure 4.1a**) showed that the particles were around 100 nm in diameter and the particles were spherical with well-defined edges. DLS analysis of five replicates showed that the

effective diameter of the particles was 117.2 (±1.53) nm, with a polydispersity of 0.170. Zeta potential outcome of ten replicates was -11.09 (±0.82) mV. The latter was found to be similar to values reported in the literature [126].

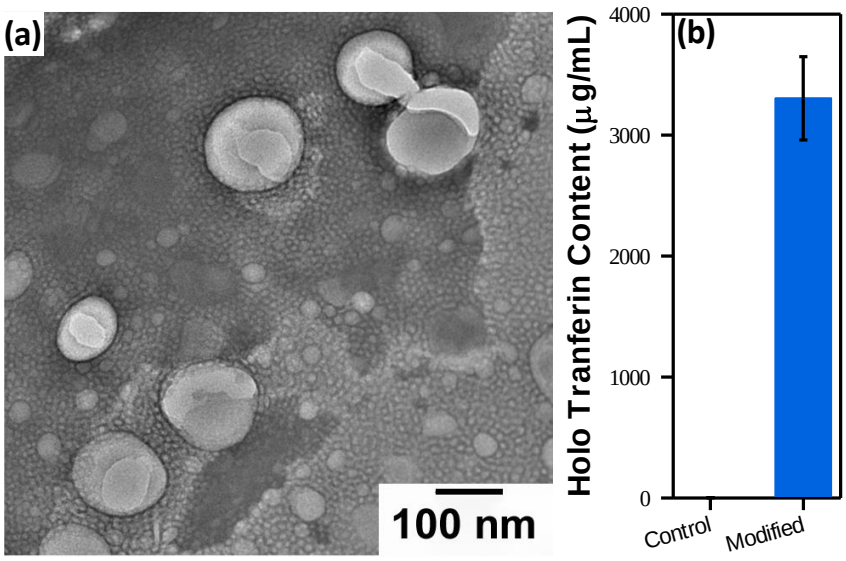

Figure 4.1: Liposomes characterization. (a) TEM image showing spherical liposomes. (b). Comparison of total protein content in holo-transferrin-conjugated liposomes with un-conjugated liposomes as the controls.

In order to understand the total transferrin present, BCA assay was performed. These results (**Figure 4.1b**) showed the concentration to be 3300 (± 334) µg/mL in holo-transferrin containing liposomes and the amount of protein in unconjugated liposome was 1.8 (± 0.17) µg/mL. Then I calculated the efficiency of loading using the total amount of holo-transferrin initial added (3850 µg/mL) during the conjugation. Calculated conjugation efficiency was 85.9 (±7.30)%. The total amount of siRNA added during the synthesis procedure was 0.72 µM. After purification of liposomes, the measured siRNA concentration was 0.66 µM. This resulted in the loading efficiency of siRNA in the liposomal particles to be 92.3 (± 2.57) %.

4.3.2 Silencing BCR-ABL in K562

In order to understand the effect of RNA interference to silence BCR-ABL gene expression in K562 cells, the RT-qPCR analysis was performed after 72 hr of exposure. The results show (**Figure 4.2a**) significant knockdown of the BCR-ABL mRNA in the sample treated with 36 nM BCR-ABL siRNA with respect to a control (untreated sample), and in addition to scrambled RNA. Compared to the control sample, there is roughly a 60% decrease in the expression of the BCR-ABL gene. Liposomes loaded with siRNA samples gave similar silencing effect compared to free siRNA. This is attributed to single culture effect, where the treatment is solely introduced to K562 cells. The cellular non-viability level achieved with the same concentration of siRNA was 46.3 (± 2.97)% [73]. In contrast, scrambled siRNA showed around 20% decrease in the expression of BCR-ABL. This correlated to the K562 cells non-viability rate of 15% [73], observed after 72 hours of incubation with a scrambled siRNA as a positive control. With increased siRNA dosage, it is expected that the knockout would proportionally increase [73]. Since I wanted to use 36 nM concentration in subsequent combination experiments, I did not perform dosage effects on the knockdown.

4.3.3 Effect of siRNA-loaded liposomes on cell viability.

In order to assess the effectiveness of loaded siRNA into holo-transferrin conjugated PEG-liposomes, cell non-viability was measured using two-color flow cytometry. The K562 cell non-viability level induced by siRNA containing holo-transferrin conjugated PEG-liposomes (**Figure 4.2b**), and PEG-liposomes, was slightly higher than those unconjugated. Compared to free-siRNA, these results show that BCR-ABL siRNA activity was not altered, suggesting the process of loading and formation of liposomes does not affect siRNA activity. These levels were similar to the apoptosis levels achieved with free siRNA, however, the necrosis level is significantly reduced. Both

scrambled and unloaded liposomes (used as positive controls) showed significantly lower non-viability levels than siRNA treated samples. This effect of inducing higher levels of apoptosis compared to necrosis is desirable.

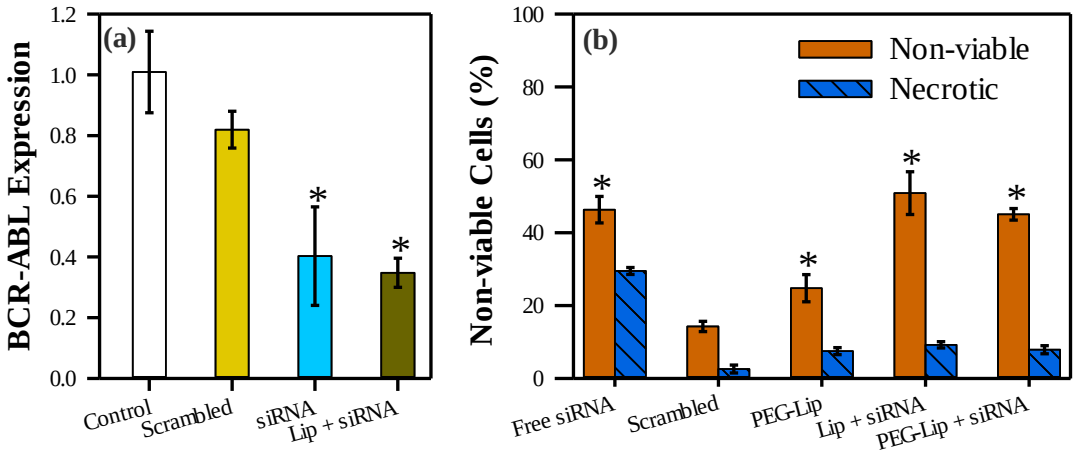

Figure 4.2: Effect of siRNA on K562 cells. (a) Real-time q-PCR analysis using expression fold change. Results show the relative fold change of BCR-ABL expression. (b) K562 cells non-viability analysis after 3 days of incubation. Indicated non-viable cells were assessed by two-color flow cytometry was used to analyze apoptosis with Annexin V and necrosis with PI. Medium sample refers to free siRNA in k562 cell medium. Lip + siRNA refers to holo-transferrin conjuagated PEG-liposomes loaded with siRNA. PEG-Lip and PEG-Lip + siRNA refer to unconjugated liposomes without and with siRNA loading, respectively. The asterisk (*) indicates $P < 0.02$ with reference to control or scrambled samples.

4.3.4 Uptake of liposomes by K562 cells.

The uptake of siRNA by K562 cells was observed using fluorescent siRNA. The control samples prepared with empty liposomes showed (**Figure 4.3**) a very low percentage of uptake; these could be attributed to the background signal. Free siRNA samples showed an uptake rate significantly higher than control samples, and it peaks after 4 days of incubation. Samples, where siRNA was loaded into holo-transferrin conjugated PEG-liposomes, showed that after 1 day of incubation, the uptake percentage in K562 cells was not significantly different than that achieved with free siRNA.

However, the uptake percentage significantly differed between the two groups after 2 days of incubation. With siRNA-loaded liposomes, the uptake peaks after 4 days of incubation.

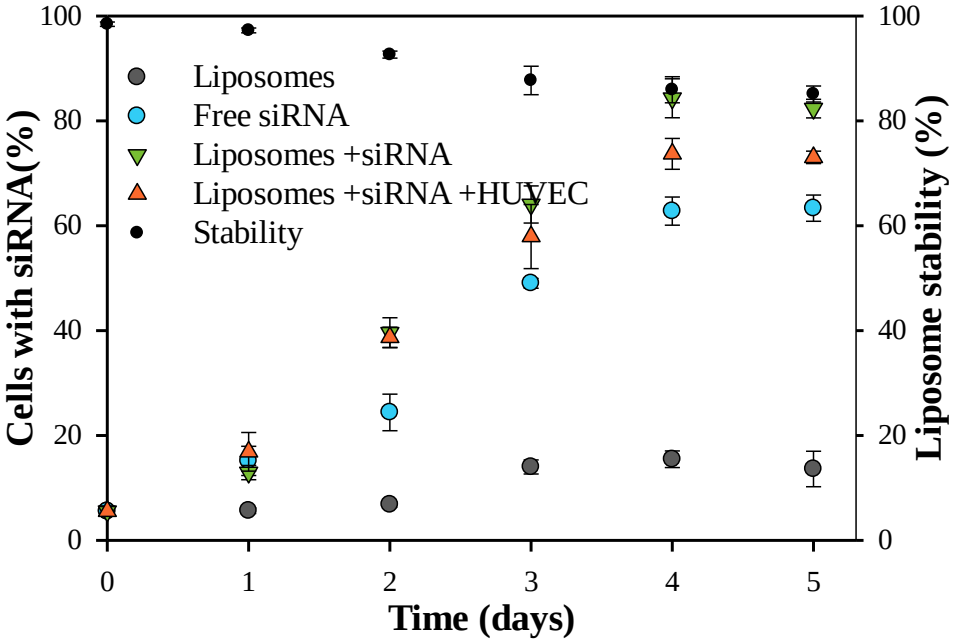

Figure 4.3: K562 cells uptake level of Alexa-Flour 488 conjugated siRNA (F-siRNA). Flow cytometry results of liposomes with no siRNA used as control samples, Free siRNA refers to F-siRNA in cell medium, Liposomes + siRNA refers to F-siRNA loaded-liposomes, and Liposomes + siRNA + HUVEC refers to F-siRNA loaded liposomes in the presence of HUVECs.

In order to test the effectiveness of prepared liposomes in targeting, I evaluated the uptake of siRNA by K562 cells in the presence of non-cancerous adherent HUVECs in co-culture. Hence, both cell types were individually harvested without the need for cell sorting. The same increasing trend was observed in the uptake of siRNA by K562 cells similar to the condition without HUVECs, with a minor reduction. Uptake peaked at 4 days of incubation. I also analyzed siRNA content in HUVECs by collecting after trypsin/EDTA treatment after 5 days. On average, 23.6 (± 1.38) % of the HUVECs had siRNA. In comparison, 73.1 (± 1.18) % of K562 cells had siRNA on day 5. When these co-cultures were observed under a microscope (**Figure 4.4**), K562 cells clustered around the adherent HUVECs, unlike monocultures where K562 cells were uniformly distributed. This could

interfere in nutrient distribution and/or liposomes to HUVECs. Based on this experiment and previous findings [73], nearly all siRNA that cells uptake induces cell death. This is interpreted by comparing the free siRNA uptake after 3 days, to the non-viability induced by free siRNA under the same conditions. The former shows 49.03 (± 0.92) %, compared to the latter which shows 46.32 (± 2.97) %.

4.3.5 Stability of liposomes in cell medium.

To test liposomes stability in cell medium, they were first loaded with fluorescent siRNA (F-siRNA). The prepared samples were incubated in cell medium under the same conditions used in all experiments, to ensure stability of liposomes under these conditions. Stable liposomal particles produce a fluorescent signal, due to loaded F-siRNA, that corresponds to their size, which is significantly larger than that of free siRNA molecules. Results show that over 5 days period, roughly 85% are intact and stable (**Figure 4.3**). The remaining percentage is attributed to undesirable release, or unsuccessful loading of F-siRNA. That percentage could also be due to dissociation of some liposomes in cell medium.

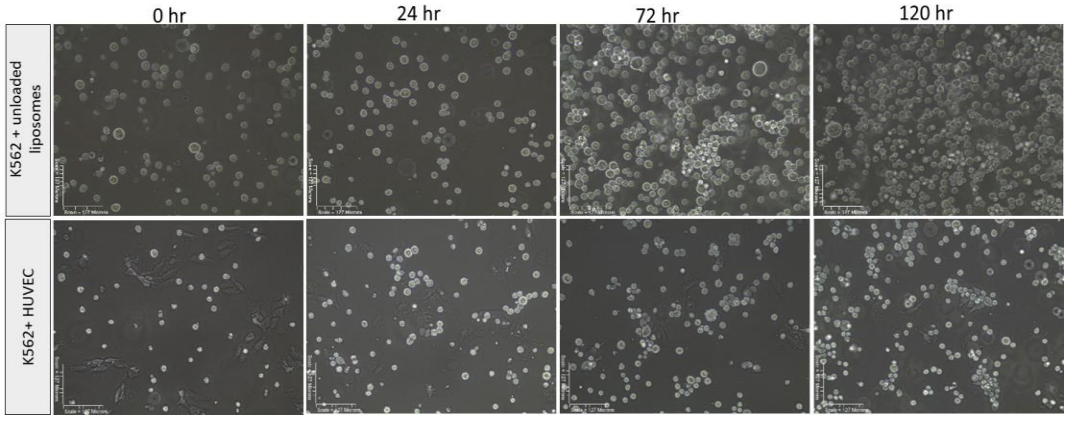

Figure 4.4: Microscopic images of K562 cells in the presence of HUVECs. The control sample microscopic images are shown for K562 cells in addition to unloaded liposomes in cell medium.

4.3.6 Effect of bolus doses of resveratrol on HUVECs.

Previously, I showed the fate of resveratrol during the 3-day cell culture in K562 cell culture medium which contains 10% FBS. The linear fit equation to the obtained data gave a value of 70.4 hours, confirming complete depletion at 72 hr. Experiments performed in the absence of cells showed an exponential decay and a half-life ($t_{1/2}$) of 89.6 hours, nearly three times longer than that reported in the plasma [92]. In co-cultures, I used 1:1 HUVECs medium and K562 cells. The absence of FBS in HUVECs culture medium reduces the total FBS content. Resveratrol uptake by cells is thought to be mediated via binding to lipoproteins and albumin [108].

Next, I tested the effect of 40 μM resveratrol alone on HUVECs viability after 3 days of exposure. Resveratrol-induced HUVECs death (**Figure 4.5a**) was not significantly different than the control cultures with no resveratrol. This is similar to that reported in the literature, although their analysis was after 24 hr and with half the resveratrol concentration [127]. Also, the presence of K562 cells did not affect the viability significantly. This suggests that the resveratrol at 40 μM dosage is not harmful to HUVECs.

Resveratrol inhibits the sphingosine kinase 1, which affects the production of S1P [128]. Level of S1P reduced in K562 cells treated with resveratrol (**Figure 4.5b**) in relation to untreated K562 cell cultures. K562 cells are hyperactive and are associated with a high uptake rate of resveratrol. A similar influence is noted in the literature [128], while different concentrations of S1P are obtained due to a different cell density used in each case. In any case, the S1P level seems to increase in presence of HUVECs, particularly at day 3. Many have shown the protective effect of resveratrol on HUVECs to inflammatory molecules [127] and oxidative stress [129].

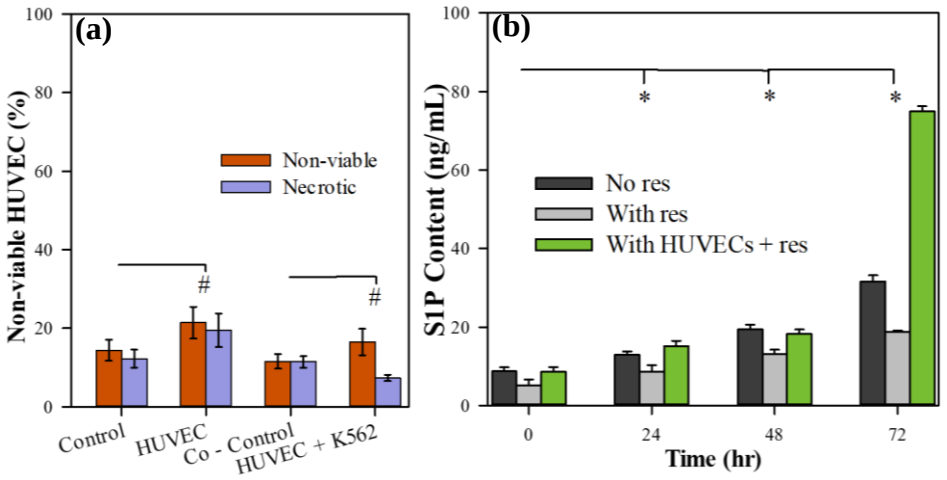

Figure 4.5: Influence of resveratrol on HUVECs viability/activity. (a) Influence of resveratrol on HUVECs viability after 72 hours. Control refers to untreated cells in cell medium, Co-Control refers to untreated cells in 50:50 cell medium. Indicated non-viable cells were assessed by two-color flow cytometry using Annexin V for apoptosis and PI for necrosis. (b) Effect of resveratrol on Sphingosine-1-phosphate levels. Values obtained from 1:1 culture medium was used as blank. Asterisk (*) indicates $P < 0.02$ relative to 0 (hr) sample, # indicates $P < 0.02$ relative to control samples.

4.3.7 The release of resveratrol from microfibers.

The release of resveratrol from different microfibers configurations, in single cell culture, as shown in **Figure 3.5b**. The presence of both polymers and resveratrol have been confirmed by FTIR [130] and differential scanning calorimetry [131]. To understand the uptake and release kinetics of resveratrol from microfibers, its content in the medium was analyzed using HPLC analysis [73]. The release of resveratrol from fibers without cells reached 100% by 72 hours of incubation from single fibers (**Figure 4.6**). Similar trends were observed in the presence of K562 cells as well as HUVECs. The highest concentration achieved was lower than the medium alone cultures. I did not account for the decay or the uptake of resveratrol by cells during the incubation time. Hence, those differences could be attributed to the uptake by cells similar to bolus experiments. Also, initial release rates in HUVECs were higher, suggesting those differences are related to the uptake rate by cells.

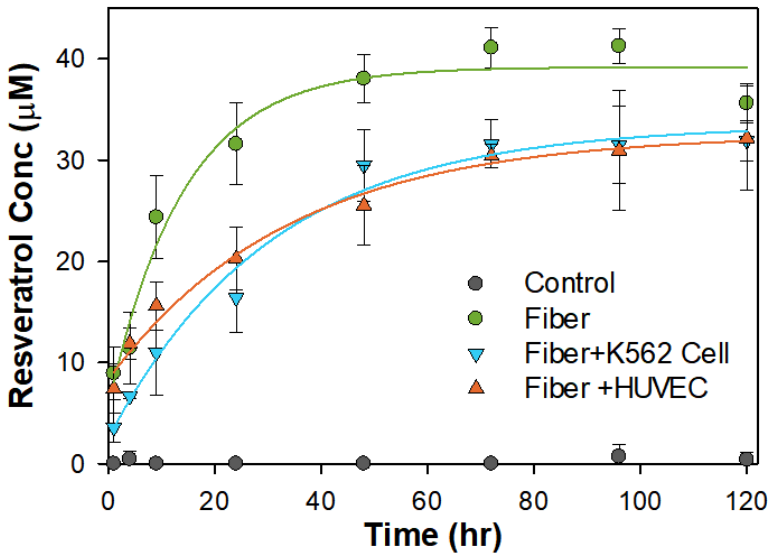

Figure 4.6: Resveratrol release and activity. Release study of resveratrol from electrospun fibers in the presence and absence of HUVECs. Control refers to unloaded electrospun single fibers.

4.3.8 Effect of combination therapy using microfibers and liposomes on cell viability.

Since our intent was to understand the effect of combination of siRNA and resveratrol control delivery devices on non-viability of K562 cells, first, I performed experiments using single fibers loaded with 40 μM resveratrol and liposomes loaded with 36 nM siRNA in two treatment modes i) fibers and liposomes added simultaneously and ii) liposomes added three days later than fibers. This delay was based on the release kinetics of resveratrol from fibers in achieving drug level, similar to the bolus doses. A gradual increase in apoptotic cells was observed when both drug delivery devices were introduced simultaneously (**Figure 4.7a**). At day 8, simultaneous addition had 86 (± 3.8) % non-viability level, which was significantly higher than the control samples prepared in PRF medium only. I did not change medium during 8-day cultures to avoid disturbance introduced to the concentration of drugs and observed cell death in controls could be due to nutrient limitation.

In cultures where liposomes were delayed by 3 days, non-viability was lower at day 3 but significantly increased on day 5 and reached 92.7 (± 1.63) % after 8 days of incubation. Reduction at day 3 is expected as there is no liposome. Over an extended time scale, however, delayed liposomes introduction resulted in higher total non-viability. Also, bolus doses of 40 μM resveratrol and liposomes loaded with 36 nM gave 78 (± 2.3)% at day 3 [73]. This suggests the possibility of achieving therapeutic levels locally, long-term, and more effectively. I also assessed the necrotic cells using the PI (**Figure 4.7b**). In relation to non-viable cells, necrotic cells were significantly lower in treated groups, similar to the control group. This also suggests that the control samples show such levels probably due to reduced nutrition level.

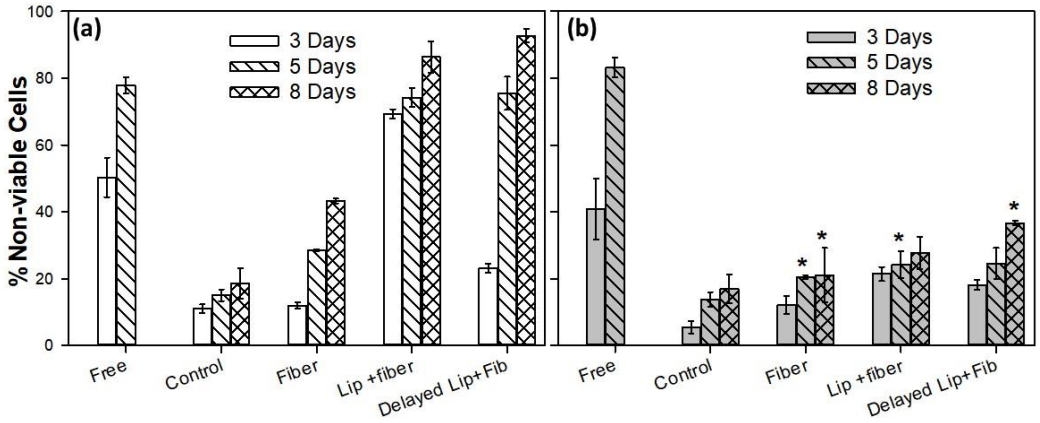

Figure 4.7: K562 cells non-viability levels investigated under different conditions. Indicated non-viable cells were assessed by two-color flow cytometry using Annexin V for apoptosis and PI for necrosis. Free samples correspond to free resveratrol in cell medium. Control samples correspond to K562 cells and cell medium without treatment. Fiber samples are single fibers loaded with resveratrol and introduced to cell medium. Lip + fiber correspond to samples treated with both loaded liposomes and loaded fibers, introduced to cell medium simultaneously. Delayed Lip + Fib samples correspond to loaded fibers introduced to cell medium immediately, and loaded liposomes introduced to cell medium after 72 hours. Part (a) shows Annexin V stained samples (non-viable cells), part (b) shows PI stained samples (necrotic cells). Asterisk (*) indicates $P < 0.02$

Next, I compared the micrographs at various time points during the culture time (**Figure 4.8**). As expected in the control group, the number of K562 cells increased progressively. Compared to control samples, K562 growth in treated samples seemed to be reduced or appeared similar to the

day zero samples. Also, cells were distributed around the fibers. In addition, the structure of microfibers seemed unaltered by the presence of neither K562 cells nor siRNA-encapsulated liposomes.

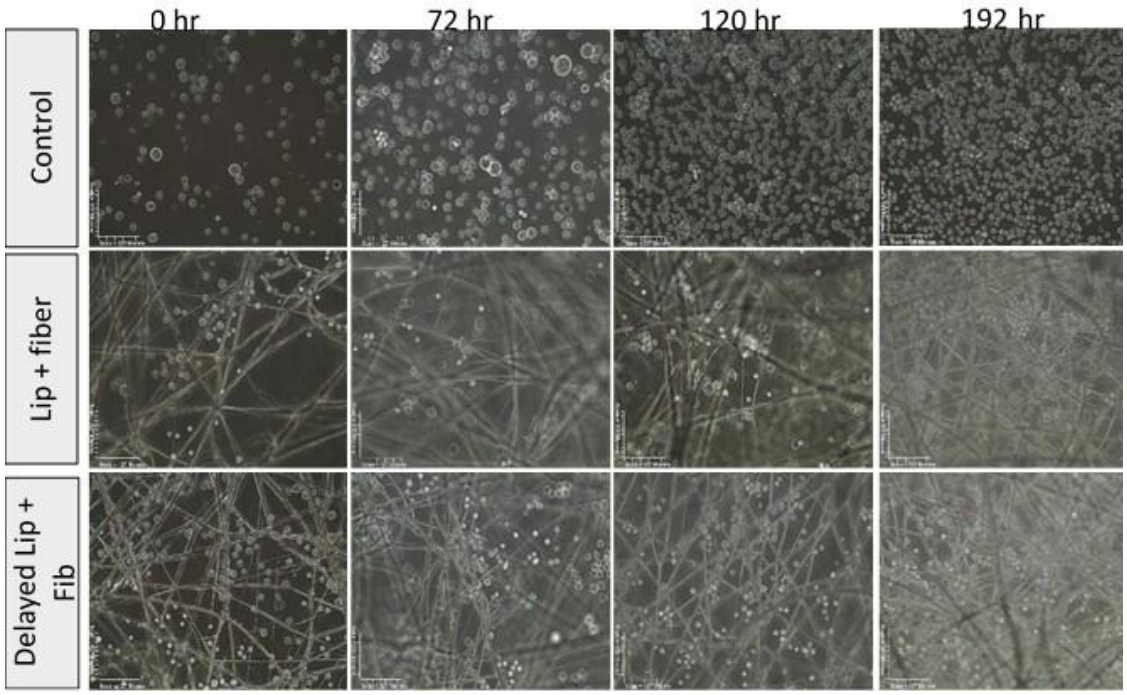

Figure 4.8: Microscopic images of the combination therapy on K562 cells. Controls correspond to monocultures in 200 PRF medium.

4.3.9 Resveratrol and siRNA combination effect on cell viability in the presence of HUVECs

In order to understand the effect of targeted combination therapy on K562 cells, I first seeded HUVECs and performed experiments similar to Section 3.7. A primary difference was the cell culture medium which was 1:1 mixture of HUECs culture medium and K562 cell culture medium. These results showed non-viability of K562 cells (**Figure 4.9a**) is not higher than that observed in monoculture results (**Figure 4.7a**) for both treatment options; non-viability levels of K562 cells were 79.99 (± 2.24) % and 94.32 (± 1.70) %. This indicates that the treatment by inducing apoptosis in K562 cells is not affected by the presence of HUVECs and that the treatment is still effective. There

also seemed to be an increase in non-viability with delayed addition of liposomes, particularly between day 3 and day 5. However, the control group showed a higher percentage of non-viable cells on day 8. When necrotic cells were analyzed (**Figure 4.9b**), there was a higher percentage of necrotic cells in all groups relative to monocultures (**Figure 4.7b**). This could be due to an enhanced effect of nutrient deficiency, with increased cell number and no replenishment of culture medium during 8-day cultures to avoid issues with drug concentration.

On the eighth day, I harvested HUVECs and tested viability (**Figure 4.9c**). These results showed 48.0 (± 4.35) % non-viable cells, and 40.9 (± 4.79) % necrotic cells in treatment groups and comparable numbers in control. The increase in non-viability levels in controls could be due to lack of nutrition over 8 days of incubation in 1:1 RPMI: PRF 200 cell medium.

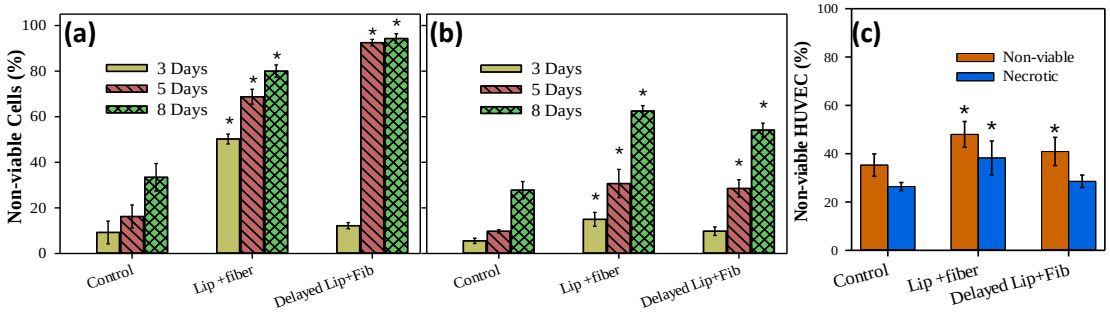

Figure 4.9: K562 cells non-viability levels investigated under different conditions. Indicated non-viable cells were assessed by two-color flow cytometry using Annexin V for apoptosis and PI for necrosis. Control samples correspond to K562 cells and HUVECs in 1:1 RPMI and 200 medium without treatment. Lip + fiber correspond to samples treated with both loaded liposomes and loaded fibers, introduced to the co-culture cell medium simultaneously. Delayed Lip + Fib samples correspond to loaded fibers introduced to the co-culture cell medium immediately, and loaded liposomes introduced to the co-culture cell medium after 72 hours. Parts a, and b correspond to non-viable, and necrotic, respectively. Parts c is non-viability analysis for the corresponding samples after 8 days. Part (a) shows Annexin V stained samples (non-viable cells), part (b) shows PI stained samples (necrotic cells). Part (c) shows the same analysis on HUVECs after 8 days of incubation. Asterisk (*) indicates $P < 0.02$ relative to control samples.

Micrographs captured during incubation showed the presence of adherent HUVECs in the bottom of the cell culture, while non-adherent K562 cells were above them (**Figure 4.10**). The co-culture

in the control samples is viable. On day 3, HUVECs were still intact, yet slowly lost their adhesive feature by day 8. K562 cell growth was also limited in co-culture. In any case, the stability of fibers was not altered by the presence of HUVECs.

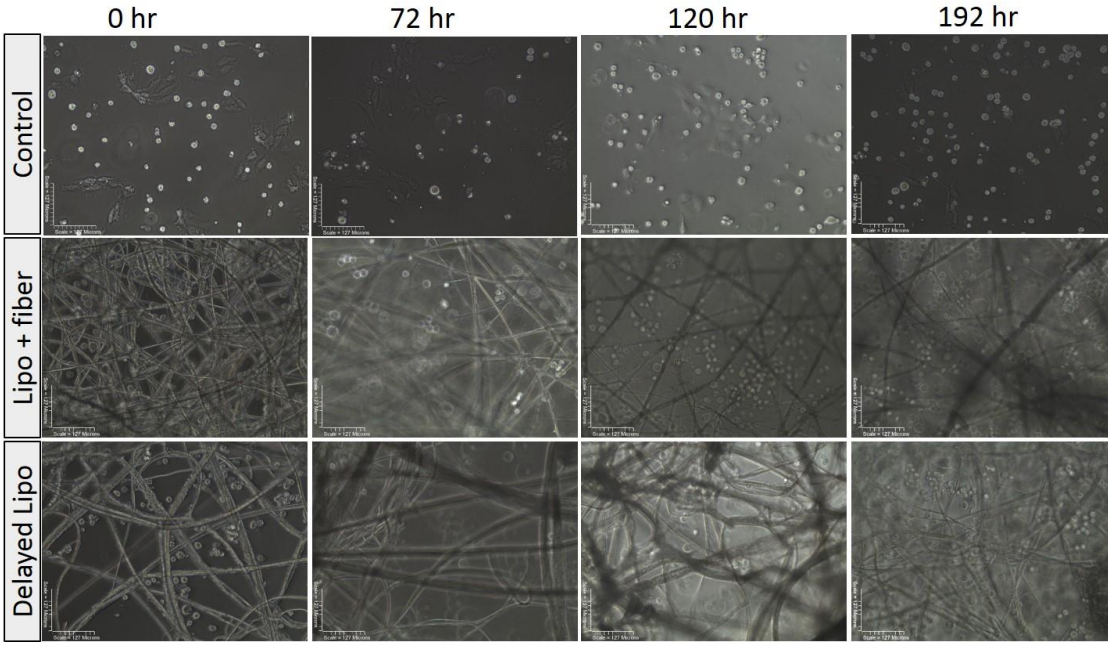

Figure 4.10: Micrographs of the combination therapy on K562 cells in presence of HUVECs. Controls correspond to co-cultures in 1:1 RPMI and 200 PRF medium.

4.4 Discussion

Available treatment options including chemotherapeutic drugs have significant side effects apart from poor solubility in an aqueous environment, short circulating times, and nonspecific delivery. Higher dosages used to achieve therapeutic levels of promulgating toxicity. In order to mitigate these issues, various controlled delivery devices with targeting have been intensely investigated [96]. For example, doxorubicin encapsulated in liposomes (e.g. DOXIL®) provides a therapeutic effect [128]. These biocompatible liposomes with very low toxicity show significant potential in many delivery systems, with high *in vivo* response [132]. PEG coating (to overcome rapid clear-

ance from circulation) and ligand attachment (to avoid non-specific binding) are important for targeting [42]. Transferrin-receptors, overexpressed in cancer cells, including K562 cells, provide higher binding efficiency and multiple fold decrease in IC_{50} value compared to non-targeted liposomes [42]. However, there has been significant side effects (e.g. hand-foot syndrome) due to premature leakage and high dosage requirement. Forming core-shell nanoparticles have been explored to minimize premature leakage [113]. Combination treatment has been explored with multiple drugs encapsulated into liposomes, or multilayered nanoparticles [62, 63].

In this chapter, I evaluated the possibility of combining two separate delivery methods to deliver two different drugs. Aside from the advantages provided by the combination of two drugs, the separate delivery systems provide flexibility and better control upon release. First, I used siRNA targeting BCR-ABL delivered through holo-transferrin conjugated PEG-liposome. Second, I prepared electrospun fiber for controlled release of resveratrol [98], which is proposed in cancer therapy [82, 83]. In Chapter III, I showed that delivering lipophilic resveratrol and achieving therapeutic levels in cell culture in five days [73]. This is a significant improvement, as clinical trials with 150 mg/day of resveratrol given to healthy volunteers for 30 days showed plasma levels in the nanomolar range [91]. This is nearly three orders of magnitude less than that required micromolar concentration to cause apoptosis in cancer cells *in vitro*. Here, I showed that resveratrol-siRNA combination is more potent over 8 days using non-adherent K562 cells and in the presence of HUVECs [87]. Others have shown complete non-viability level, using 2 μM BCR-ABL siRNA transferrin conjugated PEG-liposomes [122]. I used 36 nM BCR-ABL siRNA, in the combination delivery system, showing that 92.7 (± 1.63)% non-viability level is achievable.

Liposomal delivery of siRNA is via endocytosis, for which 100 nm diameter nanoparticles are optimal to avoid uptake by the reticuloendothelial system [133]. Others have shown that BCR-ABL siRNA causes up to 84% of protein level suppression [10]. However, to the best of our knowledge, the level of apoptosis has not been reported. Treatment with siRNA results in nearly

60% BCR-ABL gene silencing, and around 46% cell non-viability. I also observed slightly higher uptake with holo-transferrin conjugated liposomes than unconjugated liposomes. Others have shown similar silencing levels achieved with free BCR-ABL siRNA [122]. This indicates that the delivery system does not alter BCR-ABL siRNA activity. Observed non-viability level might be due to treating a population of K562 cells *in vitro* with no exposure of other cells that can contribute to selectivity. The uptake study suggests that free siRNA uptake by K562 cells is achievable, however, it is not as high as that achieved with liposomes encapsulation. The uptake level of liposomes by K562 is slightly altered in the presence of HUVECs. HUVECs contribute to the uptake of the total liposomes population, however, this uptake level is relatively low. This suggests that cancerous cells uptake of the surface modified liposomes is not significantly altered by the presence of healthy cells. Since K562 uptake is significantly higher than that of healthy cells, the delivery method is highly selective. This is attributed to the holo-transferrin conjugation, which binds to the holo-transferrin receptor, highly expressed in K562 cells.

By independently loading the two molecules of different sizes and different characteristics, one can optimize the release rates and timing of administration independently. I investigated two-time schemes. The second (delayed liposomes introduction) time scheme induces higher non-viability level. This can be attributed to uptake, and release profiles, respectively. Our approach overcomes the limitations imposed by using one delivery vehicle for the release of multiple components [134]. When introduced at the same time, both siRNA and resveratrol induce their effect on two different cellular pathways in K562 cells, simultaneously. However, a higher effect is achieved if the liposomes introduction into the system is delayed. The latter scenario allows for the maximal effect of resveratrol to take place after being released in the first 3 days. Liposomes uptake would then take place and exert its effect on K562 cells, resulting in higher non-viability levels. One could administer these intravenously and locally. The two-time schemes show how the two delivery methods can be controlled timewise to produce a maximal effect. Timing the administration of the second

delivery device is also important. Similar strategies can be easily adaptable in treating other cancer. Introducing the proposed electrospun delivery system can be applied to a broader range of cancer treatment as microfibers can also be used to deliver both lipophilic and hydrophilic molecules. As K562 cells don't attach, there is no hindrance to the resveratrol release from the fiber. However, I do not know how cell adhesion to the fiber surface affects the release and effectiveness of the delivery device. Further studies in understanding the effect of cell adhesion on release profile are needed. In any case, I believe that similar combination therapy is applicable to existing cancer treatments to reduce dosage and side effects.

In summary, BCR-ABL targeting siRNA was successfully loaded into holo-transferrin-conjugated liposomes of 110 nm in size. Formed liposomes showed 3:1 specificity between cancerous K562 cells in relation to healthy HUVECs in co-cultures. A bolus dose of 40 μM resveratrol showed increased K562 cell death [73] but did not affect HUVEC cell death in relation to controls. Serum added to the medium influences the stability of resveratrol in cultures. Measured S1P activity showed reduced content due to inhibition of sphingosine kinase 1 in K562 cells. Similar resveratrol release was observed from polycaprolactone-gelatin electrospun fibers in the presence of HUVECs. Combination of controlled release of resveratrol and targeted liposomes significantly affected K562 cell apoptosis over 8 days. Delayed addition of liposomes influenced these results further. The effect of resveratrol and siRNA can be maximized with controlled administration. The uptake study shows that K562 uptake of liposomes is not significantly altered by the presence of HUVECs. This indicates that similar uptake level is expected *in vivo*. As a result of lower uptake level, non-viability level of HUVECs is significantly lower than that in K562. The combination therapy is as effective in the presence and absence of HUVECs. These results are promising and need further *in vivo* investigation. Alternatively, I developed a model in Chapter V which can be used to predict the effects of biological conditions on the delivery system. This does not necessarily eliminate the need for *in vivo* testing, however, it can reduce the amount of required experimentation.

CHAPTER V

MODELING AND DIFFUSION ANALYSIS OF DRUG RELEASE FROM ELECTROSPUN MICROFIBERS

5.1 Introduction

Time-dependent increase in the level of non-viable cells was observed, correlating to the release profile. However, it is not clear what approach is appropriate for administering the microfibers. One option for the treatment of leukemia is to insert locally at a site near the genesis of cancerous cells, i.e., bone marrow that hub for hematopoiesis. Similar to a bone marrow biopsy procedure, or stem cell local administration [58], microfibers containing resveratrol can be placed within the bone marrow. However, the influence of blood flow along with the uptake of resveratrol by cells is not well understood.

With the advances in computational modeling, there has been an immense interest in screening therapeutic agents *in silico* with the intent of reducing the cost and time while improving the success rate of candidate drugs. However, models that translate drug stability characteristics and transient release profiles to conditions used in 3D tissue mimicking that *in vitro* conditions needs to be developed. Bioreactors provide a suitable *in vitro* 3D environment with controlled desired stimuli, to represent the bone marrow microenvironment [135]. This bioreactor configuration was assumed to mimic the bone marrow microenvironment [136]. They were used to estimate the average nutrition consumption in the bone marrow microenvironment.

In this regard, I investigated the effect of introducing a fluid flow system, mimicking that of the blood perfusion, on the release of resveratrol from electrospun microfibers.

I used a combination of experimental results and computational fluid dynamics (CFD) to assess the effect of fluid flow rate, uptake rate by cells, length of the fibrous matrix, and the porosity of the tissue surrounding the blood vessels on the concentration profile of resveratrol. I used the dimensions based on a recent study done to understand the related kinetics of chemicals secretion by the bone marrow [137]. Two cell lines were included to understand the effect of uptake rates on released stimulants: 1) endothelial cells that line the blood vessel, and 2) K562 cells suspended in the fluid and based on empirical uptake rates. Non-adherent K562 cells predominantly used in understanding the molecular mechanisms and treatment options. First, I validated the simulation approach using static and dynamic conditions. Then I extended the simulation approach and show that porosity of the tissue and uptake rates have a significant influence on the concentration profile of resveratrol.

5.2 Materials and Methods

5.2.1 Stability of resveratrol in various cell medium

To evaluate the stability of resveratrol in the culture medium, experiments were performed in 6-well plates and 2 mL medium K562 cells and HUVECs. Experiments were performed using 2×10^5 cells/mL (total number of cells, 50% each cell line in the case of co-culture), and 40 μM concentration of resveratrol in medium containing 1:1 of RPMI (used for K562 cells): 200 PRF (used for HUVEC culture) cell medium for 72 hours in 5% CO_2, and 37 °C, with and without cells. Three conditions used were i) medium alone, ii) in presence of HUVECs, and iii) in the presence of both HUVECs and K562 cells. Samples were collected every 24 hours from the initial time point and change in resveratrol concentration was assessed in samples using HPLC, as previously described [73]. Obtained concentrations were normalized to initial concentration and plotted as a function of time. Data were fitted with an exponential equation to determine the cell uptake rates.

5.2.2 Diffusion coefficient calculations

PCL-GT electrospun single fibers were formed identical to the procedure described previously. The experimentally determined concentration values were then used to calculate the corresponding total number of moles using the medium volume [73]. The dimensions of a 6-well plate were obtained from the product's data sheet. A single well has a diameter is 34.8×10^{-3} m, an area of 9.51×10^{-4} m^2, and a volume of 2 mL (amount of cell medium added in experiments). The path of diffusion can be calculated by diving the volume over the area of a single well, resulting in 0.0021 m. The diffusion flux, J, was calculated for each individual point knowing the total moles. Also, change in concentration, dC, during that time was calculated. Knowing the thickness of the fiber, diffusion flux J was plotted for the corresponding $\frac{dc_i}{dz}$. Then diffusion coefficient D was calculated using Fick's first law as shown in **Eq. 11**.

$$-J = D\frac{dC}{dz} \tag{11}$$

From the slope of the linear function. Obtained diffusivity values were used in the simulation.

5.2.3 Measuring resveratrol release with fluid flow

In order to understand the effect of fluid flow on the release profile of resveratrol, an apparatus was constructed in-house. It consisted of a variable speed syringe pump (74900 series, Cole-Parmer, Vernon Hills, IL), syringe, a 12 cm long plastic (rigid) tube with an internal diameter of 0.6 cm, microfiber boundary condition, and a waste collector (**Figure 5.1a**). A 3.8 cm long resveratrol containing PCL/GT fibers were inserted into a rigid tube, closer to the exit (**Figure 5.1b**). The opposite end of the rigid of was attached to a 10-mL syringe containing cell culture medium, which was connected to the syringe pump. The pump set to 0.001 mL/min (0.59 μm/s in simulation, calculated using the cross-sectional area of the reaction tube), used to pump RPMI (10% FBS)

medium though part 2 (**Figure 5.1c**). Entire apparatus was incubated in 5% CO_2/95% air, at 37 °C. Samples (100 µL each) were taken at the exit using a 100 µL micropipette. Eight samples were taken at 0, 10, and 50 minutes, followed by 5, 10, 24, 48, and 72 hours. The samples were analyzed using HPLC as previously described [73]. The simulation parameters were modified to match the experimental dimensions.

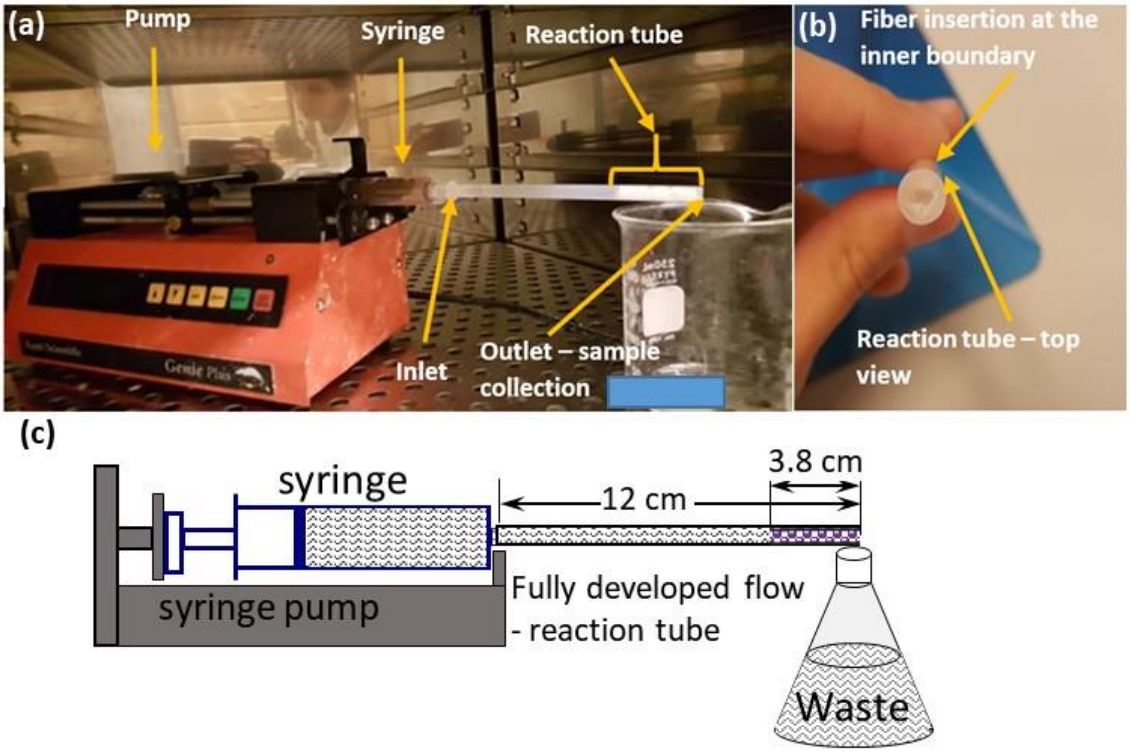

Figure 5.1: Experimental setup for model validation. (a) Experimental setup apparatus. (b) Top view of the reaction tube showing the location of the fiber insertion. (c) Illustration showing the dimensions and location of the fiber.

5.2.4 Numerical simulation of resveratrol release from fibers.

5.2.4.1 Geometry. First, a 3D cylindrical tube was drawn with a 0.8 cm radius and 3.8 cm length (**Figure 5.2a**) in COMSOL Multiphysics 5.4. These dimensions were based on a previous simulation in the bone marrow microenvironment [137]. When evaluating the presence of surrounding porous tissue, an outer shell of 2.2 cm radius (**Figure 5.2b)** was added to the geometry. In addition,

a 34-mm flat geometry was created using the dimensions of a 6-well plate, similar to prior experimental setup for the release of resveratrol from electrospun fibers. A coarse tetrahedral mesh was selected with the following element size parameters with a maximum element size of 0.00208 m and a minimum element size of 6.4×10^{-4} m. Also, the maximum element growth rate was 1.25, the curvature factor was 0.8, and the resolution of narrow regions was 0.5. Mesh independency test was performed, showing that the model is meshed independent. Physical properties (density and viscosity) of the cell culture medium were assumed to mimic that of water at 310.15 K (body temperature). Hence, two materials were defined, water, and resveratrol, defined by molecular weight and diffusion coefficient.

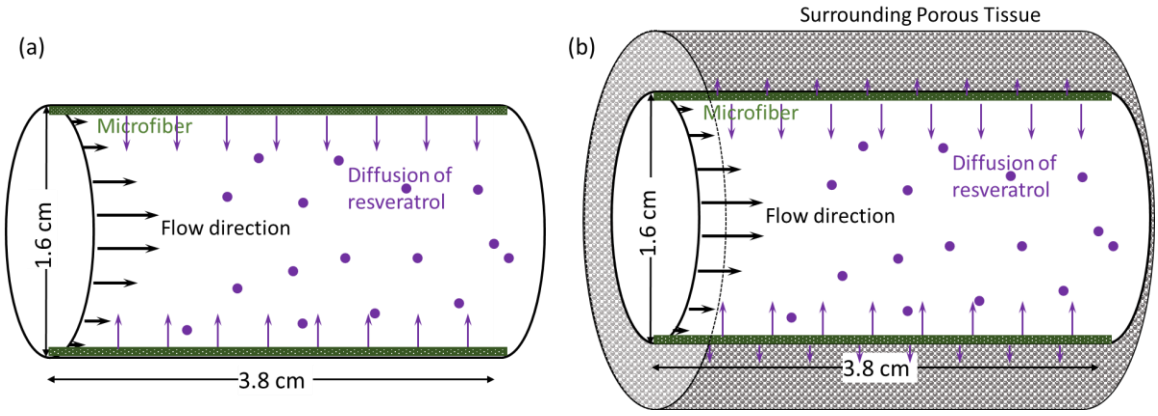

Figure 5.2: Bioreactor model geometry. (a) A schematic showing the dimensions, flow inlet, outlet, diffusion, and the microfiber location. (b) A schematic including the surrounding porous media representing the spongy microenvironment of the bone marrow.

5.2.4.2 Governing equations. It was assumed that the entrance of the tube had a fully developed laminar flow to mimic blood flow in the bone marrow, and transport of diluted chemical, representing resveratrol, from the surface boundaries. Multiphysics model was created to account for transport and laminar flow physics. The two systems are correlated using flow coupling. Fluid flow was assumed to follow incompressible Navier-Stokes equations given by **Eq. 12**, **Eq. 13**, and **Eq. 14**.

$$\rho \frac{\partial u}{\partial t} + \rho(u.\nabla)u = \nabla.[-p\delta_{ij} + \mu(\nabla u + (\nabla u)^T] \quad (12)$$

$$\nabla.(u) = 0 \quad (13)$$

$$u = -U_0 n \quad (14)$$

where ρ is the density, p is the pressure, μ is the dynamic viscosity, δ_{ij} is the Kronecker delta function, u is the fluid velocity, U_0 is the initial velocity, and n is the normal vector. Initially, simulations were performed using 1.5 mm/s velocity [137]. However, while evaluating the effect of flow rate, these values were set to various flow rates as needed. Also, for static condition, u was given a value of zero.

In order to understand the effect of stability and uptake of resveratrol, unsteady advective- diffusion equation for the diluted chemical species was used. This was represented in **Eq. 15** and **Eq. 16**.

$$\frac{\partial C}{\partial t} + \nabla.(-D\nabla C) + u.\nabla C = R \quad (15)$$

$$N = -D\nabla C + uC \quad (16)$$

where C is the concentration of resveratrol at any time t, D is the diffusion coefficient of resveratrol, R is the reaction rate, and N is the molar flux. The free diffusion coefficient was defined in the model as 1.84×10^{-7} m^2/h. The concentration profile was defined based on the release profile previously established [73]. The concentration profile, in the absence of cellular uptake, was defined from the fibers located at the boundary in **Eq. 17**.

$$C = 5.74 + 33.45\ (1 - e^{0.07t}) \quad (17)$$

When evaluating the uptake rate and stability in the culture medium, reaction rate R was defined in the integral form using exponential equations from experiments. For example, in the presence of

both HUVEC and K562 cells, the resveratrol uptake rates by cells as obtained from experiments (**Eq. 18**).

$$C_R = C_{R0}\, e^{-0.015\, t} \qquad (18)$$

where C_{R0} is the initial resveratrol loading concentration, and *t* is given in hours. When evaluating the transport of resveratrol to the surrounding porous region, the diffusion coefficient was modified to an effective diffusion coefficient (D_{eff}) (**Eq. 19**). The *transport of diluted chemical species in porous media*, D_{eff} was assumed to remain constant, isotropic, and was approximated using Mackie-Meares relationship [138].

$$D_{eff} = D\left(\frac{\varepsilon_p}{2-\varepsilon_p}\right)^2 \qquad (19)$$

where ε_p is the porosity value used in the simulation. Based on the previously published reports a porosity of 8.6% was selected first and then to test the effect of porosity it was doubled.

5.2.4.3 Boundary conditions. No slip condition was assumed at the inner surface of the cylinder, where u = 0. The Boundary condition for concentration release is defined at the surface, where material 2 (resveratrol) was defined at the inner surface only. The global definitions of *parameters* and *variables* allow modeling for concentration release from the boundary. The parametric values and model fit, as a function of time, were generated using previously established experimental results for a stagnant system [73]. These were solved using DIRECT solver system that is based on LU Factorization (12) to linearize and numerically solve the built-in PDE equations.

5.3 Results

5.3.1 Resveratrol stability as a function of medium and cellular uptake.

When resveratrol is released into the bloodstream, it is exposed to luminal endothelial cells as well as cells suspended in the bloodstream. In order to determine its fate, I performed co-culture exper-

iments using HUVECs and K562 cells. Also, a 1:1 mixture of the medium was used to accommodate the growth and survival of both the cells. Then the fate of resveratrol in the culture medium of 1:1 RPMI:200 PRF medium, in the presence of K562 cells and HUVECs, was determined over a 3-day time period. These results showed increased stability of resveratrol in culture medium with longer half-lives (**Figure 5.3a**). Others have shown similar stability of resveratrol in phosphate buffers at similar pH conditions [139], [140]. However, I previously observed that in the presence of 10% serum, degradation is much faster. Reduced serum level in the co-culture 1:1 RPMI:200 PRF medium, reduces resveratrol degradation. In the presence of HUVECs, the reduction was less compared to co-cultures, but higher than that in the medium. Cancer cells are known to have altered metabolic activity [141]. In the presence of both HUVECs and K562 cells, nearly 38% remained in the cell culture medium at the end of 72 hours. In addition, reduction in resveratrol seems to accelerate on day 3 in HUVECs, following a different trend line than the exponential decay observed in K562 cell cultures.

5.3.2 Resveratrol release profile matches with simulation results in stagnation condition.

The release rate of resveratrol from the electrospun fibers was simulated using the 6-well geometry used in experiments over five days. Five days were chosen based on available experimental results for the release of resveratrol using PCL-GT electrospun fibers in 6-well plates [73]. Similarly, flow through the reactor with zero velocity was simulated by representing simulation to occur as a *boundary condition* within the model, to generate a concentration profile (volume averaged) (**Figure 5.3b**). In flat geometry, the concentration profile reached a plateau by 80 hr. The experimentally obtained concentration showed a similar release behavior, reaching a plateau by 72 hr but a faster release in the beginning. The minor difference in the plateau value in simulations that experimentally obtained could be attributed to decay and variation in the loading of resveratrol. Effect

of variation in the loading of resveratrol in fibers can be statically observed with the highest standard deviation obtained at the indicated time point, compared to all other experimental data points in the loading efficiency. Slightly higher amount than that predicted can get loaded into the microfibers used in the experiment (including the replicates). However, these do confirm that the simulation approach is valid along with the underlying governing equations. The effect of geometry was assessed using a cylindrical fibrous structure under fluid flow. I used zero velocity, diffusion *of diluted species* is the only controlling phenomena dictating the observed final concentration profile (**Figure 5.3b**). Simulation results showed a faster release, in the beginning, relative to flat geometry. Interestingly, no plateau region was observed. I extended the simulation to 192 hr (8-days) and no plateau region was observed. Overall, the model successfully predicts the general concentration profile under stagnant conditions.

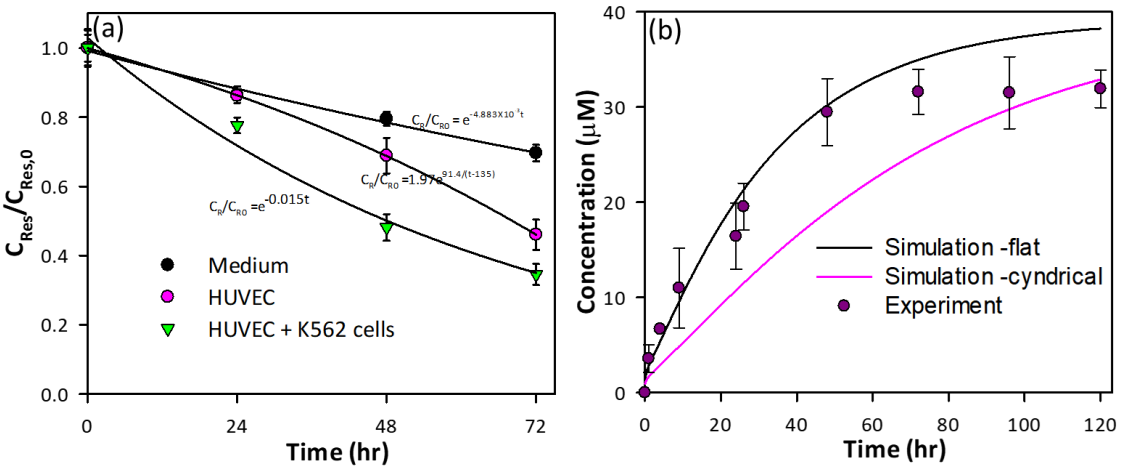

Figure 5.3: Resveratrol stability and release under non-flow conditions. (a) Resveratrol degradation analysis in 1:1 medium of HUVECs and K562 cells incubated at 37 °C and 5% CO_2. (b) Release profile simulation results in static conditions – no flow.

5.3.3 Resveratrol release profile matches with simulation results in fluid flow condition.

Experimental results were obtained using the tubular reactor set-up (**Figure 5.1**). Nearly 8 cm near the inlet was purposefully introduced so that the fluid reaches a developed flow condition with

steady-state velocity profile that used in the simulations at the inlet condition. These results (**Figure 5.4**) show that concentration profiles were identical between the experimental results and simulation results. A minor difference was in the peak value reached by resveratrol, the simulation showed a lower peak relative to experimental results. This could be attributed to a completely developed laminar flow inlet assumption in simulations, which might not have been perfectly achieved experimentally. A flow pattern mimicking a plug flow could provide such increased concentration in tubular reactors. Also, the presence of fibers and the surface roughness could alter the boundary layer leading to the variation in observed concentration profile. Due to the higher standard deviation at the peak value could also be explained by the difference in the loading of resveratrol into the fiber during preparation. In general, the model successfully predicted the actual concentration profile of resveratrol over five days, upon its release from microfibers.

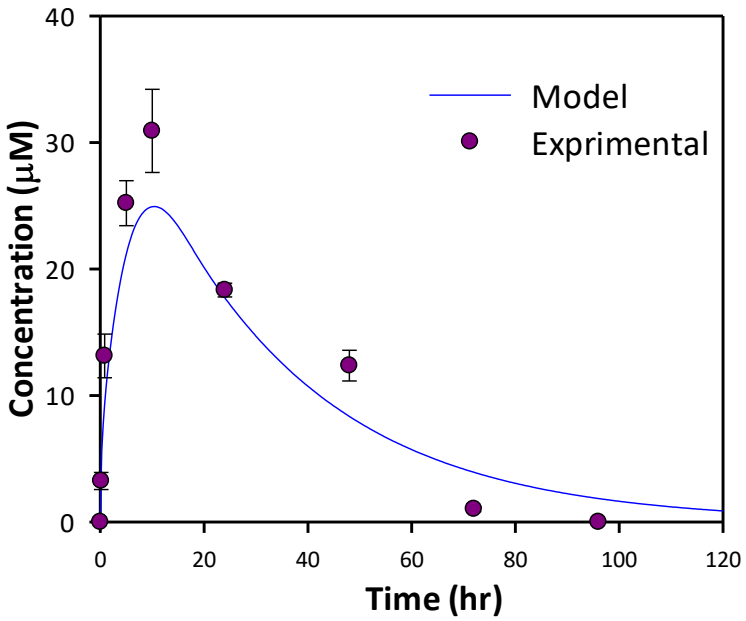

Figure 5.4: Experimental results validating the model under flow conditions. Blue model fit represents simulation results, compared to those experimentally generated (dark pink data points). The experiment and the simulation are performed under the same conditions: 37 ^{o}C, no cellular uptake, geometry/dimensions, and cell medium properties.

5.3.4 Alteration in resveratrol concentration along the length of the reactor assuming flow conditions.

After validating the simulation results with experimental results, I assessed the changes in the concentration of resveratrol along the length of the reactor. For validation, the concentration profile over time was generated by taking an average value of the concentration over the entire volume of the reactor. To determine the concentration distribution along with specific cross-sectional areas along the length of the reactor, the linear integration concept can be used and represented in the model using a *linear projection* operator [142]. To simplify this estimation, and reduce the computation time, a 2D model can be used. Expressions for the linear projection were defined as in **Eq. 20**.

$$c(z) = \frac{1}{Area} \int_0^{Radius} c(z,r).2\pi.rdr \qquad (20)$$

Where z and r are the axial and radial directions in the study. The concentration profile increases along the length of the reactor at a certain point in time (**Figure 5.5a**). This is due to the flow effect starting at the inlet of the reactor and at the outlet. Any amount of the chemical that is released at, or near the inlet, is carried towards the outlet. The overall concentration distribution at the last point in time (120 hours) is shown in **Figure 5.5b**. **Table 5.1** shows selected time points where linear integration was performed along the length of the reactor.

Table 5.1. Alterations in the resveratrol concentration along the length of the tube at various time points.

Label	Time = 0.28 h	Time = 5.56 h	Time = 120 h
Slices concentration graph – constant scale 35 0 µM	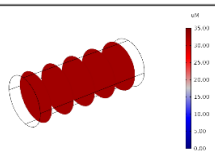	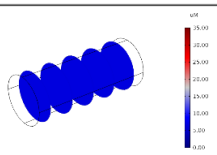	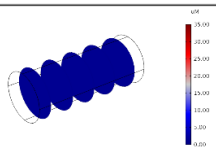
Slices concentration graph – variable scale	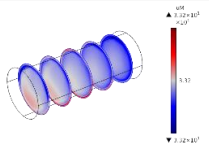	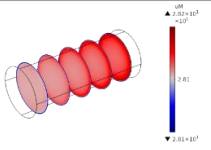	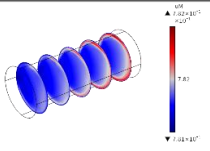
Concentration profile along the length of reactor – center line - variable scale	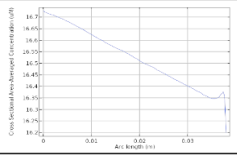	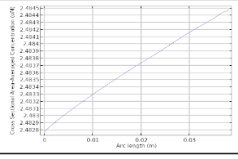	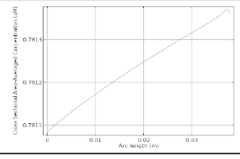

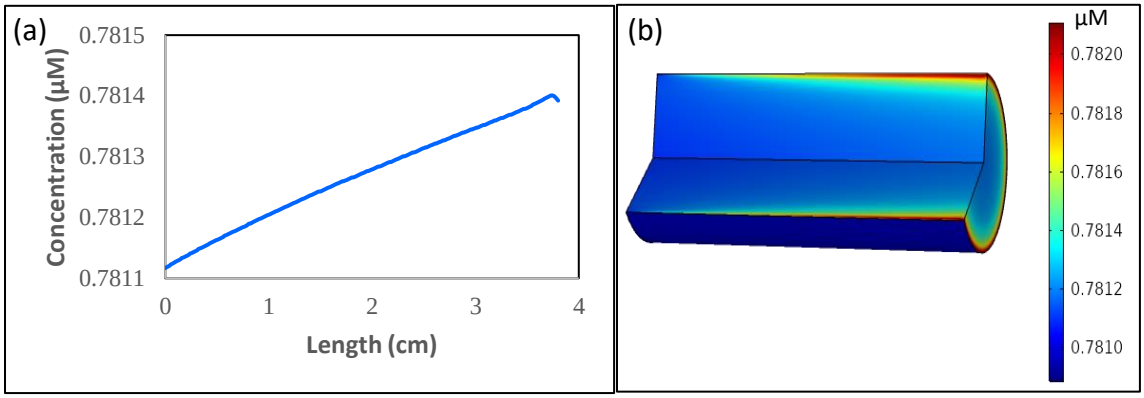

Figure 5.5: Cross-sectional area based concentration distribution by flow along the length of the bioreactor. (a) Linear integration release profile simulation at a selected point in time (120 h). (b) A 3D model of the concentration distribution.

5.3.5 Influence of various parameter on the release of resveratrol under flow conditions.

To understand the flow effects in fully developed (assumed at the entrance) laminar flow, the model was modified to include an inlet velocity. Several variables were considered, including inlet velocity, uptake rates of different cell types, and the length of the reactor.

5.3.5.1 Impact of inlet velocity on the concentration profile. The same model was used to predict the concentration profile over five days, varying three parameters: inlet velocity, cellular uptake, and reactor length (**Figure 5.6**). Inlet velocity has a direct effect on the release kinetics. The larger the velocity the faster a saturation condition is reached, and the faster resveratrol concentration starts to fall. Changing the inlet velocity within the mm/s scale does not influence the concentration profile significantly, after 100 seconds. **Figure 5.6a** shows that even 10 folds increase or decrease in the inlet velocity leads to the same general concentration profile. Lowering the inlet velocity by an order of magnitude, however, had a significant effect on the shape of concentration profile over time. As expected, the driving force reduces, leading to delayed maximum concentration level. The lower threshold is also encountered due to the wash away effect by inlet flow. While it takes longer for the maximum concentration level to be reached, the flow effect is still washing away the diffused resveratrol, leading to a lower maximum level.

The initial 2 hours of release varies based on the inlet velocity (**Figure 5.6b**). This is expected due to having the maximum driving force initially. As the initial concentration in the reactor is 0 μM, and the boundary concentration is at its maximum value, a concentration gradient is greatest, and therefore, mass transfer is greatest. Once a threshold is reached, that value stabilizes, then starts to decrease due to flow condition. The larger the inlet velocity the faster that threshold is reached. This is due to maintaining a high driving force. As the velocity is higher, the diffused resveratrol is washed away quicker, leading to lower instantons concentration inside the reactor. This driving force, however, leads to the higher release of resveratrol from the boundary per unit time. The model, hereby, satisfies the general transfer phenomena predictions. This shows that the process is convection dominant during the first few hours under the given perfusion rate.

5.3.5.2 Impact of cellular uptake on concentration profile. As the inlet velocity is fixed at 1.5 mm/s, the effect of cellular uptake rates was evaluated using experimentally generated data. the

simulation. General behavior (**Figure 5.6c**) was similar to that in **Figure 5.6a**, except that additional cellular uptake reduced the available resveratrol concentration due to fluid flow. Next, uptake rates by different cell lines were included using the expression from experimental results. First, the presence of HUVECs, which line the blood vessels, were analyzed. Due to the uptake by HUVECs, a lower release profile was observed, compared to no cellular presence. The presence of additional K562 cells further decreased that profile. This is expected due to the lower availability of the drug as the level of consumption increases. This can be further developed to include enzymatic kinetics impact of the drug stability, among other biological factors. For comparison purposes an additional profile was generated using lower velocity (three orders of magnitude lower), compared to **Figure 5.6a**, the same general curve shape is obtained at a lower concentration at each point in time, due to the uptake rates introduced.

5.3.5.3 Impact of reactor length on concentration profile. To understand the effect of varying the bioreactor's length, **Figure 5.6d** shows that increasing the length of the reactor by two, or ten folds does not have a noticeable overall effect on the concentration profile over the given period of time. Also, different orders of magnitude in length were assessed. Those scales, such as μm and m ranges produced a different release profile. Those results, however, are unrealistic, as this model is supposed to represent an insertion section to the bone marrow which is realistically represented by the length studied in the model. This shows that the process is diffusion dominant during the second part of the release. This part covers the vast majority of the time of the entire process, under the given perfusion rate.

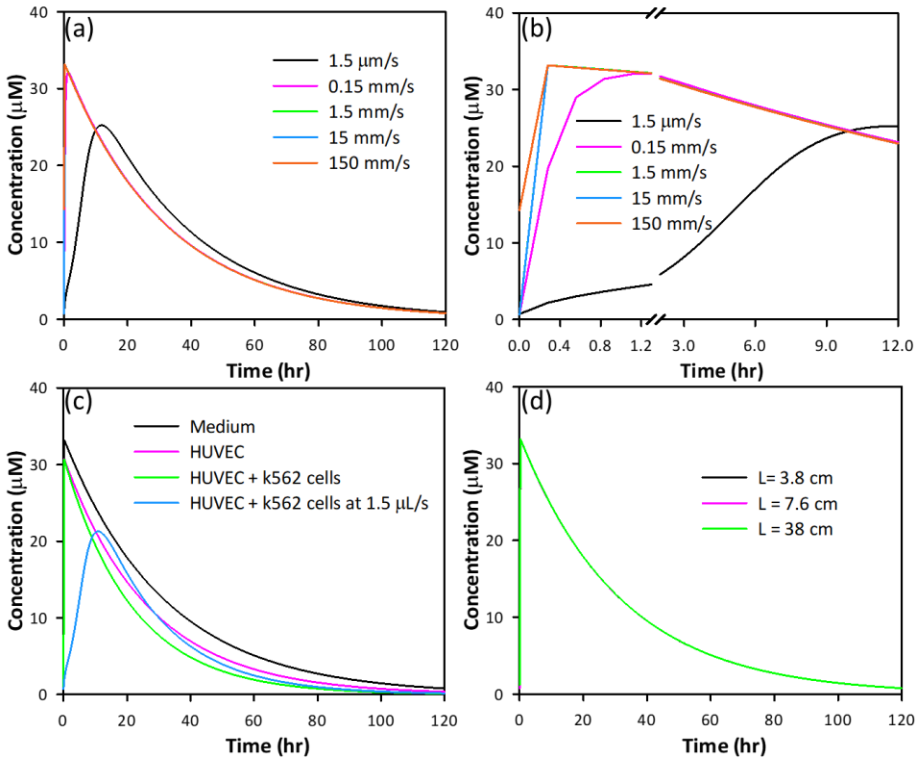

Figure 5.6: Impact of different variables on the release profile under flow conditions. (a) Varying the inlet velocity results in a different maximum release. (b) Significant differences in the release profile shown during the initial release based on inlet velocity. (c) Additional uptake rate results in lower available resveratrol levels in the reactor. (d) Changing the length of the reactor does not have a significant effect on the release simulation results.

5.3.5.4 Modeling the release in the presence of a porous medium. The simulation setup was modified to mimic the actual microenvironment of the bone marrow or tissue surrounding the blood vessel. The *laminar flow* was coupled with the *transport of diluted chemical species in porous media*, as well as *transport of diluted chemical species*. The *laminar flow* was modified in the model to account for porous domains where the solver uses the *Brinkman equation* for porous domains and the *Navier-Stokes equation* for free flow domains. The flow was coupled with both transport phenomena by adding *multiphysics*. The geometry was modified based on a previous study [137], and a porosity of 8.6% was selected using literature data [143]. For comparison purposes that porosity was then doubled (17.2%) to study the effect of varying porosity on the release

profile. **Figure 5.7a** and **Figure 5.7b** show the general concentration distribution at the 1000 seconds, and 120 hours points in time, respectively. The higher concentration distribution is observed in **Figure 5.7a**, in the inner cylinder, due to the higher effect of convection, and no flow resistance (no porosity in the inner layer). With the progression of time, the concentration shifts towards the outer shell, as laminar flow washes released resveratrol in the inner cylinder due to lower flow resistance. The porosity provides (**Figure 5.7b**) resistance for concentration drop, and hence the higher concentration distribution relative to the inner cylinder. The obtained concentration profile shows a noticeable effect of the porous medium (**Figure 5.7c**). The average, volume-based concentration profile in the presence of porous media is noticeably lower than that with no porous media, with nearly 6% reduction in the maximum level reached in the inner cylinder. When the porosity is doubled, the release profile shifts further down expectedly, due to reduced resistance by the outer shell porous media additional diffusion path. Thus based on where the material is implanted, one has to account for the diffusion through the porous medium and adjust the loading of the therapeutic agent.

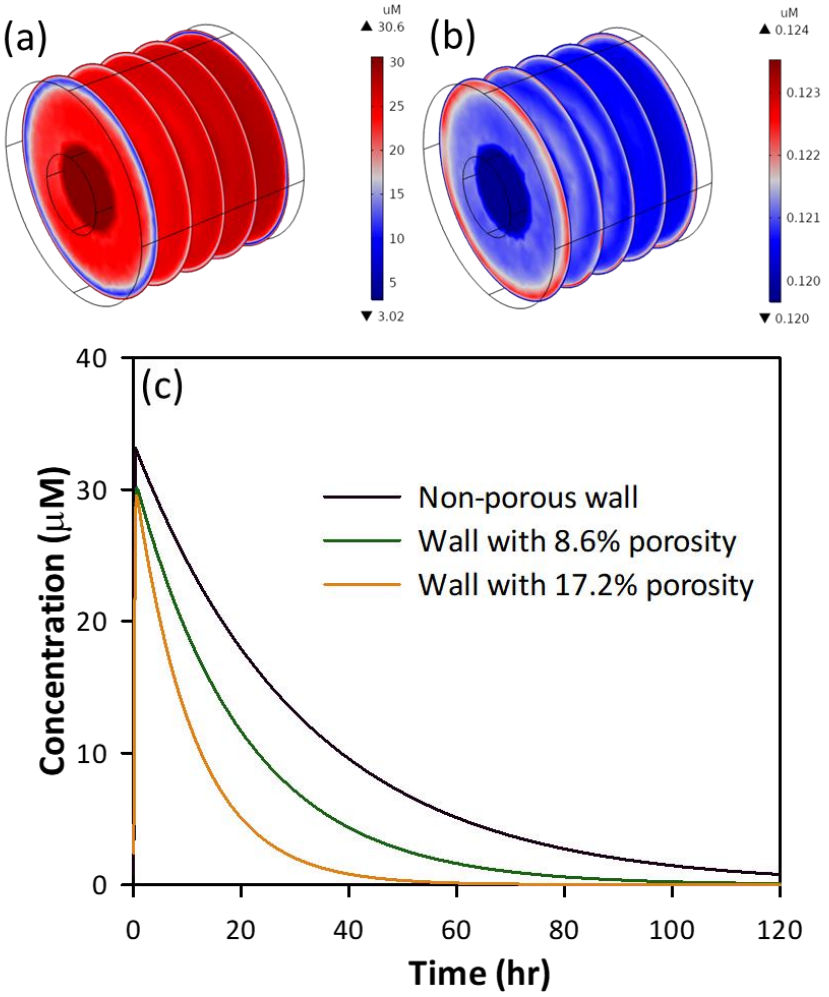

Figure 5.7: Release profile and geometry of the bioreactor in the presence of flow and outer shell porous media. Geometric representation of the concentration distribution along the length of the reactor after (a) 1000 seconds of a transfer, and (b) 120 hours of transfer. (c) Release profile simulation of the inner reaction tube in the presence of outer shell porous media.

5.4. DISCUSSION

In this chapter, I evaluated the effect of fluid flow and cellular uptake rate on the release kinetics of stimulants sequestered inside electrospun fibers. To understand the impact of fluid flow, in the bone marrow microenvironment, on the release of resveratrol from electrospun microfibers, a mathematical model was developed. I combined the time-dependent release rate from fibers along with

the uptake rates by different cells. I validated the concentration profiles from both static and dynamic conditions. The model was extended by introducing an outer porous layer to further mimic the release in a bone marrow microenvironment. This design includes experimental based relations, to define boundary conditions, and geometry. The numerical solution of the model provides crucial information regarding the controlled delivery and the effect of various parameters on that process. The inlet velocity is typically constant on individuals basis, however, the blood perfusion rate slightly differs based on the individual's age and gender [144]. This model shows the release mechanism does not significantly change based on inlet velocity changes within a similar scale. This confirms that the release process will not be affected based on the patient's age, or gender.

The presence of various cell types present in the blood and the blood vessel has a more significant effect on the release profile. As the model predicted, however, leukemic cellular uptake is higher than that by healthy cells, which is the main purpose of the treatment. The model predicted a further reduction in the available drug concentration as more cellular uptake is introduced. The model could be enhanced by adding additional cellular and enzymatic activity, within the bone marrow microenvironment. A previous model can be used as a reference for these kinetics [137]. Steady-state transport of oxygen to the surrounding tissue is well described by the Krogh cylinder approach [145] and many modifications [146]. However, coupling the time-dependent release of a therapeutic agent along with cellular uptake rate is not well understood. Some have explored the release of various drugs sequestered into stents to mitigate restenosis issues locally [147]. Another study illustrated similar kinetic behavior and results for arterial drug release from stents *in vivo* [148]. This shows that the model presented in this study provides an excellent base for future research. In any case, compared to the proposed electrospun microfibers system in this study, stents show higher rigidity and better control upon the shape uniformity.

When based on the mechanism of action, resveratrol is known to be internalized by cells. Although it is not clearly understood how to control the positioning of the proposed system, it is expected

that perfusion rate of blood in the target bone marrow tissue will not have a significant effect on microfibers displacement. It is sought to use this model as a useful tool for local delivery of resveratrol-encapsulated electrospun microfibers. The microfibers can be inserted locally in the core, fatty inner part, of the bone marrow, after the removal of the required part. Similar to how a biopsy is performed, the removed portion can be replaced with the microfibers. This can be used as a treatment [73], or to enhance treatment after chemotherapy, and a transplant, where less than 100% of the leukemia cells are removed [149]. The model predicts that changing the size of the bioreactor on a similar scale does not have a significant effect on the resultant release profile. Hence, taking the suggested geometry is recommended, while other geometries can easily be tested using the model.

Electrospun fibers are increasingly used in developing 3D structures. In addition, electrospun fibers are used in tissue regeneration and wound healing purposes, one could add various stimulants and determine the release rates [150]. With the advances in multiaxial electrospun fibers and various stimulants, one could assess the spatial distribution of components using CFD [98]. Further coupling of the pressure drop predictions across the scaffold, that I demonstrated previously, along with the nutrient consumption characteristics, one could monitor the tissue regenerative process [151]. However, such efforts need experimental validation. This can be useful in other application based on the selected system-specific parameters. Models, such as the one presented in this study, can be used to reduce animal suffering by reducing the need for *in vivo* testing. The need for the latter might not be eliminated, however, can significantly be reduced by narrowing down experimentation based on model predictions. Similar approaches can be used to understand the release profile and effect in those applications.

CHAPTER VI

CONCLUSIONS AND RECOMMENDATIONS

6.1 Conclusions

In aim 1, the influence of controlled release of resveratrol from electrospun microfibers, in combination with siRNA on cell viability was evaluated. I evaluated the apoptotic and necrotic effects of this treatment on K562 cells using Annexin V and Propidium Iodide staining. The combination effect was additive. Non-viability analysis showed resveratrol to cause higher necrotic effects compared to that of siRNA; the effect of siRNA was mainly apoptotic when introduced to the cell culture medium. Fate of resveratrol in cell culture showed reduction to zero in three days. Factorial design-based analysis suggested a range of effective concentrations of both drugs in achieving 100% cell death. In order to improve bioavailability of resveratrol, electrospun microfibers were successfully formed using PCL-GT combination in three different configurations. Controlled release of resveratrol was observed for five days and its effect on cell death was confirmed, inducing higher apoptotic effect, using three different configurations. Upon the controlled release of 40 μM resveratrol from single fibers, roughly 45% non-viable leukemia cells, after 8 days of incubation was measured. However, this percentage dropped to roughly 20% in the presence of 36 nM free BCR-ABL siRNA, which lead to further analysis in aim 2.

In aim 2, the effect of siRNA-loaded liposomes, in combination with controlled release of resveratrol on cell viability, was assessed.

The second delivery system is introduced to provide better control on the diffusion-dependent release, and eliminate possible side interactions. Liposomes 123 (±6.65) nm in size were formed using established techniques. Extrusion and dialysis were performed to obtain the desired size and purity. Holo-transferrin was conjugated to the surface of liposomes by a thiolation reaction, with 85.9 (±7.30)% conjugation efficiency. Roughly 50% of non-viable leukemia cells was measured after treatment. PCL-GT microfibers containing resveratrol were then introduced in combination with siRNA-containing holo-transferrin-derived nano-liposomes. The treatment was tested in both single cultures of K562 cells, and co-cultures, in the presence of HUVECs. The treatment introduction was tested in a timely manner, showing that the delayed addition of liposomes increases K562 non-viability to 92.7 (±2.00)% and 94.32 (±1.70)%, in the absence and presence of HUVECs, respectively. HUVECs non-viability level was significantly lower. To better understand the impact of fluid flow, present in a biological microevironment, a CFD model was built and various parameters were tested as part of aim 3.

In aim 3, experiments were performed to study the stability of resveratrol in different medium and cellular presence conditions. The release profile was analyzed experimentally and was also simulated under both flow and non-flow conditions. These results validated as the experimental data supported that predicted by the model in each case. Several variables were then tested using the model, such as inlet velocity, cellular uptake rate, bioreactor's length, and outer shell porous media. Results show that the release profile is mainly impacted by cellular uptake and the presence of porous media. The model provides a powerful tool that predicts the behavior of the release profile generated by the proposed delivery method. This delivery method can be implemented as a local treatment, and based on the model, is mainly controlled by mass transfer.

6.2 Recommendations

Numerous single and multi-drug treatments have been explored, both *in vitro* and *in vivo*, for their potential in treating cancer. Although the studies have shown the main effects of these treatments on cancer cells, further information is required. This includes treatment's effect on cellular pathways, and cellular processes, such as apoptosis and autophagy. To minimize side effects, lower the required dosage, and enhance drug release control, drug delivery devices are designed and modified mainly for targeting purposes. In this project, a novel drug delivery system has been introduced with a promising potential in treating leukemia. It is sought that this project can be used as a background for future studies in this area.

The author foresees a great advantage in combining two different delivery vehicles for the purposes of delivering multiple, different drugs. This method enables better control upon the release of both locally and systemically administered drugs. It further provides a way to control the time of administration of each drug, and whether simultaneous, or scheduled effect of each drug, is required. For example, microfibers can be locally administered, and the drug release can be modeled and controlled, as opposed to systemic administration of nanoparticles, which is eventually determined by cellular uptake alone. In addition to the controlled release, electrospun microfibers allow a higher loading capacity relative to that of nanoparticles. For instance, some drugs are effective when administered in the micromolar range, while no effect is observed with lower doses. In such cases, nanoparticles provide maximum loading capacity that is not sufficient, or that would require high nanoparticles concentration. One study shows that the maximum loading capacity of 75 million-mole of doxorubicin per mole of liposomes [152]. Accordingly, I suggest that a researcher should follow a selection process to determine the appropriate combination delivery for their treatment under study.

This method, like others, is associated with certain drawbacks. To address some, local administration might be challenging. It might introduce further unforeseen problems when tested *in vivo*, or in clinical trials. Such delivery vehicles are to be scaled up if successful. This introduces more challenges regarding time and cost of manufacturing. The overall take away message is to take the state of the art introduced in this work, as a starting point for future studies in the delivery of combination therapies for cancer treatment.

Results of simulation show that the release profile is mainly impacted by cellular uptake and the presence of porous media, provided a realistic geometry and flow conditions as that found in a bone marrow microenvironment. This model provides a powerful tool that predicts the behavior of the release profile generated by the proposed delivery method. This delivery method can be implemented as a local treatment, and based on the model, is mainly controlled by mass transfer. It is recommended to further extend this study to investigate the diffusion of drug molecules inside the fibers. This can be done by varying the ratio of PCL to GT in the core fiber gel. To further enhance the diffusion model, the diffusion coefficient discussed earlier, can be included. The overall diffusion process can then be broken down into three major steps: (1) diffusion of resveratrol within the fiber core, (2) transfer of resveratrol molecules through the interface between fiber surface and cell medium, and (3) diffusion through cell medium. The partition coefficient provides information about the concentration ratio at the interface between the two mediums at equilibrium.

I have also successfully shown that applying chemical engineering tools in the field of pharmaceuticals is a powerful addition to the field. Models, such as the one presented in this study, can be used to reduce animal suffering by reducing the need for *in vivo* testing. The need for the latter might not be eliminated, however, can significantly be reduced by narrowing down experimentation based on model predictions.

REFERENCES

1. Bray F, Ferlay J, Soerjomataram I, et al. Global cancer statistics 2018: GLOBOCAN estimates of incidence and mortality worldwide for 36 cancers in 185 countries. CA: a cancer journal for clinicians. 2018.
2. Rosen L, Rosen G. Chronic Myeloid Leukemia (CML): American Cancer Society 2016 [11/4/2016]. Available from: http://www.cancer.org/cancer/leukemia-chronicmyeloidcml/
3. Mughal TI, Schrieber A. Principal long-term adverse effects of imatinib in patients with chronic myeloid leukemia in chronic phase. Biologics : Targets & Therapy.
4. DeLeve LD. Liver sinusoidal endothelial cells and liver regeneration. The Journal of clinical investigation. 2013 May;123(5):1861-6. doi: 10.1172/JCI66025. PubMed PMID: 23635783; PubMed Central PMCID: PMC3635729.
5. Jang M, Cai L, Udeani GO, et al. Cancer chemopreventive activity of resveratrol, a natural product derived from grapes. Science (New York, NY). 1997 Jan 10;275(5297):218-20. PubMed PMID: 8985016; eng.
6. Davis ME, Zuckerman JE, Choi CHJ, et al. Evidence of RNAi in humans from systemically administered siRNA via targeted nanoparticles [10.1038/nature08956]. Nature. 2010 04/15/print;464(7291):1067-1070. doi: http://www.nature.com/nature/journal/v464/n7291/suppinfo/nature08956_S1.html.
7. Bartlett DW, Davis ME. Insights into the kinetics of siRNA-mediated gene silencing from live-cell and live-animal bioluminescent imaging. Nucleic Acids Research. 2006;34(1):322-333. doi: 10.1093/nar/gkj439.
8. Shen S, Xia J-X, Wang J. Nanomedicine-mediated cancer stem cell therapy. Biomaterials. 2016 2016/01/01/;74:1-18. doi: http://dx.doi.org/10.1016/j.biomaterials.2015.09.037.
9. Lee SJ, Kim MJ, Kwon IC, et al. Delivery strategies and potential targets for siRNA in major cancer types. Advanced drug delivery reviews. 2016 2016/09/01/;104:2-15. doi: http://dx.doi.org/10.1016/j.addr.2016.05.010.
10. Valencia-Serna J, Gul-Uludağ H, Mahdipoor P, et al. Investigating siRNA delivery to chronic myeloid leukemia K562 cells with lipophilic polymers for therapeutic BCR-ABL down-regulation. Journal of Controlled Release. 2013;172(2):495-503.
11. Pan H, Hu Q, Wang J, et al. Myricetin is a novel inhibitor of human inosine 5′-monophosphate dehydrogenase with anti-leukemia activity. Biochemical and Biophysical Research Communications. 2016 9/2/;477(4):915-922. doi: http://dx.doi.org/10.1016/j.bbrc.2016.06.158.
12. Herudek J. Structural and functional characterization of RNA-binding domain in human IMPDH proteins: Masaryk University 2013.
13. Cassuto O, Dufies M, Jacquel A, et al. All tyrosine kinase inhibitor-resistant chronic myelogenous cells are highly sensitive to ponatinib. Oncotarget. 2012;3(12):1557-1565.
14. Breccia M, Gentilini F, Cannella L, et al. Ocular side effects in chronic myeloid leukemia patients treated with imatinib. Leukemia Research. 2008 7//;32(7):1022-1025. doi: http://dx.doi.org/10.1016/j.leukres.2007.10.016.

15. Pretel-Irazabal M, Tuneu-Valls A, Ormaechea-Pérez N. Adverse Skin Effects of Imatinib, a Tyrosine Kinase Inhibitor. Actas Dermo-Sifiliográficas (English Edition). 2014 9//;105(7):655-662. doi: http://dx.doi.org/10.1016/j.adengl.2014.07.010.
16. Shen Q, Liu S, Chen Y, et al. Proliferation inhibition and apoptosis induction of imatinib-resistant chronic myeloid leukemia cells via PPP2R5C down-regulation. Journal of hematology & oncology. 2013;6(1):1.
17. Finotti A, Bianchi N, Fabbri E, et al. Erythroid induction of K562 cells treated with mithramycin is associated with inhibition of raptor gene transcription and mammalian target of rapamycin complex 1 (mTORC1) functions. Pharmacological Research. 2015 1//;91:57-68. doi: http://dx.doi.org/10.1016/j.phrs.2014.11.005.
18. Bianchi N, Osti F, Rutigliano C, et al. The DNA-binding drugs mithramycin and chromomycin are powerful inducers of erythroid differentiation of human K562 cells. British Journal of Haematology. 1999;104(2):258-265. doi: 10.1046/j.1365-2141.1999.01173.x.
19. Widemann B. Mithramycin for children and adults with solid tumors or ewing sarcoma United States: National Cancer Institute (NCI); 2012 [11/4/2016]. Available from: https://clinicaltrials.gov/ct2/show/NCT01610570
20. Kim H-B, Kim M-J, Lee S-H, et al. Amurensin G, a novel SIRT1 inhibitor, sensitizes TRAIL-resistant human leukemic K562 cells to TRAIL-induced apoptosis. Biochemical Pharmacology. 2012 8/1/;84(3):402-410. doi: http://dx.doi.org/10.1016/j.bcp.2012.03.014.
21. Srdic-Rajic T, Nikolic K, Cavic M, et al. Rilmenidine suppresses proliferation and promotes apoptosis via the mitochondrial pathway in human leukemic K562 cells. European Journal of Pharmaceutical Sciences. 2016 1/1/;81:172-180. doi: http://dx.doi.org/10.1016/j.ejps.2015.10.017.
22. He R, Liu B, Yang C, et al. Inhibition of K562 leukemia angiogenesis and growth by expression of antisense vascular endothelial growth factor (VEGF) sequence. Cancer Gene Ther. 2003 //print;10(12):879-886.
23. Yang C, Cai H, Meng X. Polyphyllin D induces apoptosis and differentiation in K562 human leukemia cells. International Immunopharmacology. 2016 7//;36:17-22. doi: http://dx.doi.org/10.1016/j.intimp.2016.04.011.
24. Chandramohan Reddy T, Bharat Reddy D, Aparna A, et al. Anti-leukemic effects of gallic acid on human leukemia K562 cells: Downregulation of COX-2, inhibition of BCR/ABL kinase and NF-κB inactivation. Toxicology in Vitro. 2012 4//;26(3):396-405. doi: http://dx.doi.org/10.1016/j.tiv.2011.12.018.
25. Tian H, Yu Z. Resveratrol induces apoptosis of leukemia cell line K562 by modulation of sphingosine kinase-1 pathway. International journal of clinical and experimental pathology. 2014;8(3):2755-2762.
26. De Laporte L, Shea LD. Matrices and scaffolds for DNA delivery in tissue engineering. Advanced drug delivery reviews. 2007;59(4-5):292-307.
27. Zhao X, Kim J, Cezar CA, et al. Active scaffolds for on-demand drug and cell delivery. Proceedings of the National Academy of Sciences. 2011;108(1):67-72.
28. Wang H, Mooney DJ. Biomaterial-assisted targeted modulation of immune cells in cancer treatment. Nature materials. 2018:1.
29. Weiden J, Tel J, Figdor CG. Synthetic immune niches for cancer immunotherapy. Nature Reviews Immunology. 2018;18(3):212.
30. Wraith DC. the Future of immunotherapy: A 20-Year Perspective. Frontiers in immunology. 2017;8:1668.
31. Singha K, Namgung R, Kim WJ. Polymers in small-interfering RNA delivery. Nucleic acid therapeutics. 2011;21(3):133-147.
32. Agrawal P. Significance of polymers in drug delivery system. J Pharmacovigil. 2014;3:e127.

33. Longmire M, Choyke PL, Kobayashi H. Clearance properties of nano-sized particles and molecules as imaging agents: considerations and caveats. 2008.
34. Lee SJ, Kim MJ, Kwon IC, et al. Delivery strategies and potential targets for siRNA in major cancer types. Advanced drug delivery reviews. 2016.
35. Neves AR, Queiroz JF, Costa Lima SA, et al. Cellular uptake and transcytosis of lipid-based nanoparticles across the intestinal barrier: Relevance for oral drug delivery. Journal of Colloid and Interface Science. 2016 2016/02/01/;463:258-265. doi: https://doi.org/10.1016/j.jcis.2015.10.057.
36. Singh S, Pandey VK, Tewari RP, et al. Nanoparticle based drug delivery system: advantages and applications. Indian Journal of Science and Technology. 2011;4(3):177-180.
37. Sanna V, Pala N, Sechi M. Targeted therapy using nanotechnology: focus on cancer. International journal of nanomedicine. 2014;9:467.
38. Nii T, Ishii F. Encapsulation efficiency of water-soluble and insoluble drugs in liposomes prepared by the microencapsulation vesicle method. International journal of pharmaceutics. 2005;298(1):198-205.
39. Ong SGM, Ming LC, Lee KS, et al. Influence of the encapsulation efficiency and size of liposome on the oral bioavailability of griseofulvin-loaded liposomes. Pharmaceutics. 2016;8(3):25.
40. Gutierrez JKT, Zanatta GC, Ortega ALM, et al. Encapsulation of curcumin in polymeric nanoparticles for antimicrobial Photodynamic Therapy. PloS one. 2017;12(11):e0187418.
41. Amini Y, Amel Jamehdar S, Sadri K, et al. Different methods to determine the encapsulation efficiency of protein in PLGA nanoparticles. Bio-medical materials and engineering. 2017;28(6):613-620.
42. Noble GT, Stefanick JF, Ashley JD, et al. Ligand-targeted liposome design: challenges and fundamental considerations. Trends in Biotechnology. 2014 1//;32(1):32-45. doi: http://dx.doi.org/10.1016/j.tibtech.2013.09.007.
43. Bazak R, Houri M, El Achy S, et al. Cancer active targeting by nanoparticles: a comprehensive review of literature. Journal of cancer research and clinical oncology. 2015;141(5):769-784.
44. Scott AM, Allison JP, Wolchok JD. Monoclonal antibodies in cancer therapy. Cancer Immunity Archive. 2012;12(1):14.
45. Cheung A, Bax HJ, Josephs DH, et al. Targeting folate receptor alpha for cancer treatment. Oncotarget. 2016;7(32):52553.
46. Sader M, Courty J, Destouches D. Nanoparticles functionalized with ligands of cell surface nucleolin for cancer therapy and diagnosis. Journal of Nanomedicine and Nanotechnology. 2015;6:310.
47. Wang Y, Chen X, Tian B, et al. Nucleolin-targeted extracellular vesicles as a versatile platform for biologics delivery to breast cancer. Theranostics. 2017;7(5):1360.
48. Chen Z, Chen Z, Zhang A, et al. Electrospun nanofibers for cancer diagnosis and therapy [10.1039/C6BM00070C]. Biomaterials Science. 2016;4(6):922-932. doi: 10.1039/C6BM00070C.
49. Goonoo N. Modulating immunological responses of electrospun fibers for tissue engineering. Advanced Biosystems. 2017;1(8):1700093.
50. He X, Feng B, Huang C, et al. Electrospun gelatin/polycaprolactone nanofibrous membranes combined with a coculture of bone marrow stromal cells and chondrocytes for cartilage engineering. International journal of nanomedicine. 2015;10:2089.
51. Wang J, Kang Q-s, Lv X-g, et al. Simple patterned nanofiber scaffolds and its enhanced performance in immunoassay. PloS one. 2013;8(12):e82888.
52. Fan Z-y, Zhao Y-l, Zhu X-y, et al. Folic acid modified electrospun poly (vinyl alcohol)/polyethyleneimine nanofibers for cancer cell capture applications. Chinese Journal of Polymer Science. 2016;34(6):755-765.
53. Mauro N, Scialabba C, Pitarresi G, et al. Enhanced adhesion and in situ photothermal ablation of cancer cells in surface-functionalized electrospun microfiber scaffold with graphene oxide. International Journal of Pharmaceutics. 2017;526(1):167-177.

54. Bonadies I, Maglione L, Ambrogi V, et al. Electrospun core/shell nanofibers as designed devices for efficient Artemisinin delivery. European Polymer Journal. 2017;89:211-220.
55. Han D, Sasaki M, Yoshino H, et al. In-vitro evaluation of MPA-loaded electrospun coaxial fiber membranes for local treatment of glioblastoma tumor cells. Journal of Drug Delivery Science and Technology. 2017 2017/08/01/;40(Supplement C):45-50. doi: https://doi.org/10.1016/j.jddst.2017.05.017.
56. Saha S, Duan X, Wu L, et al. Electrospun fibrous scaffolds promote breast cancer cell alignment and epithelial–mesenchymal transition. Langmuir. 2011;28(4):2028-2034.
57. Sánchez-Capelo A. Dual role for TGF-β1 in apoptosis. Cytokine & growth factor reviews. 2005;16(1):15-34.
58. Huang S, Xu L, Zhang Y, et al. Systemic and local administration of allogeneic bone marrow-derived mesenchymal stem cells promotes fracture healing in rats. Cell transplantation. 2015;24(12):2643-2655.
59. Al-Attar T, Madihally SV. Targeted Cancer Treatment Using Combination of siRNA-Liposomes and Resveratrol-Electrospun Fibers in Co-Cultures. 2019.
60. Lin TL, Newell LF, Stuart RK, et al. CPX-351 ((cytarabine: daunorubicin) liposome injection,(vyxeos)) does not prolong QTcF intervals, requires no dose adjustment for impaired renal function and induces high rates of complete remission in acute myeloid leukemia. Am Soc Hematology; 2015.
61. Hu C-MJ, Zhang L. Nanoparticle-based combination therapy toward overcoming drug resistance in cancer. Biochemical pharmacology. 2012;83(8):1104-1111.
62. Hu Q, Sun W, Wang C, et al. Recent advances of cocktail chemotherapy by combination drug delivery systems. Advanced drug delivery reviews. 2016;98:19-34.
63. Ma L, Kohli M, Smith A. Nanoparticles for combination drug therapy. ACS nano. 2013;7(11):9518-9525.
64. Mufamadi MS, Pillay V, Choonara YE, et al. A review on composite liposomal technologies for specialized drug delivery. Journal of drug delivery. 2011;2011.
65. Yu D-G, Zhu L-M, White K, et al. Electrospun nanofiber-based drug delivery systems. Health. 2009;1(02):67.
66. Español L, Larrea A, Andreu V, et al. Dual encapsulation of hydrophobic and hydrophilic drugs in PLGA nanoparticles by a single-step method: Drug delivery and cytotoxicity assays. RSC Advances. 2016;6(112):111060-111069.
67. Zhang Y, Cao Y, Luo S, et al. Nanoparticles as drug delivery systems of combination therapy for cancer. Nanobiomaterials in Cancer Therapy: Elsevier; 2016. p. 253-280.
68. Gadde S. Multi-drug delivery nanocarriers for combination therapy. MedChemComm. 2015;6(11):1916-1929.
69. Zhang M, Liu E, Cui Y, et al. Nanotechnology-based combination therapy for overcoming multidrug-resistant cancer. Cancer biology & medicine. 2017;14(3):212.
70. Qin M, Lee YEK, Ray A, et al. Overcoming cancer multidrug resistance by codelivery of doxorubicin and verapamil with hydrogel nanoparticles. Macromolecular bioscience. 2014;14(8):1106-1115.
71. Kim C, Shores L, Guo Q, et al. Electrospun microfiber scaffolds with anti-inflammatory tributanoylated N-acetyl-d-glucosamine promote cartilage regeneration. Tissue Engineering Part A. 2016;22(7-8):689-697.
72. Khalf A, Madihally SV. Recent advances in multiaxial electrospinning for drug delivery. European Journal of Pharmaceutics and Biopharmaceutics. 2017;112:1-17.
73. Al-Attar T, Madihally SV. Influence of controlled release of resveratrol from electrospun fibers in combination with siRNA on leukemia cells. European Journal of Pharmaceutical Sciences. 2018;123:173-183.

74. Khalf A, Madihally SV. Modeling the permeability of multiaxial electrospun poly(ε-caprolactone)-gelatin hybrid fibers for controlled doxycycline release. Materials Science and Engineering: C. 2017 2017/07/01/;76(Supplement C):161-170. doi: https://doi.org/10.1016/j.msec.2017.03.093.
75. Sangster J. Octanol-water partition coefficients: fundamentals and physical chemistry. John Wiley & Sons; 1997.
76. Welty J, Wicks CE, Rorrer GL, et al. Fundamentals of Momentum, Heat and Mass Transfer. Wiley; 2007.
77. Miller B, Imel AE, Holley W, et al. The role of nanoparticle rigidity on the diffusion of linear polystyrene in a polymer nanocomposite. Macromolecules. 2015;48(22):8369-8375.
78. Malvar O, Ruz J, Kosaka P, et al. Mass and stiffness spectrometry of nanoparticles and whole intact bacteria by multimode nanomechanical resonators. Nature Communications. 2016;7:13452.
79. Gounani Z, Asadollahi MA, Meyer RL, et al. Loading of polymyxin B onto anionic mesoporous silica nanoparticles retains antibacterial activity and enhances biocompatibility. International journal of pharmaceutics. 2018;537(1-2):148-161.
80. Rosenblatt KM, Bunjes H. Evaluation of the drug loading capacity of different lipid nanoparticle dispersions by passive drug loading. European Journal of Pharmaceutics and Biopharmaceutics. 2017;117:49-59.
81. Renaud S, de Lorgeril M. Wine, alcohol, platelets, and the French paradox for coronary heart disease. Lancet (London, England). 1992 Jun 20;339(8808):1523-6. PubMed PMID: 1351198; eng.
82. Novelle MG, Wahl D, Dieguez C, et al. Resveratrol supplementation: Where are we now and where should we go? Ageing research reviews. 2015 May;21:1-15. doi: 10.1016/j.arr.2015.01.002. PubMed PMID: 25625901; eng.
83. Kulkarni SS, Canto C. The molecular targets of resveratrol. Biochimica et biophysica acta. 2015 Jun;1852(6):1114-23. doi: 10.1016/j.bbadis.2014.10.005. PubMed PMID: 25315298; eng.
84. Kundu JK, Surh YJ. Cancer chemopreventive and therapeutic potential of resveratrol: mechanistic perspectives. Cancer Lett. 2008 Oct 08;269(2):243-61. doi: 10.1016/j.canlet.2008.03.057. PubMed PMID: 18550275.
85. Tian H, Yu Z. Resveratrol induces apoptosis of leukemia cell line K562 by modulation of sphingosine kinase-1 pathway. International journal of clinical and experimental pathology. 2015;8(3):2755.
86. Brizuela L, Dayon A, Doumerc N, et al. The sphingosine kinase-1 survival pathway is a molecular target for the tumor-suppressive tea and wine polyphenols in prostate cancer. FASEB journal : official publication of the Federation of American Societies for Experimental Biology. 2010 Oct;24(10):3882-94. doi: 10.1096/fj.10-160838. PubMed PMID: 20522783; eng.
87. Koeffler H, Golde D. Human myeloid leukemia cell lines: a review. Blood. 1980;56(3):344-350.
88. Puissant A, Robert G, Fenouille N, et al. Resveratrol Promotes Autophagic Cell Death in Chronic Myelogenous Leukemia Cells via JNK-Mediated p62/SQSTM1 Expression and AMPK Activation. Cancer Research. 2010;70(3):1042-1052. doi: 10.1158/0008-5472.can-09-3537.
89. Prabhu V, Srivastava P, Yadav N, et al. Resveratrol depletes mitochondrial DNA and inhibition of autophagy enhances resveratrol-induced caspase activation. Mitochondrion. 2013 2013/09/01/;13(5):493-499. doi: https://doi.org/10.1016/j.mito.2012.10.010.
90. Tomé-Carneiro J, Larrosa M, González-Sarrías A, et al. Resveratrol and Clinical Trials: The Crossroad from In Vitro Studies to Human Evidence. Current Pharmaceutical Design.;19(34):6064-6093. doi: 10.2174/13816128113199990407. PubMed PMID: PMC3782695.
91. Timmers S, Konings E, Bilet L, et al. Calorie restriction-like effects of 30 days of Resveratrol (resVida™) supplementation on energy metabolism and metabolic profile in obese humans. Cell metabolism. 2011;14(5):10.1016/j.cmet.2011.10.002. doi: 10.1016/j.cmet.2011.10.002. PubMed PMID: PMC3880862.

92. Almeida L, Vaz-da-Silva M, Falcão A, et al. Pharmacokinetic and safety profile of trans-resveratrol in a rising multiple-dose study in healthy volunteers. Molecular Nutrition & Food Research. 2009;53(S1):S7-S15. doi: 10.1002/mnfr.200800177.
93. Sergides C, ChirilĂ M, Silvestro L, et al. Bioavailability and safety study of resveratrol 500 mg tablets in healthy male and female volunteers. Experimental and Therapeutic Medicine. ;11(1):164-170. doi: 10.3892/etm.2015.2895. PubMed PMID: PMC4726856.
94. Bode LM, Bunzel D, Huch M, et al. In vivo and in vitro metabolism of trans-resveratrol by human gut microbiota. The American Journal of Clinical Nutrition. 2013;97(2):295-309.
95. Kim TH, Shin YJ, Won AJ, et al. Resveratrol enhances chemosensitivity of doxorubicin in multidrug-resistant human breast cancer cells via increased cellular influx of doxorubicin. Biochimica et Biophysica Acta (BBA) - General Subjects. 2014 2014/01/01/;1840(1):615-625. doi: https://doi.org/10.1016/j.bbagen.2013.10.023.
96. Vendrely V, Peuchant E, Buscail E, et al. Resveratrol and capsaicin used together as food complements reduce tumor growth and rescue full efficiency of low dose gemcitabine in a pancreatic cancer model. Cancer Letters. 2017 2017/04/01/;390(Supplement C):91-102. doi: https://doi.org/10.1016/j.canlet.2017.01.002.
97. Kumari A, Yadav SK, Yadav SC. Biodegradable polymeric nanoparticles based drug delivery systems. Colloids Surf B Biointerfaces. 2010 Jan 1;75(1):1-18. doi: 10.1016/j.colsurfb.2009.09.001. PubMed PMID: 19782542.
98. Khalf A, Madihally SV. Recent advances in multiaxial electrospinning for drug delivery. European journal of pharmaceutics and biopharmaceutics : official journal of Arbeitsgemeinschaft fur Pharmazeutische Verfahrenstechnik eV. 2017 Mar;112:1-17. doi: 10.1016/j.ejpb.2016.11.010. PubMed PMID: 27865991.
99. Heisterkamp N, Jenster G, ten Hoeve J, et al. Acute leukaemia in bcr/abl transgenic mice. Nature. 1990 Mar 15;344(6263):251-3. doi: 10.1038/344251a0. PubMed PMID: 2179728; eng.
100. Deininger MWN, Goldman JM, Melo JV. The molecular biology of chronic myeloid leukemia. Blood. 2000;96(10):3343-3356.
101. Khalf A, Madihally SV. Modeling the permeability of multiaxial electrospun poly(epsilon-caprolactone)-gelatin hybrid fibers for controlled doxycycline release. Mater Sci Eng C Mater Biol Appl. 2017 Jul 01;76:161-170. doi: 10.1016/j.msec.2017.03.093. PubMed PMID: 28482513.
102. Zhu Z, Klironomos G, Vachereau A, et al. Determination of trans-resveratrol in human plasma by high-performance liquid chromatography. Journal of Chromatography B: Biomedical Sciences and Applications. 1999 1999/03/19/;724(2):389-392. doi: http://dx.doi.org/10.1016/S0378-4347(98)00586-6.
103. Khalf A, Singarapu K, Madihally SV. Cellulose acetate core-shell structured electrospun fiber: fabrication and characterization. Cellulose. 2015 Apr;22(2):1389-1400. doi: 10.1007/s10570-015-0555-9. PubMed PMID: WOS:000350876300035; English.
104. Hong JK, Madihally SV. Three-dimensional scaffold of electrosprayed fibers with large pore size for tissue regeneration [Research Support, N.I.H., Extramural]. Acta Biomater. 2010 Dec;6(12):4734-42. doi: 10.1016/j.actbio.2010.07.003. PubMed PMID: 20620245; PubMed Central PMCID: PMC2957508. eng.
105. Sultanova Z, Kaleli G, Kabay G, et al. Controlled release of a hydrophilic drug from coaxially electrospun polycaprolactone nanofibers. International journal of pharmaceutics. 2016 Mar 21;505(1-2):133-138. doi: 10.1016/j.ijpharm.2016.03.032. PubMed PMID: 27012983.
106. Repanas A, Glasmacher B. Dipyridamole embedded in Polycaprolactone fibers prepared by coaxial electrospinning as a novel drug delivery system. J Drug Deliv Sci Tec. 2015 Oct;29:132-142. doi: 10.1016/j.jddst.2015.07.001. PubMed PMID: WOS:000362608900016; English.
107. He M, Xue JJ, Geng H, et al. Fibrous guided tissue regeneration membrane loaded with anti-inflammatory agent prepared by coaxial electrospinning for the purpose of controlled release. Appl

Surf Sci. 2015 Apr 30;335:121-129. doi: 10.1016/j.apsusc.2015.02.037. PubMed PMID: WOS:000351614000018; English.
108. Niu X-F, Liu B-Q, Du Z-X, et al. Resveratrol protects leukemic cells against cytotoxicity induced by proteasome inhibitors via induction of FOXO1 and p27 Kip1. BMC cancer. 2011;11(1):99.
109. Bharali DJ, Siddiqui IA, Adhami VM, et al. Nanoparticle delivery of natural products in the prevention and treatment of cancers: current status and future prospects. Cancers. 2011;3(4):4024-4045.
110. Jeong H, Samdani KJ, Yoo DH, et al. Resveratrol cross-linked chitosan loaded with phospholipid for controlled release and antioxidant activity. International Journal of Biological Macromolecules. 2016 2016/12/01/;93(Part A):757-766. doi: https://doi.org/10.1016/j.ijbiomac.2016.09.018.
111. Li TP, Wong WP, Chen LC, et al. Physical and Pharmacokinetic Characterizations of trans-Resveratrol (t-Rev) Encapsulated with Self-Assembling Lecithin-based Mixed Polymeric Micelles (saLMPMs). Sci Rep. 2017 Sep 06;7(1):10674. doi: 10.1038/s41598-017-11320-y. PubMed PMID: 28878397; PubMed Central PMCID: PMCPMC5587738.
112. Shao J, Li X, Lu X, et al. Enhanced growth inhibition effect of Resveratrol incorporated into biodegradable nanoparticles against glioma cells is mediated by the induction of intracellular reactive oxygen species levels. Colloids and Surfaces B: Biointerfaces. 2009 2009/08/01/;72(1):40-47. doi: https://doi.org/10.1016/j.colsurfb.2009.03.010.
113. Huang X, Dai Y, Cai J, et al. Resveratrol encapsulation in core-shell biopolymer nanoparticles: Impact on antioxidant and anticancer activities. Food Hydrocolloids. 2017 3//;64:157-165. doi: https://doi.org/10.1016/j.foodhyd.2016.10.029.
114. Wang H, Hao L, Wang P, et al. Release kinetics and antibacterial activity of curcumin loaded zein fibers. Food Hydrocolloids. 2017 2017/02/01/;63:437-446. doi: https://doi.org/10.1016/j.foodhyd.2016.09.028.
115. Rong D, Chen P, Yang Y, et al. Fabrication of Gelatin/PCL Electrospun Fiber Mat with Bone Powder and the Study of Its Biocompatibility. Journal of functional biomaterials. 2016;7(1):6.
116. Liu S, Pan G, Liu G, et al. Electrospun fibrous membranes featuring sustained release of ibuprofen reduce adhesion and improve neurological function following lumbar laminectomy. Journal of Controlled Release. 2017 2017/10/28/;264:1-13. doi: https://doi.org/10.1016/j.jconrel.2017.08.011.
117. Llorens E, Ibanez H, del Valle LJ, et al. Biocompatibility and drug release behavior of scaffolds prepared by coaxial electrospinning of poly(butylene succinate) and polyethylene glycol. Mat Sci Eng C-Mater. 2015 Apr 1;49:472-484. doi: 10.1016/j.msec.2015.01.039. PubMed PMID: WOS:000350514100055; English.
118. Vaishnaw AK, Gollob J, Gamba-Vitalo C, et al. A status report on RNAi therapeutics. Silence. 2010 Jul 08;1(1):14. doi: 10.1186/1758-907x-1-14. PubMed PMID: 20615220; PubMed Central PMCID: PMCPMC2908561. eng.
119. Wang T, Shigdar S, Shamaileh HA, et al. Challenges and opportunities for siRNA-based cancer treatment. Cancer Lett. 2017 Feb 28;387:77-83. doi: 10.1016/j.canlet.2016.03.045. PubMed PMID: 27045474.
120. Deininger MW, Goldman JM, Melo JV. The molecular biology of chronic myeloid leukemia. Blood. 2000;96(10):3343-3356.
121. Bharti AC, Aggarwal BB. Role of Nutraceuticals in Cancer Chemosensitization. Vol. 2. Academic Press; 2017.
122. Mendonça LS, Firmino F, Moreira JN, et al. Transferrin receptor-targeted liposomes encapsulating anti-BCR-ABL siRNA or asODN for chronic myeloid leukemia treatment. Bioconjugate chemistry. 2009;21(1):157-168.
123. Derycke AS, Kamuhabwa A, Gijsens A, et al. Transferrin-conjugated liposome targeting of photosensitizer AlPcS4 to rat bladder carcinoma cells. Journal of the National Cancer Institute. 2004;96(21):1620-1630.

124. Lee JW, Chen Q, Knowles DM, et al. β-Glucuronidase is an optimal normalization control gene for molecular monitoring of chronic myelogenous leukemia. The Journal of Molecular Diagnostics. 2006;8(3):385-389.
125. Shibata Y, Malhotra A, Dutta A. Detection of DNA fusion junctions for BCR-ABL translocations by Anchored ChromPET. Genome medicine. 2010;2(9):70.
126. Smith MC, Crist RM, Clogston JD, et al. Zeta potential: a case study of cationic, anionic, and neutral liposomes. Analytical and bioanalytical chemistry. 2017;409(24):5779-5787.
127. Pan W, Yu H, Huang S, et al. Resveratrol Protects against TNF-alpha-Induced Injury in Human Umbilical Endothelial Cells through Promoting Sirtuin-1-Induced Repression of NF-KB and p38 MAPK. PLoS One. 2016;11(1):e0147034. doi: 10.1371/journal.pone.0147034. PubMed PMID: 26799794; PubMed Central PMCID: PMCPMC4723256.
128. Fugit KD, Xiang T-X, Choi DH, et al. Mechanistic model and analysis of doxorubicin release from liposomal formulations. Journal of Controlled Release. 2015 2015/11/10/;217:82-91. doi: https://doi.org/10.1016/j.jconrel.2015.08.024.
129. Zhou X, Chen M, Zeng X, et al. Resveratrol regulates mitochondrial reactive oxygen species homeostasis through Sirt3 signaling pathway in human vascular endothelial cells [Original Article]. Cell Death &Amp; Disease. 2014 12/18/online;5:e1576. doi: 10.1038/cddis.2014.530 https://www.nature.com/articles/cddis2014530#supplementary-information.
130. Ghasemi-Mobarakeh L, Prabhakaran MP, Morshed M, et al. Electrospun poly([var epsilon]-caprolactone)/gelatin nanofibrous scaffolds for nerve tissue engineering. Biomaterials. 2008;29(34):4532-4539.
131. Zhang YZ, Feng Y, Huang ZM, et al. Fabrication of porous electrospun nanofibres. Nanotechnology. 2006;17.
132. Mendonça LS, Pedroso de Lima MC, Simões S. Targeted lipid-based systems for siRNA delivery. Journal of Drug Delivery Science and Technology. 2012 2012/01/01/;22(1):65-73. doi: https://doi.org/10.1016/S1773-2247(12)50006-7.
133. Schroeder A, Levins CG, Cortez C, et al. Lipid-based nanotherapeutics for siRNA delivery. Journal of internal medicine. 2010;267(1):9-21.
134. Sun H, Yarovoy I, Capeling M, et al. Polymers in the Co-delivery of siRNA and Anticancer Drugs for the Treatment of Drug-resistant Cancers. Topics in current chemistry (Journal). 2017 Apr;375(2):24. doi: 10.1007/s41061-017-0113-z. PubMed PMID: 28176270; eng.
135. Sladkova M, de Peppo GM. Bioreactor systems for human bone tissue engineering. Processes. 2014;2(2):494-525.
136. Usuludin SBM, Cao X, Lim M. Co-culture of stromal and erythroleukemia cells in a perfused hollow fiber bioreactor system as an in vitro bone marrow model for myeloid leukemia. Biotechnology and bioengineering. 2012;109(5):1248-1258.
137. Ma CYJ, Panoskaltsis N, Kumar R, et al. Simulation of ex vivo bone marrow culture: Application to chronic myeloid leukaemia growth model. Biochemical engineering journal. 2012;61:66-77.
138. Podichetty JT, Dhane DV, Madihally SV. Dynamics of diffusivity and pressure drop in flow-through and parallel-flow bioreactors during tissue regeneration. Biotechnology progress. 2012;28(4):1045-1054.
139. Zupančič Š, Lavrič Z, Kristl J. Stability and solubility of trans-resveratrol are strongly influenced by pH and temperature. European Journal of Pharmaceutics and Biopharmaceutics. 2015;93:196-204.
140. Ha E-S, Kuk D-H, Kim J-S, et al. Solubility of trans-resveratrol in Transcutol HP+ water mixtures at different temperatures and its application to fabrication of nanosuspensions. Journal of Molecular Liquids. 2019.
141. Reznik E, Luna A, Aksoy BA, et al. A landscape of metabolic variation across tumor types. Cell systems. 2018;6(3):301-313. e3.

142. Ruhl C. Analyze your Simulation Results with Projection Operators February 12, 2014 [March 11, 2019]. Available from: https://www.comsol.com/blogs/analyze-simulation-results-projection-operators/
143. Malo M, Rohrbach D, Isaksson H, et al. Longitudinal elastic properties and porosity of cortical bone tissue vary with age in human proximal femur. Bone. 2013;53(2):451-458.
144. Amin-Hanjani S, Du X, Pandey DK, et al. Effect of age and vascular anatomy on blood flow in major cerebral vessels. Journal of Cerebral Blood Flow & Metabolism. 2015;35(2):312-318.
145. Secomb TW. Krogh-cylinder and infinite-domain models for washout of an inert diffusible solute from tissue. Microcirculation. 2015 Jan;22(1):91-8. doi: 10.1111/micc.12180. PubMed PMID: 25377492; PubMed Central PMCID: PMCPMC4286507.
146. Goldman D. Theoretical models of microvascular oxygen transport to tissue. Microcirculation. 2008 Nov;15(8):795-811. doi: 10.1080/10739680801938289. PubMed PMID: 18608981; PubMed Central PMCID: PMCPMC3057578.
147. Chen Y, Xiong Y, Jiang W, et al. Numerical simulation on the effects of drug-eluting stents with different bending angles on hemodynamics and drug distribution. Medical & biological engineering & computing. 2016;54(12):1859-1870.
148. Balakrishnan B, Dooley JF, Kopia G, et al. Intravascular drug release kinetics dictate arterial drug deposition, retention, and distribution. Journal of Controlled Release. 2007;123(2):100-108.
149. Introna M, Pievani A, Borleri G, et al. Feasibility and safety of adoptive immunotherapy with CIK cells after cord blood transplantation. Biology of Blood and Marrow Transplantation. 2010;16(11):1603-1607.
150. Hong JK, Madihally SV. Next generation of electrosprayed fibers for tissue regeneration [Research Support, N.I.H., Extramural Review]. Tissue Eng Part B Rev. 2011 Apr;17(2):125-42. doi: 10.1089/ten.TEB.2010.0552. PubMed PMID: 21210761; PubMed Central PMCID: PMCPMC3062468. eng.
151. Podichetty JT, Bhaskar PR, Khalf A, et al. Modeling pressure drop using generalized scaffold characteristics in an axial-flow bioreactor for soft tissue regeneration. Ann Biomed Eng. 2014 Jun;42(6):1319-30. doi: 10.1007/s10439-014-1009-5. PubMed PMID: 24719051.
152. Crommelin D, Van Bloois L. Preparation and characterization of doxorubicin-containing liposomes. II. Loading capacity, long-term stability and doxorubicin-bilayer interaction mechanism. International journal of pharmaceutics. 1983;17(2-3):135-144.

APPENDIX A

GANTT CHART

Task	Fall 2016	Spring 2017	Summer 2017	Fall 2017	Spring 2018	Summer 2018	Fall 2018	Spring 2019
SPECIFIC AIM 1								
Evaluate the influence of controlled release of resveratrol, in combination with siRNA on cell viability								
SPECIFIC AIM 2								
Assess the effect of siRNA-loaded liposomes, in combination with controlled release of resveratrol on cell viability								
SPECIFIC AIM 3								
Design a bioreactor to mimic the bone marrow microenvironment, and study the latter's effect on the proposed treatment								
Repeat Failed Experiments								
Data Analysis								
Dissertation writing								

APPENDIX B

SUPPLEMENTARY STATISTICAL, FLOW CYTOMETRY, AND QPCR DATA

B.1 ANOVA Analysis

Anova: Single Factor method was used in excel to perform all statistical analysis shown in the paper. The Figure below shows an example of that performed on the qPCR data.

Target	Sample	Cq Mean	Cq Std. Dev		Delta Ct	DD Ct	2^-(DDCt)	Average	STD DEV				
GUSB	b1	24.60	0.15	scrambled	2.48	0.43	0.74	0.82	0.060647	1			
GUSB	b2	24.35	0.13		2.32	0.27	0.83						
GUSB	b3	24.95	0.07		2.22	0.17	0.89						
GUSB	c1	25.83	0.17	control	1.97	-0.08	1.06	1.01	0.134304	2			
GUSB	c2	25.69	0.01		1.85	-0.19	1.14						
GUSB	c3	28.20	0.15		2.32	0.28	0.83						
GUSB	s1	26.08	0.09	siRNA	2.71	0.66	0.63	0.40	0.162407	3	Silenced	P < 0.02	vs. control
GUSB	s2	25.03	0.10		3.73	1.68	0.31						
GUSB	s3	25.32	0.10		3.96	1.91	0.27						
Primer	b1	27.08	0.14										
Primer	b2	26.67	0.06	Control Avg	2.05								
Primer	b3	27.17	0.04										
Primer	c1	27.79	0.12										
Primer	c2	27.54	0.04										
Primer	c3	30.53	0.29										
Primer	s1	28.79	0.17										
Primer	s2	28.76	0.27										
Primer	s3	29.28	0.30										

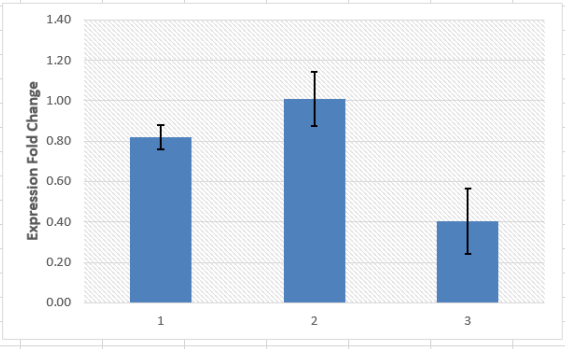

0.74	1.06
0.83	1.14
0.89	0.83

Anova: Single Factor

SUMMARY

Groups	Count	Sum	Average	Variance
Column 1	3	2.45888	0.819627	0.005517
Column 2	3	3.028239	1.009413	0.027056

ANOVA

ce of Varia	SS	df	MS	F	P-value	F crit
Between G	0.054028	1	0.054028	3.317345	0.142652	7.708647
Within Gro	0.065146	4	0.016287			
Total	0.119175	5				

1.06	0.63
1.14	0.31
0.83	0.27

Anova: Single Factor

SUMMARY

Groups	Count	Sum	Average	Variance
Column 1	3	3.028239	1.009413	0.027056
Column 2	3	1.208686	0.402895	0.039564

ANOVA

ce of Varia	SS	df	MS	F	P-value	F crit
Between (	0.551795	1	0.551795	16.56543	0.015222	7.708647
Within Gr	0.13324	4	0.03331			
Total	0.685035	5				

0.74	0.63
0.83	0.31
0.89	0.27

Anova: Single Factor

SUMMARY

Groups	Count	Sum	Average	Variance
Column 1	3	2.45888	0.819627	0.005517
Column 2	3	1.208686	0.402895	0.039564

ANOVA

ce of Varia	SS	df	MS	F	P-value	F crit
Between (	0.260497	1	0.260497	11.55687	0.027289	7.708647
Within Gr	0.090162	4	0.02254			
Total	0.350659	5				

B.2 Histogram plots- non-viability determination procedure

A cell quest software was used to obtain histogram and dot plot for samples analyzed in non-viability experiments. The histogram plots were statistically analyzed to obtain the percentage of non-viable (in case of Annixen V staining) and necrotic (in case of PI staining). A default log-log scale is set for each stain.

After running samples in the flow cytometer, readings were recorded on the template file in Cell Quest. The recorded data were then called back in the form of a histogram plot:

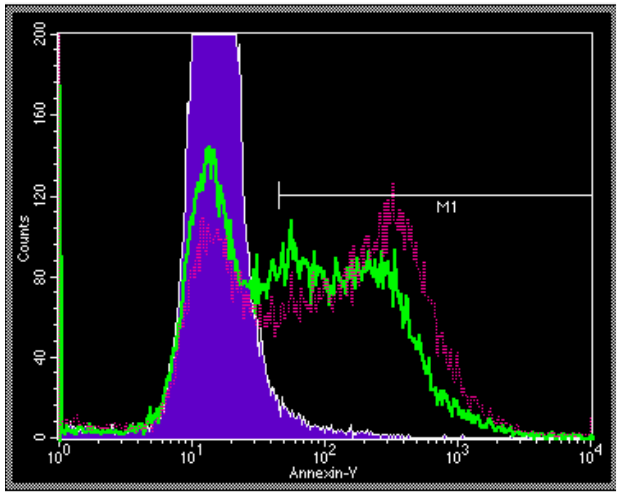

The purple curve refers to a control population incubated for 3 days. Based on that control, non-viability analysis is determined for the green (siRNA-loaded PEG-liposomes) and pink (siRNA-loaded Holo-Transferrin-Conjugated PEG-liposomes) after 3 days of incubation.

Statistical analysis is obtained in Cell Quest as follows:

Control sample:

Marker	Left, Right	Events	% Gated	% Total	Mean	Geo Mean	CV	Median	Peak Ch
All	1, 9910	40000	100.00	100.00	17.10	14.48	323.10	14.72	1
M1	45, 9910	741	1.85	1.85	105.18	74.71	374.45	63.21	47

siRNA-loaded PEG-liposomes sample:

Marker	Left, Right	Events	% Gated	% Total	Mean	Geo Mean	CV	Median	Peak Ch
All	1, 9910	40000	100.00	100.00	142.16	53.40	207.72	50.03	1
M1	45, 9910	21012	52.53	52.53	254.10	165.51	146.99	156.79	53

siRNA-loaded Holo-Transferrin-Conjugated PEG-liposomes:

Marker	Left, Right	Events	% Gated	% Total	Mean	Geo Mean	CV	Median	Peak Ch
All	1, 9910	40000	100.00	100.00	226.91	77.84	192.01	90.58	1
M1	45, 9910	24602	61.50	61.50	357.83	229.96	143.60	237.14	321

Dot plots were also generated and the difference between live and dead populations is clearly observed. Side scatter is plotted against forward scatter, where the top controls, and the bottom is siRNA-loaded Holo-Transferrin-Conjugated PEG-liposomes sample:

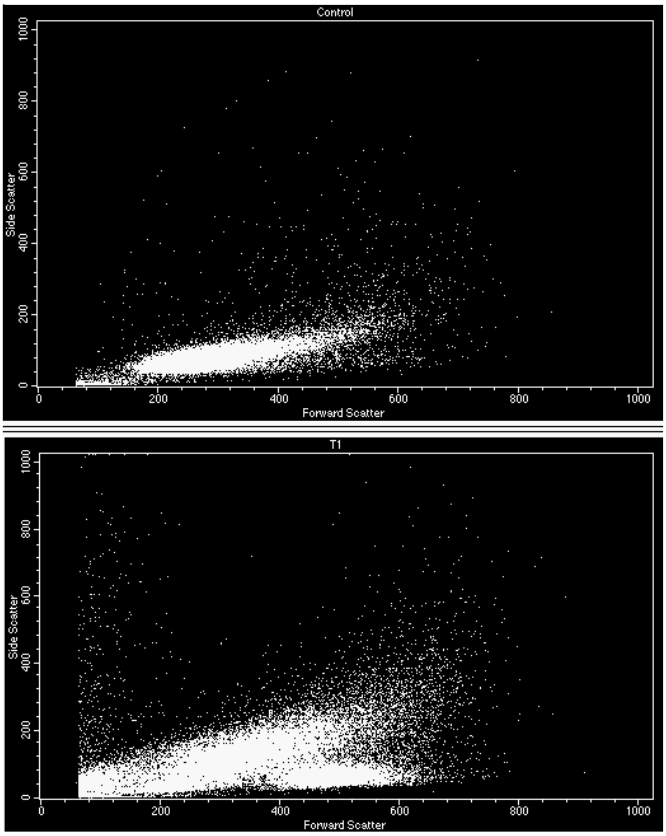

B.3 Real-time qPCR supplementary graphs

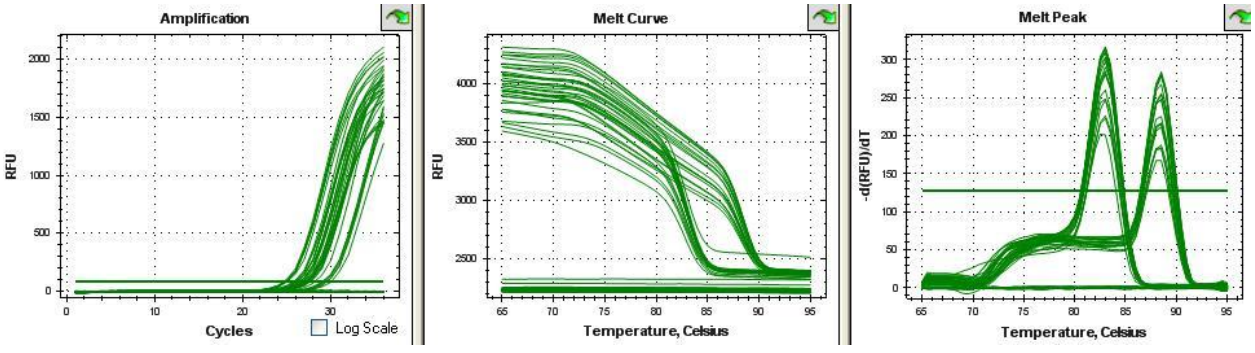

VITA

Thikrayat Al-Attar

Candidate for the Degree of

Doctor of Philosophy

Dissertation: THERAPEUTIC INVESTIGATION AND MODELING OF RESVERATROL AND SIRNA TARGETED COM-BINATION DELIVERY TO LEUKEMIA CELLS

Major Field: Chemical Engieering

Biographical:

Education:

Completed the requirements for the Doctor of Philosophy in chemical engineering at Oklahoma State University, Stillwater, Oklahoma in July, 2019.

Completed the requirements for the Master of Science in chemical engineering at University of California at Berkeley, Berkeley, California in 2016.

Completed the requirements for the Bachelor of Science in chemical engineering at United Arab Emirates University, Al Ain, U.A.E. in 2015.

Experience:

- Doctoral Research and Teaching Assistat, Oklahoma State University, OK, Aug 2016 – May 2019
- Product Development Student Consultant, Stanford Research Institute (SRI) International, CA, Jan – May 2016
- Engineering Intern, Agthia Group PJSC, U.A.E., Feb – May 2014

Professional Memberships:

- American Institute of Chemical Engineers, AIChE
- Omega Chi Epsilon, chemical engineering honor society